Simulating water flow in Hydrus 1D coupled with volumetric water content from electromagnetic induction-based model.

by

Saquib Mohammed Haroon

B.S., North South University, 2019

A THESIS

submitted in partial fulfillment of the requirements for the degree

MASTER OF SCIENCE

Department of Civil Engineering
Carl R. Ice College of Engineering

KANSAS STATE UNIVERSITY
Manhattan, Kansas

2022

Approved by:

Co-Major Professor
Dr. Weston Koehn

Approved by:

Co-Major Professor
Dr. Stacey E Tucker-Kulesza

Copyright

Abstract

Understanding groundwater flow dynamics is vital for a number of applications which includes water budget modeling, crop modeling and to understand long term soil water interactions. One of the challenges in simulating water flow in HYDRUS 1D model is the initial condition at which the model is analyzed. This thesis proposes a coupled HYDRUS 1D and Electromagnetic Induction (EMI) based Volumetric Water Content (VWC) prediction model to simulate accurate water flow. The main objective of this thesis is to calibrate, evaluate, and forecast the movement of water in Hydrus-1D coupled with a multifrequency EMI sensor. To achieve the intended objectives, an EMI based prediction model was developed to predict VWC from the Apparent Electrical Conductivity (ECa) of an EMI sensor. ECa surveys were conducted and VWC was obtained using a Time domain Reflectometer (TDR) sensor in a field located south of Manhattan, Kansas. The TDR sensors were calibrated to the site and correlation between ECa and VWC was studied. Five different Regression models which include linear, logarithmic, power, exponential and 2nd order Quadratic models were developed, and their performance analyzed. Regression models for relative and absolute changes were also studied along with a nonlinear Waxman-Smits model. Mean Absolute Error (MAE) was used to select the best model amongst the 17 models. The logarithmic model was found to be the best model to predict VWC from EMI sensors as it had the least MAE of 1.46% amongst all the models. The developed EMI based VWC prediction model was used to predict VWC and was used as an initial condition in HYDRUS 1D. Atmospheric conditions and free drainage condition was used as boundary conditions to predict VWC for later dates which were then compared with the VWC obtained from the EMI based model. The HYDRUS 1D model had a good level of correlation

with the EMI based model and the MAE was found to be 1.49% indicating the potential to use a coupled HYDRUS 1D and EMI based model to predict future groundwater flow in near surface soil.

Table of Contents

List of Figures

List of Tables

Acknowledgements

I would like to thank my advisor Dr. Stacey E. Tucker-Kulesza for believing in me and providing me all support that was required throughout this project. I have learnt immensely while doing this project under your guidance and have definitely matured more as a researcher. I will always cherish my time working under your guidance in a remarkably diverse lab. I would also equally like to thank Dr. Weston Koehn for helping me immensely during this research. Thank you for all the support from going out to the field along with me to helping me in my analysis to helping me improve my writing skills. I have received immense support and would always be thankful my whole life. Thank you very much. I would also like to express my gratitude to Dr. Stephen Welch and Dr. Phillip Alderman for their kind support and suggestions throughout my research.

Again, I am grateful to my friends Jace, William, Calvin, and Wenqian who have been my greatest motivator and people whom I've always looked into for all types of support. Thank you very much.

Finally, I would like to thank the National Science Foundation who funded this research through Award #1826820: "RII Track-2 FEC: Building Field-Based Ecophysiological Genome-to-Phenome Prediction". This multidisciplinary project helped me grow as a researcher at the same time building other needed soft skills.

Dedication

Dedicated to my mom - My biggest source of Inspiration

Chapter 1 - Introduction

1.1 Background

With advances in precision agriculture, understanding temporal and spatial variability in soil properties have become a very vital part in agricultural modeling as well as in effective soil management (Corwin and Lesch 2005). Unfortunately, delineating soil properties with traditional field and lab-based methods are inefficient and not cost-effective means to characterize an entire crop production field. New agricultural models and precision agriculture methods can be improved with continuous and dynamic data that cover an entire site as opposed to traditional, discrete sampling methods. Geophysical methods present a viable means for subsurface characterization and to understand the spatial and temporal variability. A number of geophysical methods like Ground Penetrating radar (GPR), Time domain reflectometry (TDR), Electrical Resistivity Tomography (ERT) and Electromagnetic Induction (EMI) have a huge potential to be used to understand the variability in soil properties (Allred, Daniels, and Ehsani 2008; Lück et al. 2009). Apparent Electrical conductivity (ECa) is electrical conductivity measured through EMI as well as ERT geophysical methods, ECa represents the soil electrical conductivity for a bulk volume of soil. Previous researchers have found that ECa is correlated with soil properties such as clay content, temperature, water content, salinity and soluble salt (e.g., Corwin and Lesch 2005; Doolittle and Brevik 2014). This has led to ECa to be considered as a vital parameter in developing prediction models for soil properties. The high resolution at which soil ECa is measured from field geophysical methods has the potential to understand variability in soil properties over very short distances. With the increase in interest in sensing technologies, these methods have had increased interest amongst researchers for understanding soil properties. Currently, geophysical methods are not able to predict water flow dynamics in soil, which is important to hydrologists, agricultural

modelers as well as hydrogeologists. Parameters such as infiltration, soil water profile, and fluxes are important parameters that are vital for different analysis and application such as water budget models and root water uptake models. Nonetheless, geophysical models can provide us with real time prediction of current soil properties, predominantly volumetric water content, which has the potential to be used in numerical simulations for better estimation of water movement in soil.

Conventional methods of soil sampling make it very tedious to determine soil properties such as water content at lower horizons. Geophysical methods have the potential to solve this problem. EMI sensors, which are based on electromagnetic theory, measure ECa in a non-invasive and non-destructive method (Brevik, Fenton, and Horton 2004). EMI sensors are unique because the measurements do not require direct contact with the soil. This allows surveyors to map ECa over large fields with less effort and time compared to other geophysical methods. EMI works by transmitting electromagnetic waves into the soil from a primary coil, also called the transmitter coil, which induces an eddy current due to the conductive nature of soil. The eddy current in return generates a secondary electromagnetic wave which is sensed by a secondary coil in the EMI sensor. The EMI sensor provides us response by normalizing the secondary electromagnetic wave with respect to the primary magnetic wave which is used to derive the apparent electrical conductivity. The apparent electrical conductivity is then computed from the normalized response, which is also dependent on the frequency applied, the permeability of the free space and the coil spacing. The theory is explained in greater detail in Chapter 3

There are two different types of commercially available EMI sensors. The first one is the multi-coil EMI sensor which consist of one transmitter and several receiver coils. The transmitter coil transmits an electromagnetic wave at a single frequency and the ECa is determined based on the distance between the transmitter and receiver coils as a function of depth. A smaller coil

separation reaches lower depths while larger coil separation corresponds to larger depths, which allows one to capture soil variability along different depths with one measurement. Another type of EMI sensor is a multifrequency EMI sensor in which the transmitter coil emits multiple frequencies for a fixed coil separation. The frequency is inversely proportional to the depth of investigation i.e., a higher frequency travels shorter distances (and therefore the depth of investigation is shallower) while smaller frequencies travel deeper distances.

The main objective of this thesis is to calibrate, evaluate, and forecast the movement of water in soil using HYDRUS-1D coupled with a multifrequency EMI sensor. One of the challenges to a reliable HYDRUS 1D model is the setup of initial soil water conditions before running a water flow simulation. HYDRUS recommends setting up an initial soil water content that can be as close to present condition. However, obtaining present soil water content at near surface depth is a tedious task, particularly if one wants to evaluate the movement of water over an entire field. This study examines movement of water in soil using a HYDRUS 1D model coupled with an EMI based VWC prediction model in an agricultural site in Kansas. The methodology has the potential to accurately understand soil water dynamics in soil.

To meet the objectives of this research, a prediction model is developed to predict VWC from ECa of EMI sensor. ECa at a field in Ashland Bottom was obtained by running multiple EMI surveys. A TDR sensor was used to gather VWC for these prediction models. Soil surveys were conducted from March 2021 to December 2021 using a GEM-2 EMI sensor. VWC was also obtained using traditional sampling methods for laboratory characterization and the TDR sensor during this timeframe. The HYDRUS model was created using the meteorological data for the time frame. Lab tests were conducted to determine the texture of soil which was used as an input in HYDRUS . The VWC obtained was used as an initial condition in HYDRUS 1D and soil water

content was simulated for later dates and matched with that of HYDRUS 1D model predicted values. The research is aimed at accurate simulation of water movement over different periods of time. Further parameters such as infiltration, fluxes and soil water content can be accurately obtained when HYDRUS 1D models is used in conjunction with EMI sensor based models.

1.2 Thesis Organization

This thesis is divided into 6 Chapters. Chapter 1 provides a background on the research conducted with a brief overview on EMI, ECa, VWC and multifrequency EMI sensors. Chapter 2 is an extensive literature review on the use of geophysical models in characterization of soil variability, the working of EMI and TDR sensors and how HYDRUS models have been used with previous geophysical models. Chapter 3 provides the details on the theories that helps in running the EMI and the TDR sensor. The working of HYDRUS has also been explained in Chapter 3. Chapter 4 explains the methodology and site characteristics. The method to calibrate TDR sensor is also explained. Chapter 5 explains the results obtained which includes the prediction model of VWC from ECa as well as the comparison of results from our predicted model with that of HYDRUS models. Chapter 6 gives a general discussion, conclusions and recommendations based on the results from the study.

Chapter 2 - Literature Review

2.1 Electromagnetic Induction Method in understanding soil variability

Precision agriculture has been an area of high interest for researchers. Research have pointed out the need of understanding temporal and spatial soil variability to support decisions that would generate the best crop yields (Peralta and Costa 2013). Soil electrical conductivity has been used in precious agriculture. Early research involved directly analyzing the variability in soil ECa to understand soil spatial and temporal variability. Clay et al. (2001) analyzed the ECa in four different fields in eastern South Dakota using the Geonics EM 38 multi coil EMI sensor. They determined that ECa was an excellent parameter for understanding the spatial structure of soil. They further concluded that well drained soils had lower ECa than poorly drained soils and attributed the differences in ECa to water leaching salts as well as water content of the soil.

Previous research has employed models to estimate VWC, θ, from the ECa (Garré, Javaux, Vanderborght, Pagès, & Vereecken, 2011). Garre et al. (2011) analyzed the dielectric constant measured using a TDR sensor to develop equations between ECa and VWC. ECa refers to the conductivity that is obtained by assuming that the subsurface is homogenous in nature (Won et al. 1996). Researchers have also evaluated the possibility of predicting the variability in soil properties using the ECa. Carroll and Oliver (2005) examined the relationship between ECa measured with an EMI sensor and soil physical properties. For their research they studied two sites in southern England and used the EM 38 sensor to survey the sites for recording the ECa. Soil was sampled at depths of 0-15cm and 30-60 cm. They measured soil organic matter, particle size fraction, and bulk density. VWC was measured using a Delta-T theta probe which works on the principle of impedance. Carroll and Oliver (2005) concluded that the correlation was moderately positive between ECa and VWC when measurements were taken in autumn. However, correlations

were stronger for measurements taken in drier soil in the summer. They concluded that the difference can be explained by the structural correlation. They also concluded that the soil moisture had a very high impact on the ECa such that the influence of other soil properties was negligible. Similarly, Sudduth et al. (2005) used the EM 38 sensor along with a coulter-based sensor (Veris 3100) to understand soil physical and chemical properties. They carried out their research in 12 different fields across six states in the North Central United states for soil samples up to a depth of 120cm. Regression models for predicting soil moisture, clay content, silt content and cation exchange capacity as a function of both single and multiple ECa variables were developed. An R^2 and standard error were used to analyze the performance of models. In their research, they concluded that ECa was highly correlated with clay content and cation exchange capacity for all fields. They also determined that water content, silt content, sand content, organic carbon was more variable across different type of fields. Another research used a contact (ERT) and a non-contact (EMI) electrical conductivity sensor to map variability in soil properties for two very different situations (Serrano, Shahidian, and da Silva 2014). One part was conducted in a condition with low soil moisture content and with high and differentiated vegetation development. The other condition was soil with a high soil moisture content but with short and relatively homogenous vegetation development. The authors concluded that in spite of correlation among the raw ECa values among both the sensors, the non-contact sensor had an inconsistency for the two different conditions. They further recommended that non-contact sensor was more suitable for soils that had less dense soil vegetation. Robinson et al. (2012) used a differencing approach to separate the influence of soil properties such as texture and mineralogy to estimate relative changes in soil moisture. The relative change is obtained by subtracting the bulk soil electrical conductivity of the driest seasonal soil map. A Dualem 1-S sensor was used to obtain the bulk electrical conductivity.

A Campbell TDR 100 was used to obtain water content which is based on the Topp's Equation (Topp, Davis, and Annan 1980). The authors found that correlations improved due to a proposed differencing approach. In this method, they subtracted the lowest EcA from all other values. A similar method was used in this research. With the strong correlation from their differencing approach, the authors also indicated that ECa might not be dependent on soil moisture for some soils.

In addition to soil water content, researchers have been interested in understanding what other soil properties have an impact on ECa. Martinez et al. (2009) used the EM38 sensor, which is a multi-coil sensor, to determine if ECa obtained from the EMI sensors could be used to determine soil organic carbon. They conducted an exploratory data analysis as well as Fuzzy K-means Classification and concluded that ECa accounted for 30% of the total soil organic carbon variability. It was further said that in spite of a low point to point correlation among soil organic carbon and ECa, geostatistical methods can be useful for spatial estimation of soil organic carbon. Peralta and Costa (2013) evaluated if different soil properties as well as nutrients could be a potential estimator for ECa. ECa was compared with clay content, organic content, soil moisture, cation exchange capacity, pH, and nitrogen concentrations using statistical methods such as principal components stepwise regression and analysis of variance (ANOVA). The results from their principal component stepwise regression indicated that spatial variability of ECa was correlated with clay content, organic content, soil moisture and cation exchange capacity. However other properties such as pH, and nitrogen did not have any significant dependence on the ECa. Ultimately they emphasized the potential of ECa to compute sampling zones. ECa has also been used to understand the relationship between soil electrical conductivity and soil salinity. Ding and Yu (2014) used an EM 38 sensor to identify a relationship between soil conductivity and soil

salinity. They used salinity indices derived from remote sensing images. Ding and Yu (2014) concluded that combining geophysical methods such as EMI with remote sensing images and spectral indices indicated an accurate method to monitor, evaluate and predict soil salinity.

The use of a multi frequency sensor in understanding soil spatial variability has seen increased research interest due to its ease in use and the ability to predict soil properties at numerous depths. The sensor used in this research is the Geophex GEM-2 ski which has been used in various applications. For example, the GEM-2 has been used to locate abandoned brine wells in Hutchinson, Kansas (Xia et al. 2004), to understand permafrost controls on hydrology in Alaska (Walvoord et al. 2015), to delineate near-lake groundwater flow (Ong et al. 2010), to map hydrocarbon contaminant dispersion (Yaccup and Brabham 2012), for the detection of boulders (Liu et al. 2022) and in precision agriculture (Badewa et al. 2018). Badewa et al. (2018) used the multi frequency EMI GEM-2 sensor along with a multi coil EMI CMD-MINIEXPLORER to obtain ECa for a managed podzols in Pasadena, Newfoundland, Canada. The authors emphasized on the requirement of a site-specific calibration when developing a prediction model for soil moisture content. The study confirmed the relationship between the ECa and soil moisture content through a correlation pattern. They concluded that regions of low soil moisture content corresponded to regions of low ECa and regions of higher soil moisture content corresponded to regions of higher ECa. This implies that soil moisture content was a major driver for the ECa. The authors also found out that the ECa for both the multi coil and muti frequency EMI sensors were similar but noted that the depth of investigation for both the sensors might be different.

One major setback for the GEM-2 sensor is the lack an official inversion software to provide an accurate measurement of true conductivity and the depth of investigation. Researchers have instead developed inversions for GEM-2 for different conditions. Elwaseif et al. (2017)

developed a MATLAB based frequency domain electromagnetic inversion code called FEMIC which included all relevant processes like data filtering, forward modelling, inverse modelling, and calculating the depth of investigation. FEMIC was developed on the nonlinear least-squares inversion algorithm coupled with an analytical forward model. The forward model is based on the formulation of the electromagnetic potential on the surface of a layered earth. Liu et al. (2022) developed a 3D inversion scheme with compact finite element method and Gauss Newton optimization to delineate 3D structure of boulders. Their results show a higher horizontal resolution and the ability to visualize a three-dimensional contour of the boulder. Brosten et al. (2011) analyzed different methods to identify the depth of investigation. Methods included the depth of penetration method (McNeill 1980), depth of exploration method (Callegary, Ferré, and Groom 2007), skin depth (Won et al. 1996), depth of investigation (Oldenburg and Li 1999), correlation loss (Moysey, Singha, and Knight 2005; Singha, Day-Lewis, and Moysey 2007) and the model resolution method (Menke 1984). The estimated depth of investigation in the different methods ranged from as low as 1.2m to 23.4m with the skin depth method showing a high of 23.4m. All methods other than the skin depth method indicated a depth between 1.2m to 2.7m. This skin depth seemed incorrect, a similar issue was encountered in this research. With an extremely high frequency, the skin depth was around 4m which should not be the case. This is why the depth was determined using a depth weighted method which is discussed in the methodology of this thesis.

2.2 Geophysical model integration into HYDRUS-1D models

The movement of water in variably saturated media has been of interest to researchers. HYDRUS-1D and HYDRUS (2D/3D) are software packages that use the finite element model (FEM) for simulating the movement of water, heat and multiple solutes in variably saturated media

(Šimůnek, van Genuchten, and Šejna 2008). The simulations can be run in one, two and three dimensions and are based on the solution to the Richard's Equation for saturated-unsaturated water flow and convection-dispersion type equation for heat and solute transport (Šimůnek, van Genuchten, and Šejna 2016). Over the years, researchers have been interested in integrating geophysical models to numerical models. With the increase in the interest in precision agriculture, numerical models integrated with geophysical models have the potential to solve complex problems. Blonquist, Jones, and Robinson (2006) used a time domain transmission soil moisture sensor to estimate VWC for a certain depth. The main objective was to compare irrigation scheduling in turfgrass based on meteorological data and data from a time domain transmission sensor. A HYDRUS-2D model was also developed to simulate drainage below the plant rooting depth and to infer dynamics of VWC for depth of 10cm. The authors compared the values of VWC obtained from the time domain transmission sensor to that of the VWC obtained from the HYDRUS-2D model. They concluded that HYDRUS models have the potential to simulate future VWC conditions and used the HYDRUS model to quantify how well a sensor-controlled irrigation system worked. However, the authors emphasized on the use of a scaling factor as they found out that the HYDRUS models overestimate infiltration through the soil. The authors also emphasized on the use of threshold VWC from EMI based models which is the minimum VWC below which irrigation needs to be started to be used while scheduling irrigation.

Although the use of HYDRUS models with EMI sensors have been very limited, HYDRUS models have been used extensively with other geophysical methods. Lehmann et al. (2013) used ERT and TDR surveys to analyze the spatial and temporal evolution of wetting patterns in slope region which was underlain by a shallow sandstone bedrock. The wetting pattern was simulated in HYDRUS-2D. Numerous researches have used ground penetrating radar (GPR) data models along

with HYDRUS models to understand sub soil properties. Saintenoy, Schneider, and Tucholka (2008) used GPR to monitor water infiltration in sand. A GPR system was used to record the trace every second for water injected through an 81-cm long tube placed in a hole. The water content was found and compared to a 2-D HYDRUS model. They concluded that GPR reflections were able to trace the wetting front in soil. Similarly, Haarder et al. (2011) used GPR to visualize unsaturated flow phenomenon, such as unstable wetting fronts and preferential flow. They infiltrated blue dyed water along a 3m-by-3m field and collected the reflection GPR data. Water and tracer movement were simulated using HYDRUS-1D models and were used to support the conclusion that GPR had a very good potential as a nondestructive method to understand flow phenomena.

Jadoon et al. (2012) used a HYDRUS-1D model along with time lapse GPR data to determine hydraulic parameters. For verifying their model, they compared data from GPR derived water content profile with that of water content obtained from TDR. Their results showed a higher reliability in using GPR along with HYDRUS-1D models to characterize shallow subsurface hydraulic properties and to monitor water dynamics in a large field scale. In another study, soil hydraulic properties were obtained using GPR data acquired in a single ring infiltrometer infiltration test (Léger, Saintenoy, and Coquet 2014). The complex refractive index method was used to convert water content profiles into dielectric permittivity profiles. Experiments were carried out in sandy soil and were converted with the inverted parameters. This literature review highlights that while GPR has been used the most to date, overall geophysical methods have been used extensively along with HYDRUS models.

Chapter 3 - Theory

3.1 Electromagnetic Induction (EMI)

Electromagnetic induction sensors involve a transmitter and receiver coil. The working of the EMI sensor is based on Maxwells equation describing electric and magnetic fields, primarily the Maxwell Faraday's Law and the Maxwell-Amperes Law (Sears 1963). The laws state that a time varying magnetic field induces an electric field while a changing electric field will induce a magnetic field. A transmitter coil transmits the primary magnetic field which reaches the soil surface. Due to the conductive nature of the surface, circular eddy currents are formed which creates a phase shift. The magnitude of the current loops is proportional to the electrical conductivity. According to Maxwell's Law, a changing electric field induces a magnetic field and the loop of eddy current produces the secondary magnetic field. The secondary magnetic field is sensed by the receiver coil. This is amplified and formed into output voltage through which the ECa is formed. Figure 1 is a schematic of a GEM-2 EMI sensor. The bucking coil removes the primary field from the receiver coil.

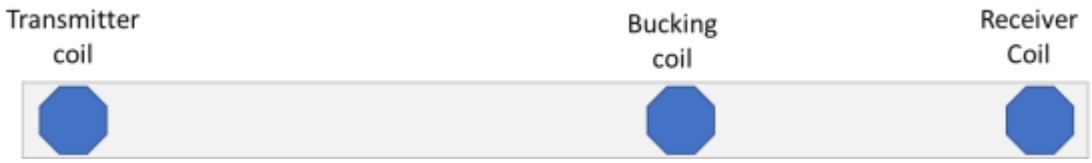

Figure 3-1: Coil configuration in GEM-2 EMI sensor

The ratio of the magnitudes of the out of phase secondary magnetic field to the primary magnetic field is used to determine the ECa which is a weighted average value over a certain depth. Factors that affect the secondary magnetic field are shown in Figure 2.

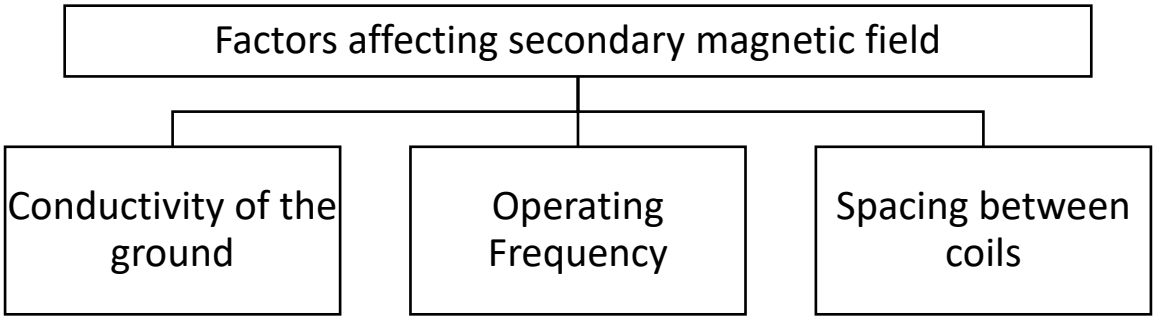

Figure 3-2: Factors affecting secondary magnetic field

The secondary magnetic field is a function of a number of factors which include the conductivity of the ground, the frequency at which the instrument is operating as well as the spacing between the transmitter and receiver coils (McNeill 1980). The measured quantity of the instrument which is the ratio of the secondary magnetic field to the primary magnetic field are related to the abovementioned factors in free space through Equation 1

$$\left(\frac{B_s}{B_p}\right)_H = 2[1 - \frac{3}{(\gamma s)^2} + [3 + 3\gamma s + (\gamma s)^2]\frac{e^{-\gamma s}}{(\gamma s)^2} \quad (1)$$

where $\gamma = \sqrt{i\omega\mu_0\sigma}$, $\omega = 2\pi f$ is the angular frequency, f is the frequency in Hz, σ is the ECa in S/m, μ_0 is the permeability of free space, B_s is the secondary magnetic field at the receiver coil, B_p is the primary magnetic field at the receiver coil, s is the intercoil spacing in m, $i = \sqrt{-1}$ and H indicates horizontal dipole configuration. Skin depth is defined as the half space distance through which a propagated wave has travelled when the amplitude is 1/e of that of the surface (Singh and Mogi 2003). The skin depth is computed using Equation 2

$$\delta = \sqrt{\frac{2}{\omega\mu_0\sigma}} = \frac{\sqrt{2i}}{\gamma} \quad (2)$$

where all variables have previously been defined. Rewriting Equation 2 and multiplying by the coil spacing gives

$$\gamma s = \sqrt{2i}\,\frac{s}{\delta}\ . \tag{3}$$

The ratio $\frac{s}{\delta}$ is defined as the induction number, B, and is equal to the coil spacing divided by the skin depth. The induction number is given by

$$\gamma s = \sqrt{2i}B\ . \tag{4}$$

If γs is exceedingly small than 1, then equation 1 which is the ratio of secondary magnetic field to the primary magnetic field reduces to

$$\frac{B_s}{B_p} \cong \frac{iB^2}{2} = \frac{i\omega\mu_0\sigma s^2}{4}\ . \tag{5}$$

If B is smaller than unity, the coil spacing should be smaller than the skin depth which gives

$$\omega \ll \frac{2}{\mu_0\sigma s^2} \tag{6}$$

and thus, the apparent electrical conductivity is given by

$$\sigma_a = \frac{4}{\omega\mu_0 s^2}\left[\frac{B_s}{B_p}\right] \tag{7}$$

It is assumed that the current loop generated below the surface is independent of any other soil factors which helps in understanding the integrated response of the surface measurement of EMI. The sensitivity functions, ϕ^H, of the EMI sensor with the depth from the soil surface is given by

$$\phi^H(z) = 2 - \frac{4z}{\sqrt{4z^2+1}} \tag{8}$$

where z is the depth in cm.

3.2 GEM-2 Sensor

The GEM-2 multifrequency EMI sensor consists of a transmitter coil, a buckling coil and a receiver coil (Won et al. 1996). The transmitter coil and the receiver coil have a coil separation distance of about 1.66m. The bucking coil removes the primary field transmitted from the transmitter coil in the receiver coil. The frequencies applied are converted into digital bit stream which is then used to construct the desired waveform. The pulse width modulation technique is used to construct the arbitrary waveform from the digital bitstream. The GEM-2 sensor operates in both the horizontal coplanar (HCP) and the vertical coplanar (VCP) data mode as shown in Figure 3

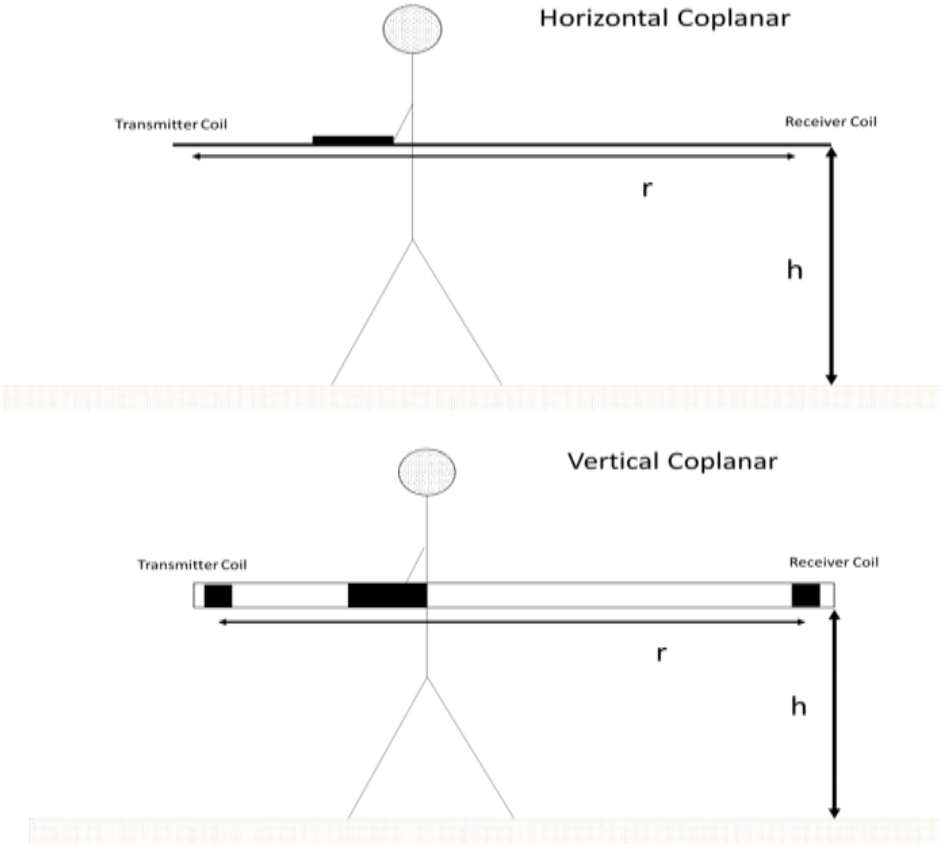

Figure 3-3: Horizontal and Vertical coplanar coil configuration

The GEM-2 sensor can be operated from 30 Hz to 93 KHz and has the capability to collect data points at the rate of 10,000 data points per acre per hour. Since the coil spacing between the

transmitter and the receiver coil is fixed, the transmitter frequency is changed for different depths. This is termed as frequency sounding. In phase and quadrature data is derived from the GEM-2 sensor which is converted into part per million and is defined as

$$ppm = 10^6 * \frac{secondary\ magnetic\ field\ at\ receiver\ coil}{primary\ magnetic\ field\ at\ receiver\ coil} \quad (9)$$

The in-phase and quadrature ppm data can be used to derive information about our target by inverting these data. The ECa, which is the electrical conductivity imagining the surfaced below the sensor is represented by a homogenous and isotropic half-space, can be derived from the inversion of these in-phase and quadrature ppm data. The secondary field normalized against the primary field is termed as the mutual coupling ratio and is defined for the HCP and VCP configuration as equation 10 and equation 11, respectively

$$Q = \frac{B_s}{B_p} - 1 = -r^3 \int_0^\infty \lambda^2 R(\lambda) J_0 \lambda r e^{-2\lambda} d\lambda \quad (10)$$

$$Q = \frac{B_s}{B_p} - 1 = -r^2 \int_0^\infty \lambda R(\lambda) J_1 \lambda r e^{-2\lambda h} d\lambda \quad (11)$$

where R is the Kernel function corresponding to a uniform half space and is defined in Equation 12

$$R(\lambda) = \frac{\lambda - \sqrt{\lambda^2 + i2\pi f\mu\sigma}}{\lambda - \sqrt{\lambda^2 + i2\pi f\mu\sigma}} \quad (12)$$

here B_s is the secondary field at receiver coil, B_p is the primary field at receiver coil, r is the coil separation, h is the sensor height, J_0 is the zeroth order Bessel Function, J_1 is the first order Bessel Function, f is the transmitter frequency in Hertz, μ is the magnetic susceptibility, σ is the earth conductivity.

The zeroth order and the first order Bessel function as defined above are the Bessel function of the first kind and is generally given by

$$J_\alpha\,(x) = \sum_{m=0}^{\infty} \frac{-1^m}{m!\,\Gamma(m+\alpha+1)} \left(\frac{x}{2}\right)^{2m+\alpha} \tag{13}$$

α is the order if the Bessel Function and Γ(x) is the gamma function which is defined as

$$\Gamma(m) = (m-1)! \tag{14}$$

Equations 10 and 11 can be solved by linear digital filter method with known filter coefficients along with the standard form of Bessel Function which is beyond the scope of this thesis.

3.3 Time Domain Reflectometry (TDR)

A Field Scout TDR 350 soil moisture meter was used to determine the VWC in soil. A TDR sensor works by measuring the propagating time of electromagnetic waves. The electromagnetic waves propagate through a coaxial cable to a metal probe. The impedance difference between the coaxial cable and the probe reflects a part of the electromagnetic wave while the remainder of the wave travels through the probe to its end where it is reflected (Noborio 2001). The round-trip time is measured and is described as

$$t = \frac{2L\kappa^{0.5}}{c} \tag{15}$$

where t is the round trip time in seconds, L is the TDR probe length in meters, κ is the dielectric constant, c is the velocity of electromagnetic wave in free space ($3*10^{-8}$ m/s). Rearranging Equation 15 gives

$$\kappa = \left(\frac{ct}{2L}\right)^2 \tag{16}$$

where all variables have previously been defined. The VWC, θ, is then calculated using the Topps equation (Topp et al. 1980) which is

$$\theta = -5.3 * 10^{-2} + 2.92 * 10^{-2}\kappa - 5.5 * 10^{-4}\kappa^2 + 4.3 * 10^{-6}\kappa^3 \quad (17)$$

where all variables have previously been defined. Jacobsen and Schjønning (1993) determined that the relationship between soil moisture content and dielectric constant is almost linear. Furthermore, the dielectric constant is also influenced weakly by soil texture, bulk density, clay content and the organic matter.

3.4 Richard's Equation for flow of water

The HYDRUS model which was used in the current research measures flow of water by solving the Richards equation for unsaturated flow (Richards 1931). The Richards equation is based on Darcy's Law which describes the flow of fluid through a porous medium and was developed for saturated flow. The continuity equation for one dimensional unsteady unsaturated flow in a porous medium is given by

$$\frac{\partial \theta}{\partial t} = -\frac{\partial q}{\partial z} \quad (18)$$

where q is the Darcy flux, θ is the VWC. From Darcy's Law,

$$q = -K(\theta)\frac{\partial h}{\partial z} \quad (19)$$

where $K(\theta)$ is the hydraulic conductivity, $\frac{\partial h}{\partial z}$ is the head loss per unit length, q is the Darcy flux. The total head which is given by

$$h = \psi + z \quad (20)$$

Here h is the total head, ψ is the matric head and z is the elevation above a vertical datum.

Darcy's Law can thus be expressed by

$$q = -K(\theta)\frac{\partial(\psi + z)}{\partial z} \quad (21)$$

Where where q is the Darcy flux, θ is the VWC and $K(\theta)$ is the hydraulic conductivity. Substituting the Darcy's law into the continuity equation we get

$$\frac{\partial \theta}{\partial t} = -\frac{\partial}{\partial z}[K\left(\frac{\partial \psi}{\partial z} + \frac{\partial z}{\partial z}\right)] \tag{22}$$

Which gives us

$$\frac{\partial \theta}{\partial t} = -\frac{\partial}{\partial z}[K\left(\frac{\partial \psi}{\partial z} + 1\right)] \tag{23}$$

Equation 23 is the one-dimensional form of the Richards equation which is used for modeling water flow though unsaturated medium in HYDRUS models.

3.5 van- Genuchten single porosity model

The van Genuchten-Mualem single porosity model was selected as the Hydraulic model in HYDRUS. The van Genuchten-Mualem model used the following equation to calculate soil hydraulic properties

$$\theta = \left\{\theta_r + \frac{\theta_s - \theta_r}{[1 + |\alpha h|^n]^m}\right\} \; when \; h < 0 \tag{24}$$

$$\theta = \theta_s \; when \; h \geq 0 \tag{25}$$

$$K(h) = KsS_e^l\left[1 - \left(1 - S_e^{\frac{1}{m}}\right)^m\right]^2 \tag{26}$$

$$m = 1 - \frac{1}{n} \; for \; n > 1 \tag{27}$$

where h is the hydraulic head in cm, θ_r is the residual water content, θ_s is the saturated water content, θ is the water content, α is the inverse of air entry value, n is the pore size distribution index, m is a coefficient related to pore size distribution index, K_s is the saturated hydraulic conductivity in cm/day, S_e is effective water content, l is pore connectivity.

Chapter 4 - Methodology

A six-step methodology was used for this research. In the first step, the frequency corresponding to a depth of 50cm was identified using ground truthing. Secondly, the TDR sensor was calibrated to the site to obtain accurate values of VWC. Thirdly, ECa values were obtained using the EMI surveys at the same time volumetric water content was obtained using the TDR sensor. Once the ECa and VWC data were obtained, different relationship models were tested with ECa as the independent variable and VWC as the dependent variable. Finally, a HYDRUS-1D model was developed using atmospheric boundary condition at the top and the free flow drainage boundary condition at the bottom and the VWC from EMI based model as the initial condition. The water content at different days at a depth of 50cm was obtained and compared with the VWC obtained from the EMI based volumetric water content model. Figure 5 outlines the six-step methodology used in this research.

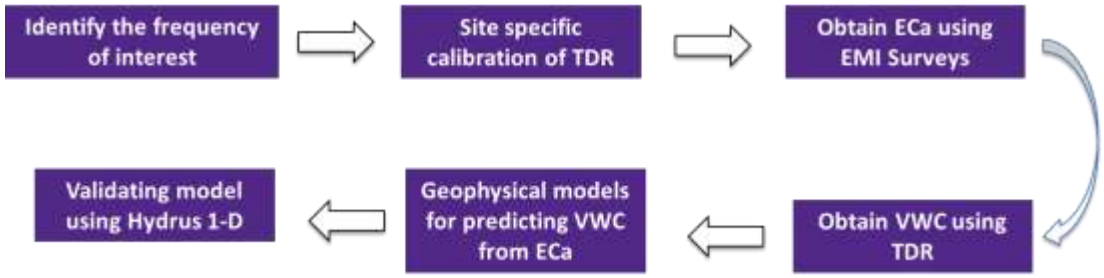

Figure 4-1: Methodology used in this study

4.1 Survey Site

The research was carried out in the Kansas State University Agronomy Research Farm located in Ashland Bottoms, which is towards the south of Manhattan, KS. Data were collected throughout different months in 2021. The total precipitation in Manhattan during 2021 was 743.38mm. The minimum temperature and maximum temperature in 2021 were -30.2 ºC and 39.4 ºC, respectively. The Ashland Bottom farm is used for farming throughout the year with

wheat being the major crop. The soil texture in the farm is loamy silt according to USDA classification while USCS classification classifies it as silt with high plasticity (MH). The specific gravity of the soil sample is 2.67. The map of the site area can be found in Figure 6.

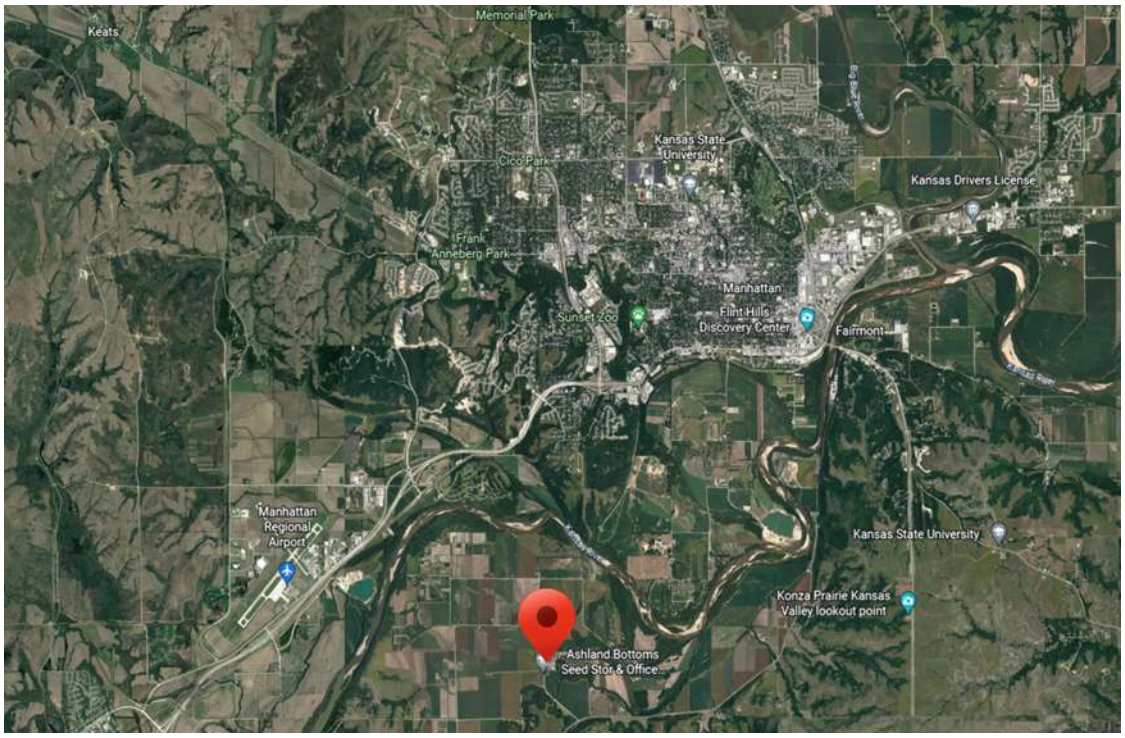

Figure 4-2: The location of the research field used in this research

4.2 EMI Survey

EMI surveys were conducted using the GEM-2 multifrequency EMI sensor. Initially, frequencies from 540 Hz to 93 KHz were used to collect the ECa. Both VCP and HCP coil configurations were evaluated, however, later only the HCP coil configuration was used. This is because the VCP coil configuration has more noise than the HCP soil configuration. To prevent instrumental drift, it was recommended that the sensor be warmed up for a period of 30 minutes before measurements were taken. Although the GEM-2 sensor can transmit up to fifteen frequencies simultaneously, it is recommended that only three to five frequencies be used at once. This is due to the fact that the total energy is shared by each of the frequencies. The more

frequencies used; the less energy is available for each frequency which in turn degrades the signal to noise ratio. Hence a maximum of five frequencies were used for each survey. The sensor was carried at a height of 1m from the ground. Maximum effort was given to ensure that the same speed of walking was used to ensure that no datapoint was aggregated due to lower walking pace, as the GEM-2 sensor collected data every 1/30th of a second.

The GEM-2 sensor provides in phase and quadrature data at the end of the survey which needs to be inverted to determine the apparent electrical conductivities. WinGEM2, the default software from Geophex was used to convert the in phase and quadrature data into apparent electrical conductivities. It is commonly recommended that raw ECa data should be converted to a standard soil temperature of 25°C. The ratio model (Ma et al. 2011) was used for this research,

$$ECa_{25} = \frac{ECa(t)}{1 + \delta(T - 25)} \tag{28}$$

where ECa_{25} is the ECa at common soil temperature i.e.,25°C; $ECa(t)$ is the ECa measured at site, δ the temperature slope correction which is 0.0191°C^{-1} and T is the measured soil temperature. Data were collected from April 2021 to December 2021.

4.3 VWC Data

Point based measurements of VWC were obtained using a time domain reflectometer (TDR) sensor, which is a probe-based sensor and measures reflections of velocity pulses along a conductor. Two probes of 10.16 cm (4 in) and 20.32 cm(8 in) length are embedded in the soil through which a rapid voltage pulse is propagated through the soil and the resulting travel time of the propagated pulse is measured. Propagation velocity, which can be determined from travel time of the propagated pulse, is related to the dielectric constant which is the ratio of permittivity of a substance to the permittivity of free space. Topp et al. (1980) first formulated the relationship

between dielectric constant and VWC, which is used to measure VWC from a TDR sensor (see Equation 17). The VWC was collected using 20.32 cm TDR sensor probes along with the EMI survey. VWC was calculated at a depth of 50 cm depth by digging up to 30 cm and then using the 20 cm probe to collect data from the 50 cm probe. A total of 70 samples of VWC at a depth of 50cm were recorded throughout the year. Emphasis was given to ensure that the VWC had a wide range of values so that both the dry as well as wet characteristics were accounted for. The TDR sensor needs to be calibrated to the site in order to collect accurate data. The steps used for the site calibration of the TDR sensor to collect VWC is explained in the next section

4.3.1 Site specific calibration of TDR sensor

The following steps were used for calibrating the TDR sensor:

1. Four undisturbed soil cores were collected directly from the field. Since the volume of the cores are known, the bulk density can be measured and then the cores dried in the oven. After 24 hours, remove the soil cores and measure the dry mass. Calculate the dry density by diving the dry mass by the volume. Take the average of the dry density for the four cores as the dry density of the soil at the field.
2. Sieve a grab soil sample through a 2 mm sieve to remove the soil structure, then oven dry the sample for 24 hours.
3. Measure the mass of the dry soil. Then, determine the volume of water needed to reach the desired VWC. The Gravimetric water content, GWC, can thus be calculated as

$$GWC = \frac{\theta * \rho_w}{\rho_d} \tag{29}$$

Where GWC is the gravimetric water content, $\theta$is the volumetric water content, $\rho_d$is the bulk density and ρ_w is the density of water

4. Now determine the amount of water that needs to be added this can be calculated using the equations below

$$GWC = \frac{Mass\ of\ water}{Mass\ of\ soil} \quad (30)$$

   Once the amount of water is determined, use a sprayer to spray the water uniformly throughout the soil sample. Keep on spraying and mixing till the determined amount of water has been sprayed. Ensure that the water is uniformly sprayed in the whole sample.

5. Compact the soil in a cylindrical PVC pipe. Determine the volume of the cylinder in which the soil is to be compacted. Now calculate the amount of soil that needs to be contacted by multiplying the volume of the cylinder with the bulk density measured at step 1. Ensure that the soil is compacted perfectly so that the desired bulk density is maintained.
6. Now using the TDR sensor measure the VWC. Ensure that the TDR is calibrated to free air and distilled water so as to remove any uncertainty. Record the VWC measured by the TDR.
7. Take a subsample of the soil core from the area at which the tip of the TDR sensor reached to measure the VWC. Record the wet mass and the put the subsample of the soil core in the oven for 24 hours.
8. After 24 hours, measure the dry mass. Calculate the VWC by multiplying the gravimetric water content with the dry density recorded in step 1. This is the lab measured volumetric water content.
9. Repeat steps 1-8 for a range of VWC and record the TDR and lab measured volumetric water content.

10. Develop a regression model between the lab measured VWC the TDR measured VWC by keeping the TDR VWC as the independent variable and the lab VWC as the dependent variable. The developed equation can be used to determine the actual value of VWC from the lab value of VWC. Ensure that the model performance metrics are withing an acceptable range.

The TDR sensor was calibrated to the site used in this research based on the above methodology. The correlation coefficient was found to be 0.997, indicating a remarkably high level of correlation between the actual value and the TDR value. Figure 7 shows the site-specific calibration between the lab measured VWC and the VWC obtained from TDR sensor.

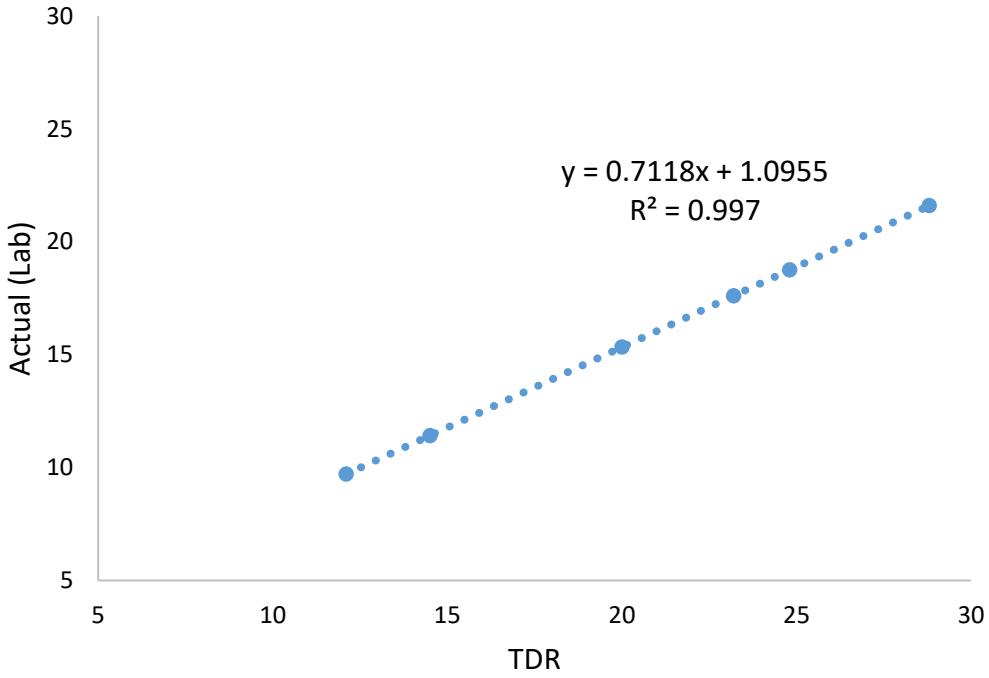

Figure 4-3: Site specific calibration for the TDR sensor

4.4 Identifying the depth of investigation

One of the biggest challenges of using a multifrequency EMI sensor is the difficulty in obtaining the depth at which the signals correspond. The depth of investigation has been said to be closely related to the skin depth. The skin depth is defined as the depth at which the current density reaches 1/e or 37% of its value of that of the surface. The skin depth is a function of the medium conductivity, magnetic permeability and the angular frequency of the wave. The skin depth is calculated using equation 31

$$\delta = \sqrt{\frac{2}{\sigma\mu\omega}} \tag{31}$$

where $\omega = 2\pi f$ is the angular frequency of the wave in degrees per sencond, σ is the conductivity of the medium in siemens, μ is the magnetic permeability, δ is the skin depth in m.

In order to understand the true depth of investigation, the true conductivity needs to be known. However, the GEM-2 EMI sensor cannot be used to determine the true conductivity. The GEM-2 sensor can be used to determine the ECa which is the electrical conductivity representing the true bulk volume assuming soil electrical conductivity is homogenous. This ECa in turn gives an apparent depth of investigation, which is not useful to the problem in this research. A number of inversion models have been developed over years (e.g., Elwaseif et al. 2017; Liu et al. 2022), no models have verification from Geophex. There are numerous other methods used by researchers to understand the depth of investigation (Brosten et al. 2011). The depth of penetration method developed by McNeill (1980) and the depth of exploration method (Callegary et al. 2007) used Low Induction Number (LIN) approximation method to determine the depth of investigation while correlation loss method (Singha et al. 2007) used 90% correlation loss to estimate the depth of investigation.

Since the ECa is the integral of the electrical conductivity for a bulk volume assuming a homogenous space, both the TDR sensor and EMI sensor were used to determine the depth of investigation in this study. The TDR sensor is also an EMI sensor which can be used to measure the ECa of small volume of soil. Since the bulk volume is small, the ECa measured through the TDR sensos is nearly that of the true value of electrical conductivity. To determine the depth of investigation for the GEM-2 sensor the following methodology was adopted.

1. The ECa from 25cm to 75 cm deep was computed at three different points- the starts of the test line, a middle point and the end line. The ECa was computed for a difference in depth of 5 cm, i.e., a point every 5 cm was recorder along with the ECa.
2. The depth weighted average of the electrical conductivity for the desired depth is calculated as

$$Weighted\ average\ ECa = \frac{\sum Depth * ECa}{\sum Depth} \quad (32)$$

   Where Weighted average ECa is the ECa at the desired depth when ECa from depths of 25cm above and below are taken into account. Depth is the particular depth for which the ECa has been measured using a TDR sensor while ECa is the apparent electrical conductivity measured at that depth using TDR sensor
3. EMI surveys using the GEM-2 multifrequency EMI sensor for different frequencies were taken and plotted. Since our intended depth of investigation is very close to the surface, we know that higher frequencies will reach shorted depths while smaller frequencies will reach higher depth. Hence emphasis was given on very high frequencies.
4. The apparent electrical conductivities obtained from the GEM-2 multifrequency EMI sensor for different frequencies were plotted along with the depth weighted average

electrical conductivity values obtained from the TDR sensor. The trends and values were matched and the frequency corresponding to the desired depth was selected.

Figure 4-4 depicts that the desired frequency for 50 cm depth corresponded to a frequency of 90 kHz. Hence, for a depth of 50cm the frequency range was 90 kHz in this research.

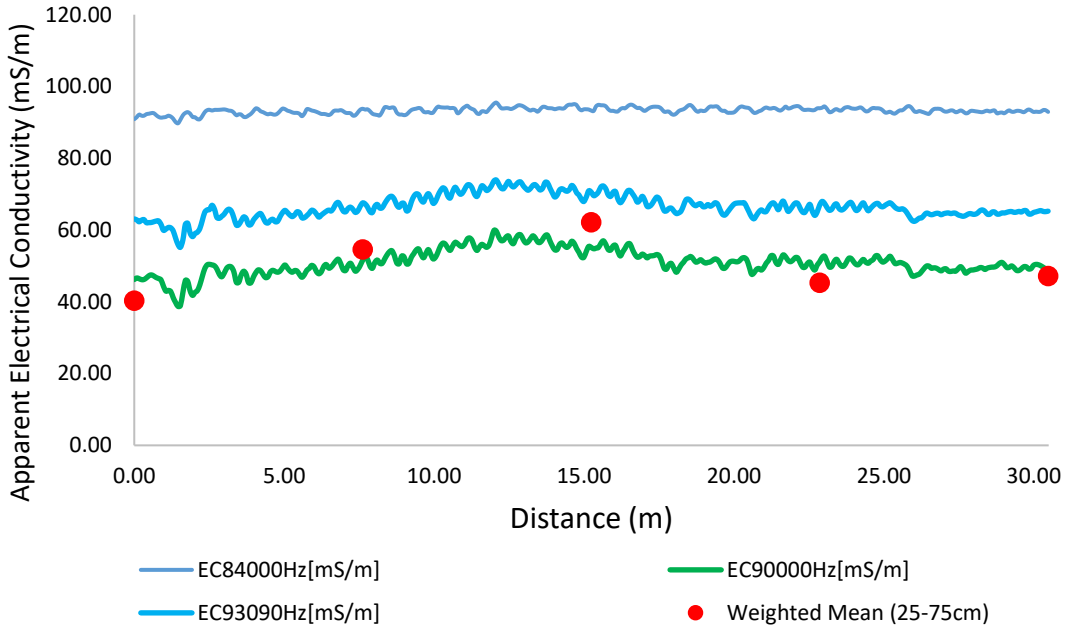

Figure 4-4: Selection of desired frequency of GEM-2 EMI sensor from depth weighted average ECa obtained using the TDR sensor

4.5 HYDRUS 1D model

A HYDRUS 1D model was created with the EMI based volumetric water content model. As described in the literature review, HYDRUS 1D models are based on the Richards equation and can be used to simulate flow of water and solutes though saturated, partially saturated and unsaturated porous media. The water flow into the soil as well as out of the soil is controlled by applying boundary conditions at both the upper and lower end. A number of built in upper and lower boundary conditions can be selected based on the requirement of the model. Unsaturated flow can be simulated using the van Genuchten-Mualem (1980) porosity models for hydraulic

flow. Additionally, atmospheric boundary conditions including precipitation and evapotranspiration can be added. HYDRUS 1D 4.17 which is the lates version of HYDRUS 1D has been used in our current research.

4.5.1 Model Settings and Input

A forward solution of water flow model was selected as the main process. The unit for the model was taken as cm. The soil was assumed to be a single homogenous soil with one layer. Vertical modeling was selected, and the depth of soil profile was taken as 50cm. The time units selected was days with the whole model being setup for a total of 154 days. The 154 days was the number of days from the first day EMI data were collected to the last day. Other values were kept as default. The print times were setup to print values of the days for which we had EMI Data. A total of 8 days were selected for print time. Other setup was kept as default HYDRUS had a built in neural network prediction model called as Rosetta Lite v1.1 which can be used to predict soil hydraulic properties based on the soil properties when measurements are not possible. Textural classes, or percentage of sand, silt, and clay, can be used as the input. A sieve and hydrometer analysis were done to find out the percentage of sand, silt, and clay. These were used as an input in Rosetta Lite v1.1 to predict the soil hydraulic parameters which was then used to develop the soil water retention curve. Table 1 shows the soil hydraulic properties used in this research. **Error! Reference source not found.** Figure 9 depicts the soil water retention curve generated from the soil hydraulic properties using the van Genuchten Single porosity model.

Table 1: Soil Hydraulic Properties obtained from the Rosetta module of Hydrus

θ_r	θ_s	α	n	K_s	l
0.034	0.46	0.016	1.37	18.41	0.5

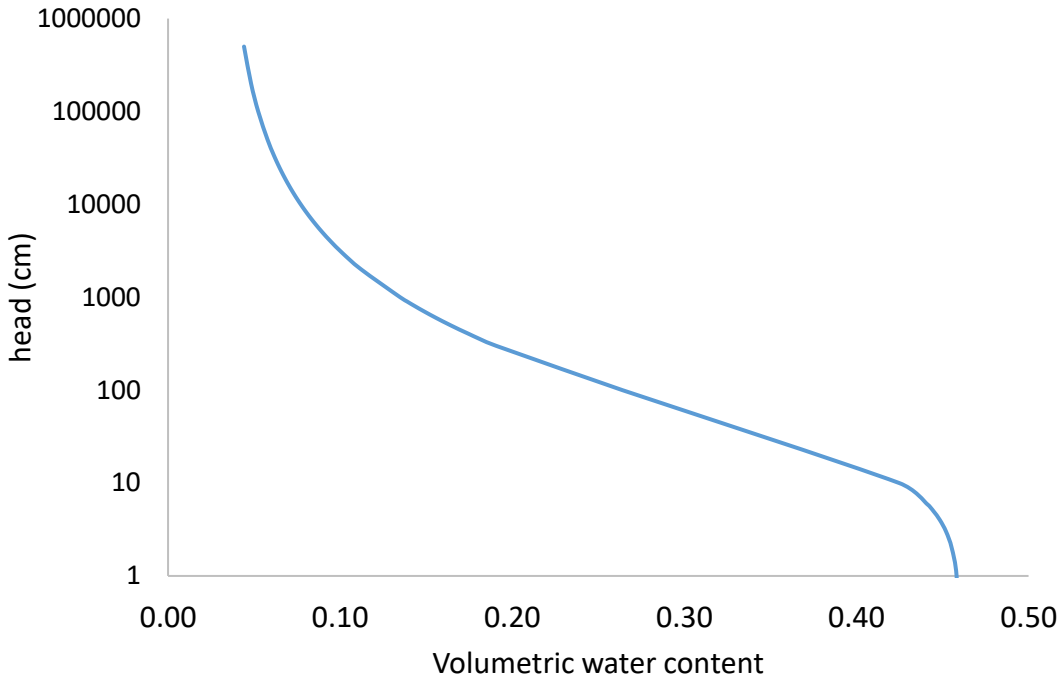

Figure 4-5: Soil water retention curve generated from the soil hydraulic properties

The boundary conditions are one of the most important parts of the model. HYDRUS 1D has a number of inbuilt boundary conditions that need to be used for simulation. The upper boundary condition that can be applied in HYDRUS 1D models include constant pressure head, constant flux, atmospheric boundary condition with surface layer, atmospheric boundary condition with surface run off, variable pressure head/flux, and triggered irrigation. The lower end boundary conditions include constant pressure head, content flux, variable pressure head, variable flux, free drainage, deep drainage, seepage face and horizontal drains.

Table 2 lists the boundary conditions used in this research. These were the most idealized boundary condition which were similar to what is expected in real life. This is because the field does not see any ponding in case of high rainfall and secondly the groundwater level was nowhere near the top 50cm.

Table 2: Upper and lower boundary conditions used in our model

Location	**Boundary Condition**

Top Layer	Atmospheric BC with surface Runoff
Bottom at 50cm depth	Free Drainage

The daily precipitation data were obtained from the KSU Mesonet (Kansas Mesonet). Daily precipitation data from 1st of July 2021 to 01st December 2021 were used in the model. Data from Ashland bottom station, which is located close to the research site, were used. During this period, the total amount of precipitation recorded was 387.04 mm with maximum rainfall occurring on 15th July which had a precipitation of 98.04mm. The minimum precipitation was 0 for a 120 days. The evapotranspiration was calculated using the single crop coefficient method The potential evapotranspiration values were obtained from the Kansas Mesonet. Since the trial line was a wheat field and most of the data collected were from a line of no crop, the Kc initial value was takes as 0.3 to compute the evapotranspiration values. The Kc initial value is the crop coefficient value at the start of the season when there is no crop.

4.6 Mean Absolute Error

Mean absolute error was used to assess the model performance. The mean absolute error can be defined as the mean measure of error between paired observations. Mean absolute error is an important parameter in analyzing prediction model performance (Willmott & Matsuura, 2005) and hence was used as a criterion in model selection. This is because mean absolute error explains the boundary of error. In other words, mean absolute error gives an idea of how different the predicted values can differ from real values. R^2 on the other hand gives us an indication on how our outcomes are replicated by the model.

Mean absolute error was computed using equation

$$MAE = \frac{\sum_{i=1}^{n} |y_i - x_i|}{n} \quad (33)$$

where y_i is the predicted value of the i^{th} term, x_i is the true value for the i^{th} term, and n is the total number of data points.

4.7 Regression models and Waxman and Smits model

Regression analysis was done to develop prediction models for predicting volumetric content from the apparent electrical conductivity. Regression analysis finds the line or curve which closely fits the data. Five different types of regression analysis were done: linear, logarithmic, exponential, power, and polynomial regression. Figures A-1 to A-5 depict the different regression models for this thesis. A comparison of a linear, logarithmic, exponential, power, polynomial and Waxman and Smits model was conducted to determine the best model for predicting VWC from field based ECa data.

The Waxman and Smits model is one of the more popular models used in geosciences. It was derived from Archie's Law (Archie 1942)which is an empirical relationship between the bulk electrical conductivity, porosity, and the degree of saturation. The Waxman and Smits model is

$$\theta = \left[\frac{(E_{ca}) - b}{a}\right]^{\frac{1}{n}} \quad (34)$$

where b, a, and n are the fitting parameters of the model and the remaining variables have previously been defined. Additionally, relative and absolute differences in electrical conductivity and VWC were analyzed to further explore the correlations gleaned from the original models.

Chapter 5 - Results

The results obtained from different analysis are presented in the next few subsections

5.1 Modeling the Corrected Apparent Electrical conductivity against the volumetric water content

The correlation between VWC and ECa of a silt loam soil was analyzed to facilitate the development of a predictive model for estimating VWC based upon the response of EMI surveys. ECa data were obtained with the GEM-2 multifrequency electromagnetic induction (EMI) sensor. Six models were compared to determine the best model for predicting VWC from field based ECa data. The functional form of the regression models can be found in appendix A. Additionally, relative, and absolute differences in electrical conductivity and VWC were analyzed to further explore the correlations gleaned from the original models.

The ECa and the VWC were obtained between March 2021 to November 2021 across different soil conditions. VWC values ranged from 25% - 37% while ECa values ranged from 37mS/m to 68 mS/m. Data obtained from the field were fit to linear, logarithmic, power, exponential and polynomial regression models to identify the nature of the relationship between ECa and VWC. The results of the linear regression model for 70 measured values of the independent and the dependent variable are shown in Figure 10 along with the frequency distribution of errors. The gaussian like distribution (Schmidt and Finan 2018) of error magnitudes in Figure 11 supports the use of a linear regression model.

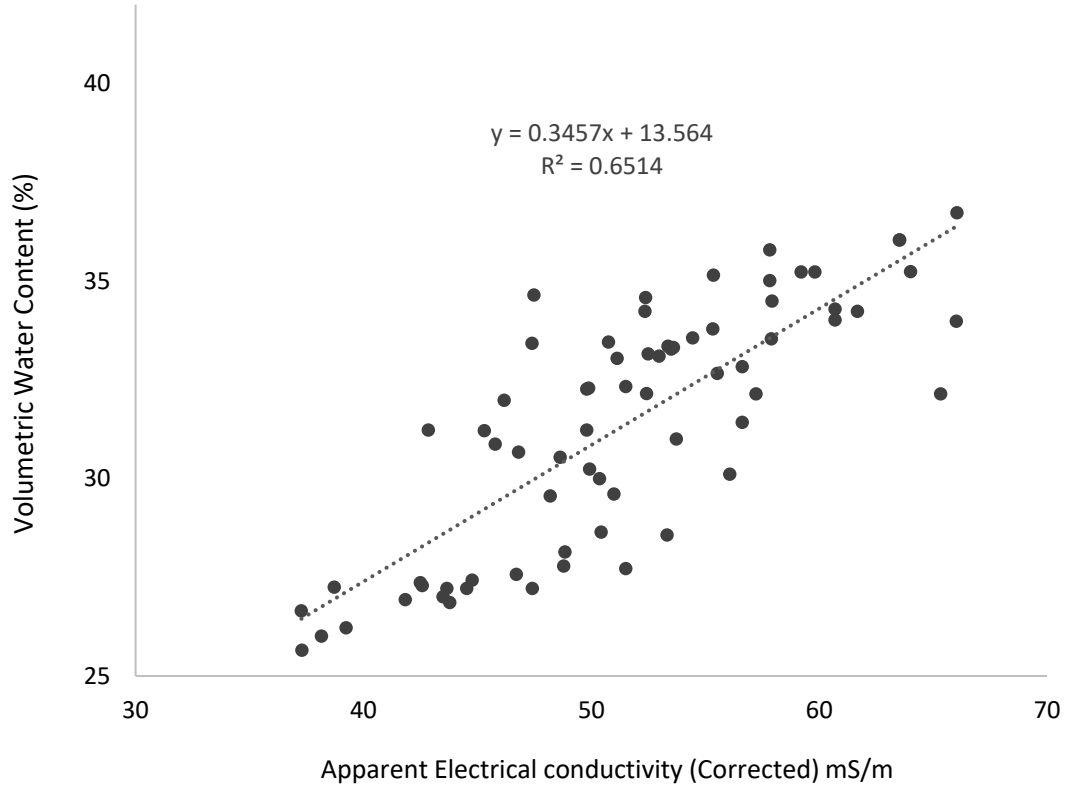

Figure 5-1: Linear fit model between apparent electrical conductivity and VWC

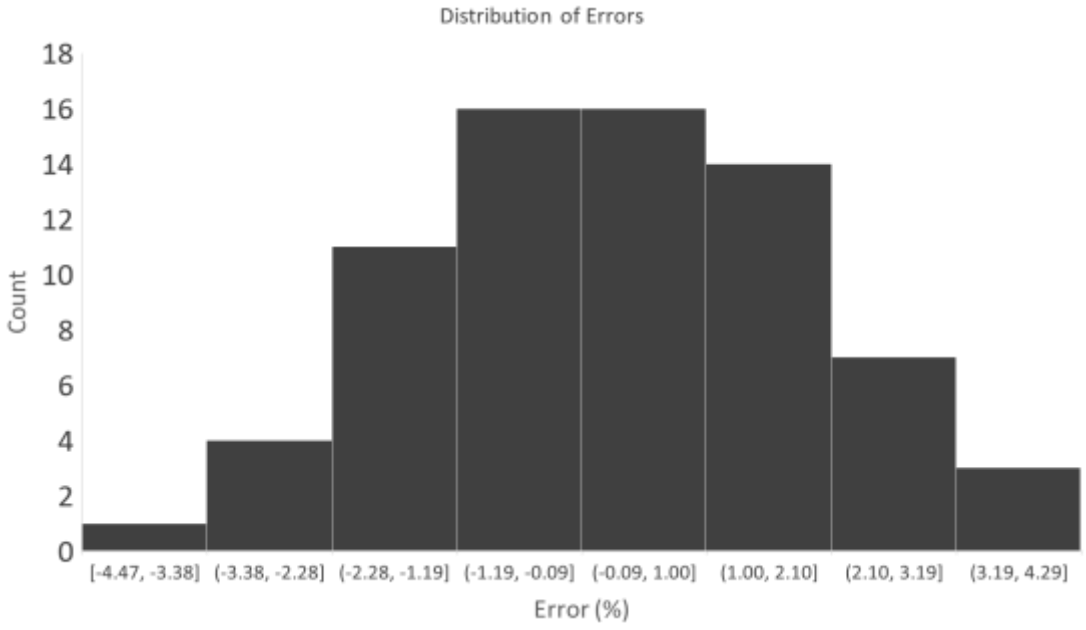

Figure 5-2: Distribution of Errors for the linear model

The computed R^2 and the mean absolute error for the linear, Logarithmic, Power, Exponential, 2nd order polynomial and Waxman and smith model is shown in Table 3.

Table 3: R^2 and MAE for the different curve fitting model analyzed

Model	R^2	MAE (%)
Linear	0.65	1.49
Logarithmic	0.66	1.46
Power	0.67	1.47
Exponential	0.65	1.51
2nd Order Polynomial	0.67	1.45
Waxman and Smith		1.74

5.2 Relative Change in Apparent Electrical conductivity as well as volumetric water content

The relative change in ECa was plotted against the relative change in VWC for three different cases. Firstly, maximum values for both ECa and VWC were taken as the reference value. In the other two cases, the minimum and the average values were taken as the reference values. The relative change in conductivity was calculated using equation 35

$$\Delta \sigma_a = \sigma_{a_{ref}} - \sigma_a(t) \quad (35)$$

where $\Delta\sigma_a$ is the relative change in ECa, $\sigma_{a_{ref}}$is the reference value from which the ECa is calculated, $\sigma_a(t)$ is any value in the dataset. Figure 5-3 shows relative change with respect to the maximum value. Figure E-3 and Figure E-4 shows the other cases in which the relative change is taken with respect to the minimum and average value.

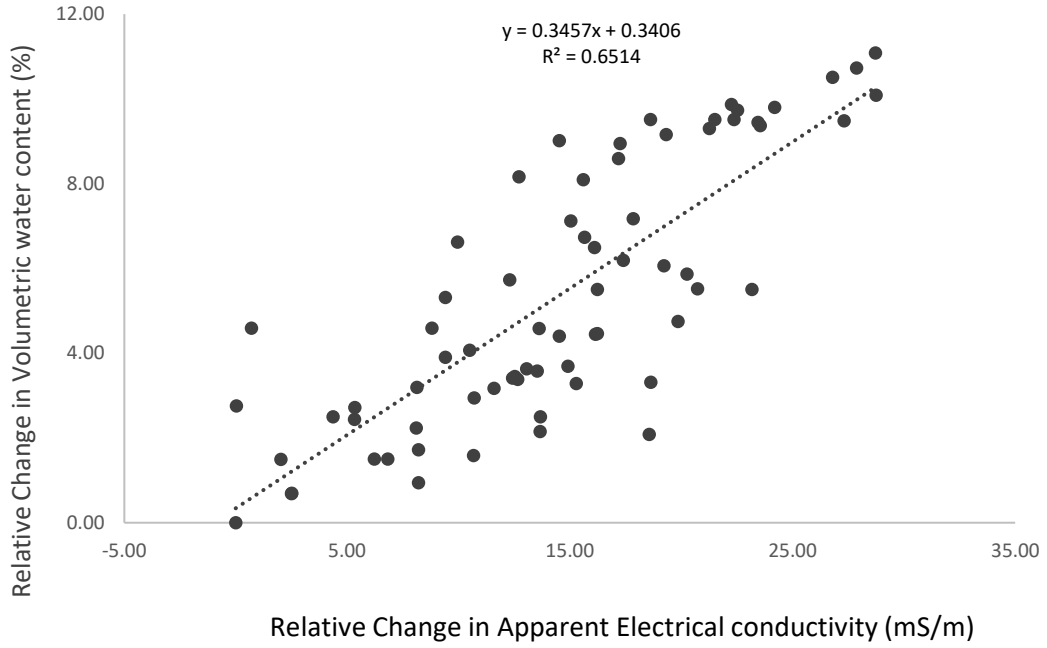

Figure 5-3: Linear model when relative change is taken with respect to the maximum value

No change is observed in the R^2 values for the three cases. The correlation coefficient has a value of 0.65 for all the three cases

5.3 Electrical conductivity modeled with the relative change in volumetric water content

The ECa was modelled against the relative change in VWC. This was done to determine how ECa is impacted for changes in VWC. Equation 1 was used to calculate the relative change in VWC. The relative change in VWC was then used as a dependent variable with the true ECa value used as the independent variable. Like previous models, the minimum, maximum and the average of the VWC were taken as the reference values three different cases. Figure 5-4 shows that when relative change in VWC is modelled against ECa, the slope changes to a negative value although the magnitude of the slope remains same. Figure 13 is the case when maximum value is

taken as the reference value, note that the region of maximum ECa has a relative change of zero. It can also be seen in Figure 13 that at lower VWC (below 27% VWC). the impact of VWC on ECa is weaker. When the minimum value is taken as reference value, the minimum ECa has zero relative change as is shown in Figure E-6 .

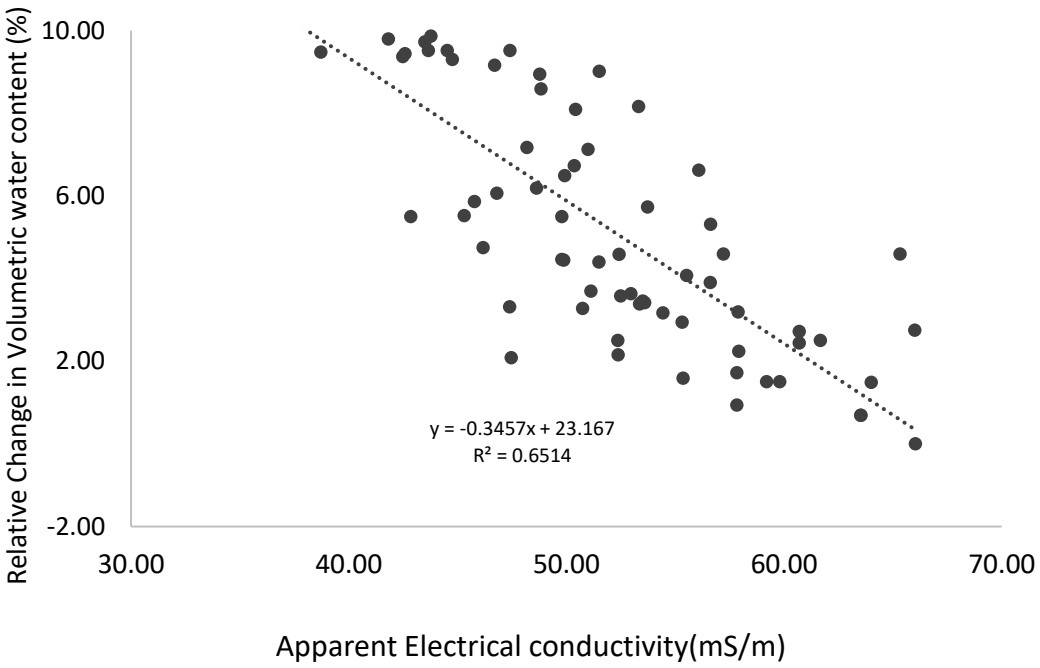

Figure 5-4: The relative change in VWC with respect to the maximum value is modelled against apparent electrical conductivity

5.4 Electrical conductivity modeled with the absolute changes

Absolute change in apparent electrical conductivity was modelled against the absolute change in VWC. The absolute change was determined with respect to a reference point. As previously done, three different reference points were selected, the maximum value, the minimum value and the average value for both dependent and independent variable. Two distinct types of models were analyzed. In the first case the absolute change in ECa was modelled against the

absolute change in VWC which is shown in Figure 14. In the second case, ECa was modelled against the absolute change in volumetric water content which is shown in Figure 15. The absolute change of ECa was computed using equation 36

$$|\Delta\, \sigma_a\,| = \left|\sigma_{a_{ref}} - \sigma_a\,(t)\right| \tag{36}$$

Where reference value is either the maximum, minimum or average of the dataset, true value is the electrical conductivity at the data point for which the absolute is to be calculated.

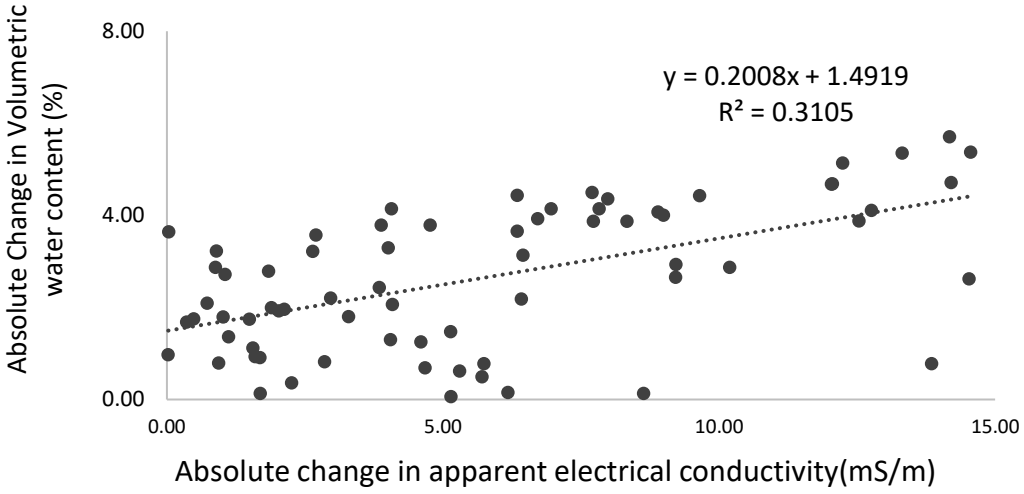

Figure 5-5: Absolute change taken with respect to the average value for both volumetric water content and apparent electrical conductivity is modelled

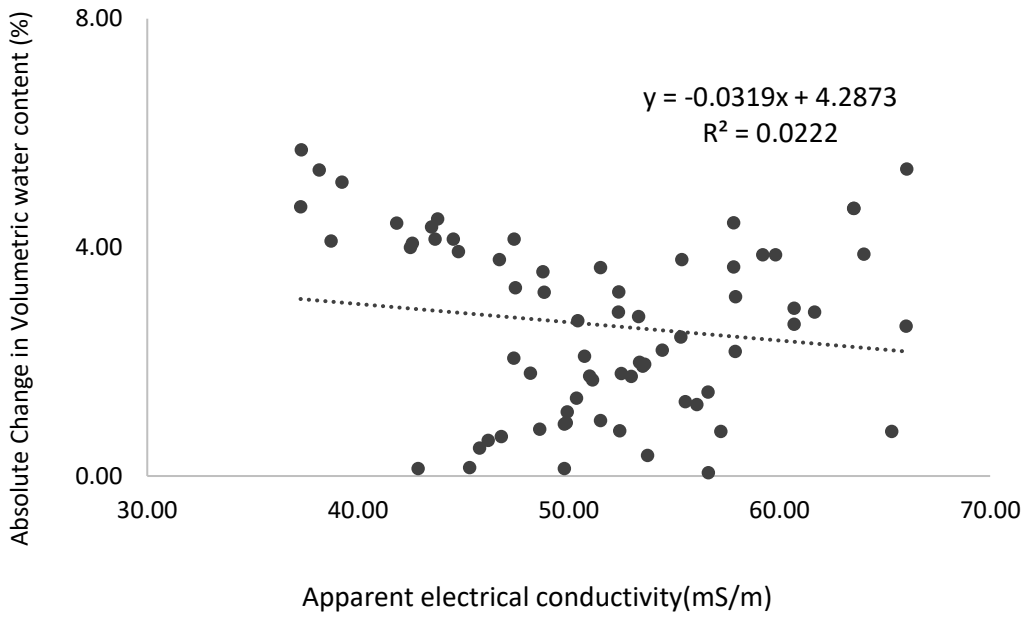

Figure 5-6: Absolute change in Volumetric water content with respect to the average value is modelled against apparent electrical conductivity

5.5 Lab Measured value as a Reference Point.

The next analysis used a known lab measurement of VWC as the reference point for VWC. The ECa obtained from the GEM-2 sensor at that point was taken as the reference point for ECa. Four different scenarios were modeled, one in which the relative difference of ECa was modeled against the relative change in VWC with respect to the lab measured volumetric water content (Figure 5-7). In the second scenario, ECa was modelled against the relative change in VWC with respect to the known point which can be found in Figure F-1. In the third and the fourth case, the absolute change was modelled instead of the relative change taken in the first two cases as shown in Figure F-7 and Figure F-8 respectively.

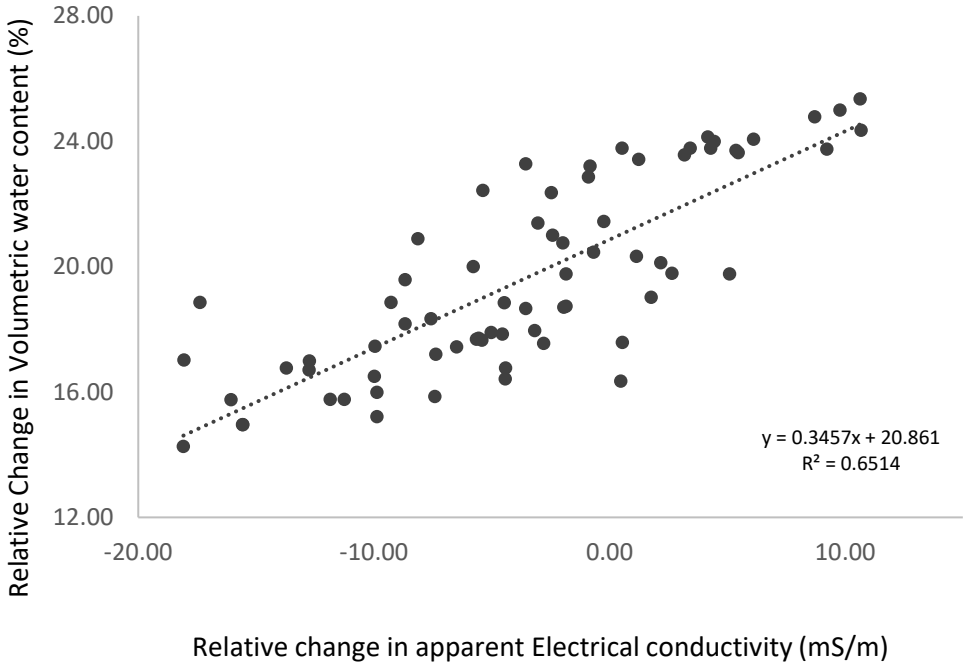

Figure 5-7: Relative change in volumetric water content with respect to a known lab value is modelled against relative change in apparent electrical conductivity of that known value

5.6 Model validation using train/test split and randomized validation

The ECa and VWC at numerous location and different time periods were divided into two different datasets, namely – training dataset and testing dataset. Approximately 80% of samples were taken from the dataset to develop a regression model (training model). Once the regression model was developed, independent variables from the test dataset were used to predict the dependent variable. The mean absolute error was calculated by finding the mean absolute difference between the original value and the predicted value. Figure 17 shows the training model developed using the training dataset.

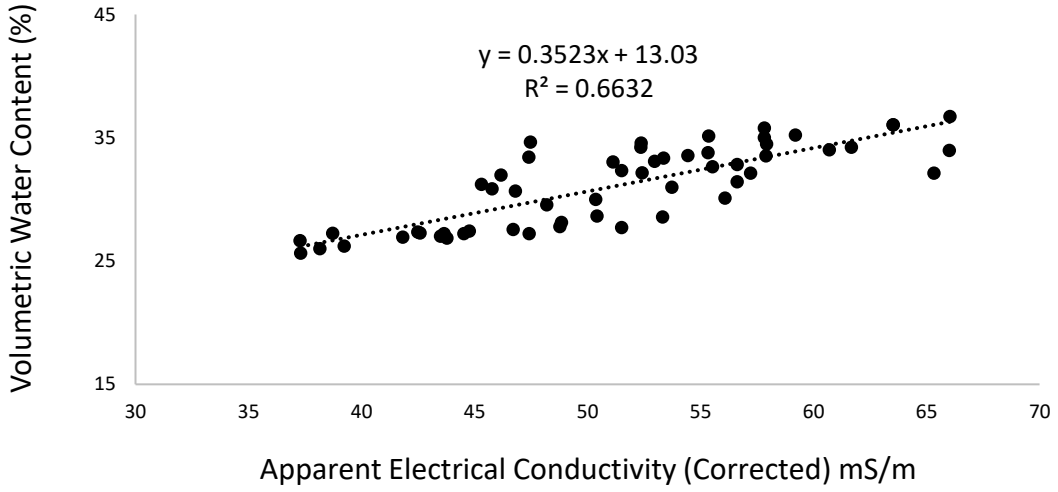

Figure 5-8: Linear model from the train dataset of the test/train split

ECa values from the test dataset were used as the input variable in the developed regression model to determine the accuracy of the regression model. Predicted values from regression model were then compared to that of original dataset. Mean absolute error was calculated and the actual and predicted values were plotted to show how predicted values differed from the original values. Figure 18 shows plot comparing the predicted values with original values. The mean absolute error in test dataset was 1.28% which was less than that in the training dataset where mean absolute error was 1.55%.

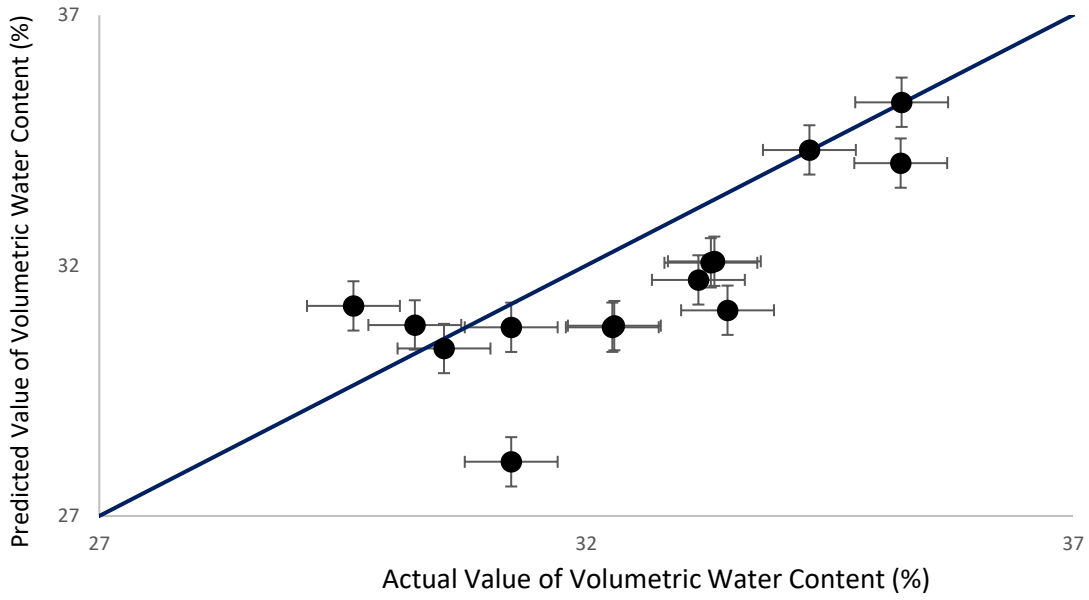

Figure 5-9: Predicted value for the test dataset obtained using the equation derived from the train dataset versus the original value for obtained from TDR

To ensure that the bias was similar across datasets, the dataset was randomized for testing and training four times in addition to the original dataset of training and testing. Mean absolute error was calculated for the four additional randomized datasets. A logarithmic regression model was also evaluated in a similar manner and randomized five times. Mean absolute error for each of the four randomized datasets along with the original data is reported in Table 4.

Table 4: Results from the Fivefold analysis for Test/Train split

Data	**Training data mean absolute error**	**Testing data mean absolute error**
Linear 1	1.55	1.28
Linear 2	1.50	1.47
Linear 3	1.49	1.63
Linear 4	1.31	2.17
Linear 5	1.50	1.52
Log 1	1.53	1.17
Log 2	1.47	1.43
Log 3	1.46	1.60
Log 4	1.28	2.11
Log 5	1.48	1.38

5.7 The significance of Mean Absolute Error

From the different models and the Fivefold analysis done, it can be seen that the mean absolute error stays within 1.17% in the best case and 2.17% in the worst case. That means at the worst end, the EMI based volumetric water content model may overestimate or underestimate the VWC by 2.11%. Soil water retention curve is important in a number of fields to understand soil as well as water dynamics in soil. Thus, an overestimation or an underestimation of VWC in a silty loam soil at different ranges would lead to an error in head of a maximum of 60cm

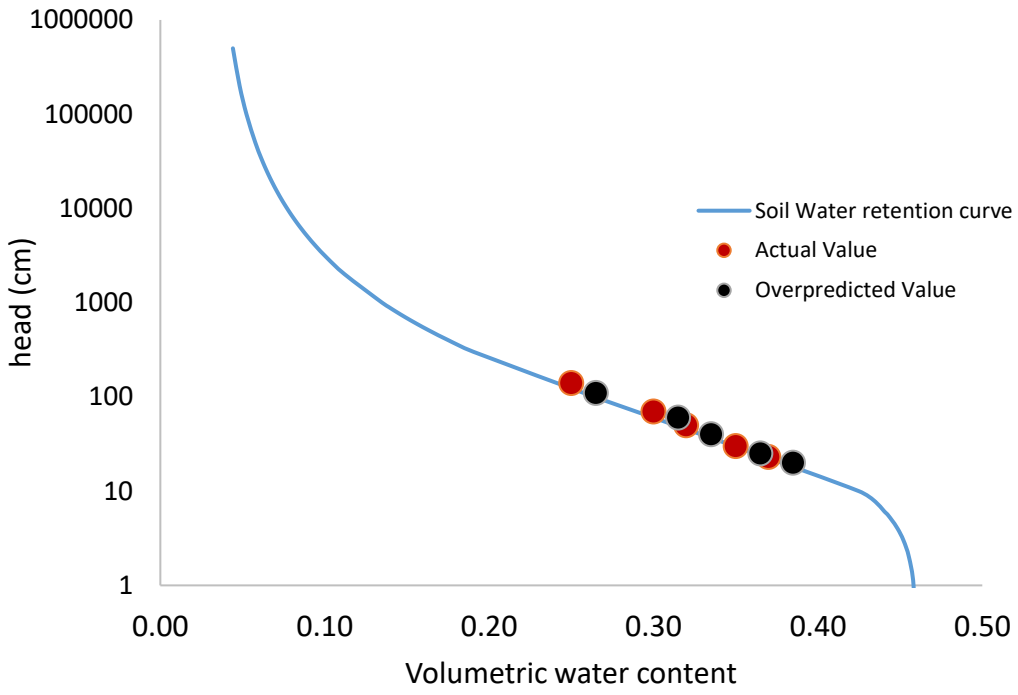

Figure 5-10: Effect of overestimating volumetric water content by the MAE

5.8 Validation using HYDRUS 1D model

A HYDRUS -1D model was setup using the atmospheric data obtained from the Ashland Bottom weather station and the boundary conditions that are deemed realistic to actual condition

for the case. Initial values for the model were set up using the VWC from the EMI based model. The water content profile for different days along the research period was obtained in HYDRUS 1D for a depth of 50 cm. The water content obtained from HYDRUS were compared with the average VWC for the whole field obtained from the EMI based VWC prediction model. The VWC obtained from the EMI based volumetric water content model for 14th July 2021, 28th July 2021, 20th August 2021, 03rd September 2021, 19th September 2021, 29th September 2021, 21st October 2021 and 3rd November 2021 were compared with the VWC obtained from the HYDRUS -1D model for each date. Figure 20 shows the values of VWC from the HYDRUS -1D model, and the VWC obtained from the average of the EMI ECa. The trend of VWC in Figure 20 for both the EMI based volumetric water content model and HYDRUS models are similar. The data obtained for 03rd September 2021 were preceded by a rain event that occurred the day before. The increase in VWC from the rain was accurately captured by both the HYDRUS as well as the EMI based volumetric water content model. VWC for both the EMI based volumetric water content model and the Hydrus model shows remarkably similar trends which further validates our EMI based volumetric water content model . The Mean absolute error between the Geophysical and Hydrus model was found to be 1.49%.

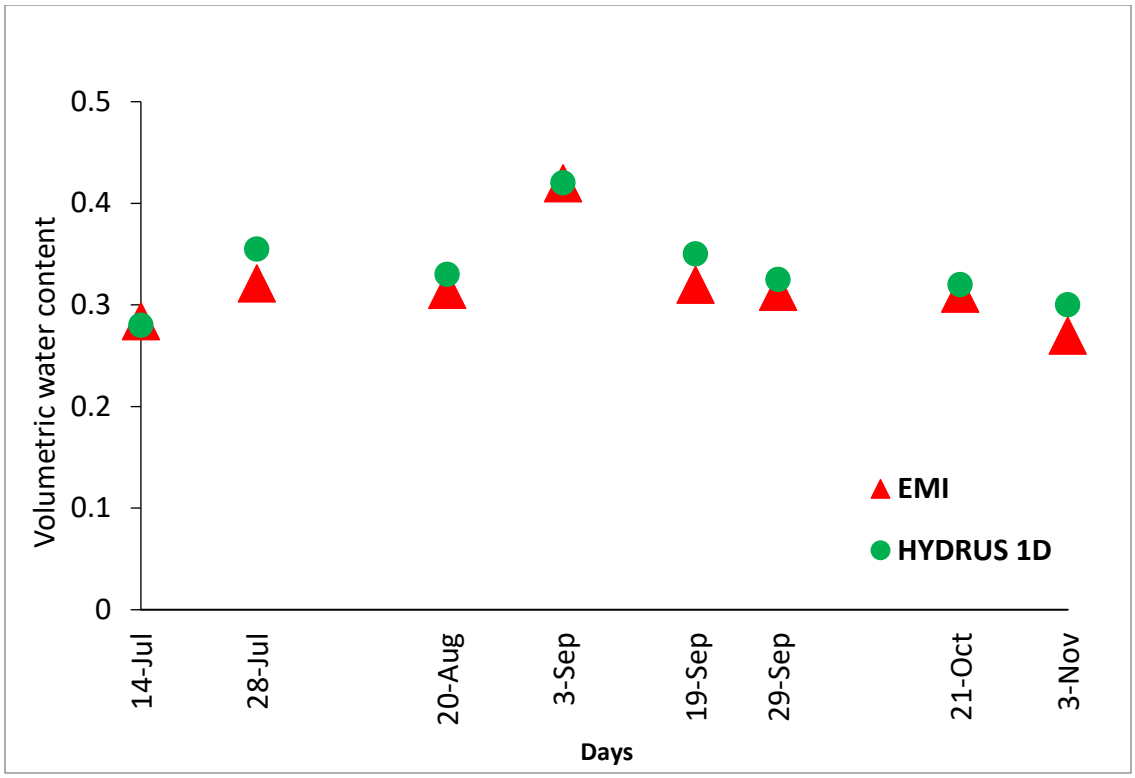

Figure 5-11: Volumetric water content obtained from the EMI based volumetric water content model and the Hydrus-1D model for different days

6 Discussion

The 17 Models analyzed are summarized in Table 5 including the R^2, MAE, the coefficients, and intercept values.

Table 5 : R^2 and MAE values for different models developed in this research

Model		Equation	R^2	MAE
Dependent Variable	**Independent Variable**			
VWC	ECa	$y = 0.3457x + 13.564$	0.6514	1.50
Relative (Minimum VWC)	Relative (Minimum ECa)	$y = 0.3457x - 0.7976$	0.6514	1.50
Relative (Maximum VWC)	Relative (Maximum ECa)	$y = 0.3457x + 0.3406$	0.6514	1.50
Relative (Average VWC)	Relative (Average ECa)	$y = 0.3457x - 4E - 15$	0.6514	1.50
Relative (Minimum VWC)	ECa	$y = -0.3457x + 12.087$	0.6514	1.50
Relative (Maximum VWC)	ECa	$y = -0.3457x + 23.167$	0.6514	1.50
Relative (Average VWC)	ECa	$y = -0.3457x + 17.795$	0.6514	1.50
Absolute (Minimum VWC)	Absolute (Minimum ECa)	$y = 0.3457x + 0.7976$	0.6514	1.50
Absolute (Maximum VWC)	Absolute (Maximum ECa)	$y = 0.3457x + 0.3406$	0.6514	1.50
Absolute (Average VWC)	Absolute (Average ECa)	$y = 0.2008x + 1.4919$	0.3105	1.03
Absolute (Minimum VWC)	ECa	$y = -0.0319x + 4.2873$	0.6514	1.32
Absolute (Maximum VWC)	ECa	$y = 0.3457x - 12.087$	0.6514	1.50
Absolute (Average VWC)	ECa	$y = -0.3457x + 23.167$	0.0222	1.50
Absolute (Lab VWC)	Absolute (GEM-2 ECa)	$y = 0.246x + 1.7447$	0.3955	1.19
Absolute (Lab VWC)	ECa	$y = 0.16x - 4.9145$	0.386	1.15
Relative (Lab VWC)	Relative (GEM-2 ECa)	$y = 0.3457x + 20.861$	0.6514	1.50
Relative (Lab VWC)	ECa	$y = -0.3457x + 37.436$	0.6514	1.50

The equations in Table 5 show the magnitude of the slope for most of the models are similar, except the absolute models. This indicates that the rate of change among the two variables

are the same irrespective of whether the variables or relative changes are correlated. The value of the intercept changes because correlations were done at different scales of unit, but the R^2 and the mean absolute error values remain the same. For models that consider absolute values of change in the ECa and VWC, when maximum and minimum values are taken as reference values the magnitude of coefficient or the slope doesn't change, however there is a shift in the graph because of the units at which the correlation. When the average value is taken as reference point the magnitude and intercept values change. This is likely due to the fact that the relation might be not exactly linear and more of a logarithmic relation as seen before where the best model was a logarithmic fit model. For models that use known laboratory values as reference values, the relative change models have similar coefficient and intercept values indicating that the model developed is similar to what is expected in the field. The absolute change model gives an indication of a better logarithmic fit rather than a linear fit.

The correlation between the spatial variation in ECa and VWC is confirmed in this research. The relationship between ECa and VWC is linear. In all the cases, regions of lower ECa corresponded to region of lower volumetric water content while regions of higher volumetric content corresponded to regions of higher ECa. Different models shown in this research were analyzed to understand the possibility of replicability of these models for other soil properties. However, in most cases the models had a similar slope further indicating the need of more research for developing a global model. With the methodology outlined above, research can continue to develop a global model for estimating VWC from ECa. Further different frequencies may be used to get VWC at different depths.

Once the correlation analysis was done, the VWC from this correlation model was used as an initial condition for modeling water flow in HYDRUS 1D. Based on atmospheric conditions,

soil water content profile was computed in Hydrus and then compared with the VWC that was predicted using the EMI based model. The results from the HYDRUS 1D model coupled with the EMI based model showed great level of correlation between them. The error between the HYDRUS 1D predicted value and the EMI based VWC value ranged from 0.04% to 3.04%.

7 Conclusions and Recommendations

This research proposes a method to couple EMI based VWC with HYDRUS 1D model to understand waterflow dynamics in near surface soil. For this purpose, the VWC predicted from the EMI based model was used as an initial condition in HYDRUS 1D model. Based on the initial condition and atmospheric condition from days after the initial day, VWC was compared and errors were computed. The results showed a remarkably elevated level of similarity with a mean absolute error of 1.49%. Hence an EMI coupled HYDRUS 1D model can be used to understand other water flow dynamics such as Infiltration and fluxes in HYDRUS 1D. This could aid hydrologists, plant modelers and hydrogeologists in understanding water flow dynamics in near surface soil.

Regression analysis between ECa and VWC was done. ECa was measured using a multi frequency EMI sensor while the VWC was measured using a time domain reflectometer sensor at 50 cm depth. The multifrequency EMI sensor was used at 90 kHz to reach the desired depth of 50cm. The TDR was calibrated to the site for accurate VWC measurements. The site-specific calibration of the TDR sensor gave us an R^2 value of 0.99 indicating a remarkably high correlation amongst the lab measured and the TDR measured VWC.

EMI surveys were conducted at the Ashland Bottom Farm south of Manhattan, Kansas for 26 days throughout 2021. A ground truthing method was used to identify the frequency corresponding to a depth of 50cm. The TDR values were also collected for numerous locations along the transect line of EMI surveys. The ECa measured using the EMI sensor was corrected for temperature and different models were developed with ECa as the independent variable. The VWC obtained from the TDR corrected model was used as the dependent variable. Different curve fitting models along with nonlinear models were evaluated to find the best fit. Relative change and

absolute change models were also considered to see if the relative models and absolute models have any significant different and could be replicated in a different soil texture. It is recommended that a logarithmic model be used for the silt loam soil analyzed in this research as the mean absolute error is the least for the logarithmic model. The following recommendations are given for application of this model to different soil types:

1. For a field that has similar soil texture, a small trial needs to be conducted before using the model. Measurements of the VWC and ECa at a minimum of three points should be recorded across different VWC levels. Based on the linear model in this research, if the predicted value has an absolute error of less than or equal to 2% of the regressed model, the model developed here may be used. Otherwise, it is recommended that a new regression model is developed based on the procedure used for this research.
2. For a field that has a different soil texture/soil type, it is recommended that a new regression model is developed. There are uncertainties when moving towards a soil of different texture. Since the depth of investigation is based on the skin depth (which is related to conductivity), there is a high probability that the EMI readings may depict soil at a different depth for the same frequency. Secondly, the relative change amongst the apparent electrical conductivity and volumetric water content might not be similar for a different soil texture.

A HYDRUS-1D model was then developed coupled with predicted VWC values from the EMI based models to compare the EMI based volumetric water content model with HYDRUS 1D models predicted VWC. Atmospheric condition along with free drainage boundary condition was used in HYDRUS 1D. VWC at different days at a depth of 50cm was computed from HYDRUS 1D and these values were compared from the VWC obtained using the EMI sensor. The VWC

from HYDRUS 1D and EMI based model had a mean absolute error of 1.49% with the day after a high-volume rainfall having a error of 0.04% while the driest day having an error of 2% Overall, this study shows that multifrequency EMI sensor can be used to understand variability in VWC for large fields.

This research tried to solve the issue of using a realistic initial condition in HYDRUS 1D by coupling HYDRUS 1D models with EMI based models. The EMI based VWC prediction model can be used to setup initial conditions and the based on the forecasted weather condition, water flow parameters can be estimated. Spatial and temporal variability in soil water content also can be understood more accurately. Future work might integrate HYDRUS 2D/3D models to analyze how EMI based models coupled with HYDRUS 2D/3D can aid in understanding and predicting water flow.

References

Allred, Barry, Jeffrey J. Daniels, and Mohammad Reza Ehsani, eds. 2008. “Past, Present, and Future Trends of Soil Electrical Conductivity Measurement Using Geophysical Methods.” in *Handbook of Agricultural Geophysics*. CRC Press.

Anon. n.d. “McNeill, J. D. (1980). Electromagnetic Terrain Conductivity Measurement at Low Induction Numbers. Geonics Ltd., Technical Note TN-6. - References - Scientific Research Publishing.” Retrieved April 18, 2022 (https://www.scirp.org/%28S%28lz5mqp453edsnp55rrgjct55%29%29/reference/referencespapers.aspx?referenceid=1203516).

Archie, G. E. 1942. “The Electrical Resistivity Log as an Aid in Determining Some Reservoir Characteristics.” *Transactions of the AIME* 146(01):54–62. doi: 10.2118/942054-G.

Badewa, Emmanuel, Adrian Unc, Mumtaz Cheema, Vanessa Kavanagh, and Lakshman Galagedara. 2018. “Soil Moisture Mapping Using Multi-Frequency and Multi-Coil Electromagnetic Induction Sensors on Managed Podzols.” *Agronomy* 8(10):224. doi: 10.3390/agronomy8100224.

Blonquist, J. M., S. B. Jones, and D. A. Robinson. 2006. “Precise Irrigation Scheduling for Turfgrass Using a Subsurface Electromagnetic Soil Moisture Sensor.” *Agricultural Water Management* 84(1):153–65. doi: 10.1016/j.agwat.2006.01.014.

Brevik, Eric C., Thomas E. Fenton, and Robert Horton. 2004. “Effect of Daily Soil Temperature Fluctuations on Soil Electrical Conductivity as Measured with the Geonics® EM-38.” *Precision Agriculture* 5(2):145–52. doi: 10.1023/B:PRAG.0000022359.79184.92.

Brosten, Troy R., Frederick D. Day-Lewis, Gregory M. Schultz, Gary P. Curtis, and John W. Lane. 2011. “Inversion of Multi-Frequency Electromagnetic Induction Data for 3D Characterization of Hydraulic Conductivity.” *Journal of Applied Geophysics* 73(4):323–35. doi: 10.1016/j.jappgeo.2011.02.004.

Callegary, J. B., T. P. A. Ferré, and R. W. Groom. 2007. “Vertical Spatial Sensitivity and Exploration Depth of Low-Induction-Number Electromagnetic-Induction Instruments.” *Vadose Zone Journal* 6(1):158–67. doi: 10.2136/vzj2006.0120.

Carroll, Z. L., and M. A. Oliver. 2005. “Exploring the Spatial Relations between Soil Physical Properties and Apparent Electrical Conductivity.” *Geoderma* 128(3):354–74. doi: 10.1016/j.geoderma.2005.03.008.

Clay, D. E., J. Chang, D. D. Malo, C. G. Carlson, C. Reese, S. A. Clay, M. Ellsbury, and B. Berg. 2001. “Factors Influencing Spatial Variability of Soil Apparent Electrical Conductivity.” *Communications in Soil Science and Plant Analysis* 32(19–20):2993–3008. doi: 10.1081/CSS-120001102.

Corwin, D. L., and S. M. Lesch. 2005. “Characterizing Soil Spatial Variability with Apparent Soil Electrical Conductivity: Part II. Case Study.” *Computers and Electronics in Agriculture* 46(1):135–52. doi: 10.1016/j.compag.2004.11.003.

Ding, Jianli, and Danlin Yu. 2014. “Monitoring and Evaluating Spatial Variability of Soil Salinity in Dry and Wet Seasons in the Werigan–Kuqa Oasis, China, Using Remote Sensing and Electromagnetic Induction Instruments.” *Geoderma* 235–236:316–22. doi: 10.1016/j.geoderma.2014.07.028.

Doolittle, James A., and Eric C. Brevik. 2014. “The Use of Electromagnetic Induction Techniques in Soils Studies.” *Geoderma* 223–225:33–45. doi: 10.1016/j.geoderma.2014.01.027.

Elwaseif, M., J. Robinson, F. D. Day-Lewis, D. Ntarlagiannis, L. D. Slater, J. W. Lane, B. J. Minsley, and G. Schultz. 2017. “A Matlab-Based Frequency-Domain Electromagnetic Inversion Code (FEMIC) with Graphical User Interface.” *Computers & Geosciences* 99:61–71. doi: 10.1016/j.cageo.2016.08.016.

Haarder, Eline B., Majken C. Looms, Karsten H. Jensen, and Lars Nielsen. 2011. “Visualizing Unsaturated Flow Phenomena Using High-Resolution Reflection Ground Penetrating Radar.” *Vadose Zone Journal* 10(1):84–97. doi: 10.2136/vzj2009.0188.

Jacobsen, O. H., and P. Schjønning. 1993. “A Laboratory Calibration of Time Domain Reflectometry for Soil Water Measurement Including Effects of Bulk Density and Texture.” *Journal of Hydrology* 151(2):147–57. doi: 10.1016/0022-1694(93)90233-Y.

Jadoon, Khan Zaib, Lutz Weihermüller, Harry Verrecken, and Sébastien Lambot. 2012. “Estimation of Soil Hydraulic Parameters by Integrated Hydrogeophysical Inversion of Time-Lapse GPR Data Measured at Selhausen, Germany.” Pp. 701–6 in *2012 14th International Conference on Ground Penetrating Radar (GPR)*.

Léger, Emmanuel, Albane Saintenoy, and Yves Coquet. 2014. “Hydrodynamic Parameters of a Sandy Soil Determined by Ground-Penetrating Radar inside a Single Ring Infiltrometer.” *Water Resources Research* 50(7):5459–74. doi: 10.1002/2013WR014226.

Lehmann, Peter, Francesca Gambazzi, Barbara Suski, Ludovic Baron, Amin Askarinejad, Sarah M. Springman, Klaus Holliger, and Dani Or. 2013. “Evolution of Soil Wetting Patterns Preceding a Hydrologically Induced Landslide Inferred from Electrical Resistivity Survey and Point Measurements of Volumetric Water Content and Pore Water Pressure.” *Water Resources Research* 49(12):7992–8004. doi: 10.1002/2013WR014560.

Liu, Rong, Xiaowu Shen, Chunfei Chen, Jianxin Liu, Jianping Xiao, Mengyu Sun, and Rongwen Guo. 2022. “Detection of Boulder Using GEM-2 EM System Based on Three-Dimensional Inversion Algorithm.” *Journal of Applied Geophysics* 196:104516. doi: 10.1016/j.jappgeo.2021.104516.

Lück, E., R. Gebbers, J. Ruehlmann, and U. Spangenberg. 2009. “Electrical Conductivity Mapping for Precision Farming.” *Near Surface Geophysics* 7(1):15–26. doi: 10.3997/1873-0604.2008031.

Ma, Ruijun, Alex McBratney, Brett Whelan, Budiman Minasny, and Michael Short. 2011. “Comparing Temperature Correction Models for Soil Electrical Conductivity Measurement.” *Precision Agriculture* 12(1):55–66. doi: 10.1007/s11119-009-9156-7.

Martinez, Gonzalo, Karl Vanderlinden, Rafaela Ordóñez, and José L. Muriel. 2009. “Can Apparent Electrical Conductivity Improve the Spatial Characterization of Soil Organic Carbon?All Rights Reserved. No Part of This Periodical May Be Reproduced or Transmitted in Any Form or by Any Means, Electronic or Mechanical, Including Photocopying, Recording, or Any Information Storage and Retrieval System, without Permission in Writing from the Publisher.” *Vadose Zone Journal* 8(3):586–93. doi: 10.2136/vzj2008.0123.

Menke, W. 1984. “The Resolving Power of Cross-borehole Tomography.” *Geophysical Research Letters* 11(2):105–8. doi: 10.1029/GL011i002p00105.

Moysey, Stephen, Kamini Singha, and Rosemary Knight. 2005. “A Framework for Inferring Field-Scale Rock Physics Relationships through Numerical Simulation.” *Geophysical Research Letters* 32(8). doi: 10.1029/2004GL022152.

Noborio, K. 2001. “Measurement of Soil Water Content and Electrical Conductivity by Time Domain Reflectometry: A Review.” *Computers and Electronics in Agriculture* 31(3):213–37. doi: 10.1016/S0168-1699(00)00184-8.

Oldenburg, D. W., and Y. Li. 1999. “Estimating Depth of Investigation in Dc Resistivity and IP Surveys.” *Geophysics* 64(2):403–16. doi: 10.1190/1.1444545.

Ong, J., J. Lane, V. Zlotnik, T. Halihan, and Eric A. White. 2010. “Combined Use of Frequency-Domain Electromagnetic and Electrical Resistivity Surveys to Delineate near-Lake Groundwater Flow in the Semi-Arid Nebraska Sand Hills, USA.” doi: 10.1007/S10040-010-0617-X.

Peralta, Nahuel Raúl, and José Luis Costa. 2013. “Delineation of Management Zones with Soil Apparent Electrical Conductivity to Improve Nutrient Management.” *Computers and Electronics in Agriculture* 99:218–26. doi: 10.1016/j.compag.2013.09.014.

Richards, L. A. 1931. “Capillary Conduction of Liquids through Porous Mediums.” *Physics* 1(5):318–33. doi: 10.1063/1.1745010.

Robinson, David A., Hiruy Abdu, Inma Lebron, and Scott B. Jones. 2012. “Imaging of Hill-Slope Soil Moisture Wetting Patterns in a Semi-Arid Oak Savanna Catchment Using Time-Lapse Electromagnetic Induction.” *Journal of Hydrology* 416–417:39–49. doi: 10.1016/j.jhydrol.2011.11.034.

Saintenoy, Albane, Sébastien Schneider, and Piotr Tucholka. 2008. “Evaluating Ground Penetrating Radar Use for Water Infiltration Monitoring.” *Vadose Zone Journal* 7(1):208–14. doi: 10.2136/vzj2007.0132.

Schmidt, Amand F., and Chris Finan. 2018. “Linear Regression and the Normality Assumption.” *Journal of Clinical Epidemiology* 98:146–51. doi: 10.1016/j.jclinepi.2017.12.006.

Sears, Francis W. 1963. “Faraday’s Law and Ampere’s Law.” *American Journal of Physics* 31(6):439–43. doi: 10.1119/1.1969576.

Serrano, João, Shakib Shahidian, and José Marques da Silva. 2014. “Spatial and Temporal Patterns of Apparent Electrical Conductivity: DUALEM vs. Veris Sensors for Monitoring Soil Properties.” *Sensors (Basel, Switzerland)* 14(6):10024–41. doi: 10.3390/s140610024.

Šimůnek, Jirí, Martinus Th. van Genuchten, and Miroslav Šejna. 2008. “Development and Applications of the HYDRUS and STANMOD Software Packages and Related Codes.” *Vadose Zone Journal* 7(2):587–600. doi: 10.2136/vzj2007.0077.

Šimůnek, Jiří, Martinus Th. van Genuchten, and Miroslav Šejna. 2016. “Recent Developments and Applications of the HYDRUS Computer Software Packages.” *Vadose Zone Journal* 15(7):vzj2016.04.0033. doi: 10.2136/vzj2016.04.0033.

Singh, Nagendra Pratap, and Toru Mogi. 2003. “Effective Skin Depth of EM Fields Due to Large Circular Loop and Electric Dipole Sources.” *Earth, Planets and Space* 55(6):301–13. doi: 10.1186/BF03351764.

Singha, Kamini, Frederick D. Day-Lewis, and Stephen Moysey. 2007. “Accounting for Tomographic Resolution in Estimating Hydrologic Properties from Geophysical Data.” Pp. 227–41 in *Geophysical Monograph Series*. Vol. 171, edited by D. W. Hyndman, F. D. Day-Lewis, and K. Singha. Washington, D. C.: American Geophysical Union.

Sudduth, K. A., N. R. Kitchen, W. J. Wiebold, W. D. Batchelor, G. A. Bollero, D. G. Bullock, D. E. Clay, H. L. Palm, F. J. Pierce, R. T. Schuler, and K. D. Thelen. 2005. “Relating Apparent Electrical Conductivity to Soil Properties across the North-Central USA.” *Computers and Electronics in Agriculture* 46(1):263–83. doi: 10.1016/j.compag.2004.11.010.

Topp, G. C., J. L. Davis, and A. P. Annan. 1980. “Electromagnetic Determination of Soil Water Content: Measurements in Coaxial Transmission Lines.” *Water Resources Research* 16(3):574–82. doi: 10.1029/WR016i003p00574.

Walvoord, M., F. Day-Lewis, J. Lane, R. Striegl, C. Voss, and T. Douglas. 2015. “Improved Understanding of Permafrost Controls on Hydrology in Interior Alaska by Integration of Ground-Based Geophysical Permafrost Characterization and Numerical Modeling.” *Undefined*.

Won, I. J., Dean A. Keiswetter, George R. A. Fields, and Lynn C. Sutton. 1996. “GEM-2: A New Multifrequency Electromagnetic Sensor.” *Journal of Environmental and Engineering Geophysics* 1(2):129–37. doi: 10.4133/JEEG1.2.129.

Xia, Jianghai, Chao Chen, Sihao Xia, David Laflen, and Stephen L. Williams. 2004. “Using High?Resolution Magnetic Method and Gradient Method to Locate Abandoned Brine Wells in Hutchinson, Kansas.” Pp. 1350–67 in *Symposium on the Application of Geophysics to Engineering and Environmental Problems 2004*, *Symposium on the Application of Geophysics to Engineering and Environmental Problems Proceedings*. Environment and Engineering Geophysical Society.

Yaccup, Rahman, and P. Brabham. 2012. “Ground Electromagnetic Survey (GEM-2) Technique to Map the Hydrocarbon Contaminant Dispersion in the Subsurface at Barry Docks, Wales, UK.” *Undefined*.

Appendix A - Curve Fitting models

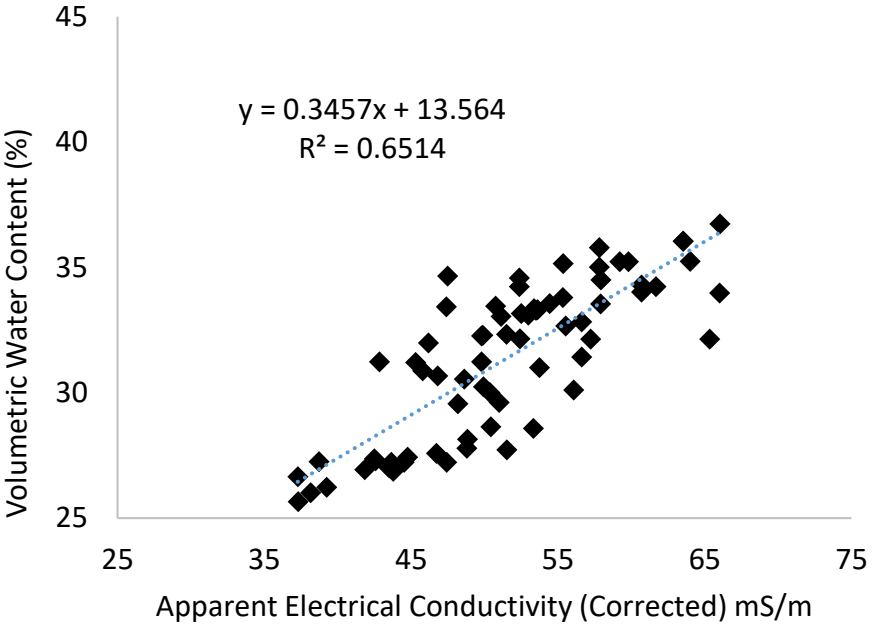

Figure A-1: Linear model between corrected apparent electrical conductivity and Volumetric water content

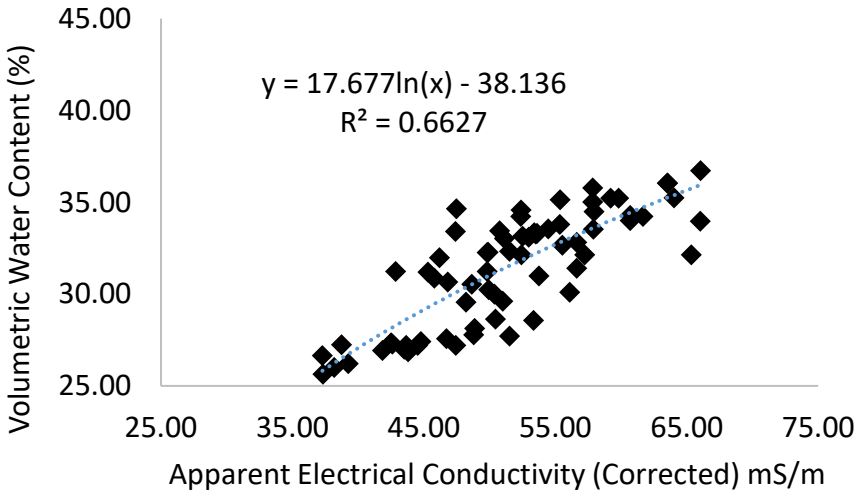

Figure A-2: Logarithmic model between corrected apparent electrical conductivity and Volumetric water content

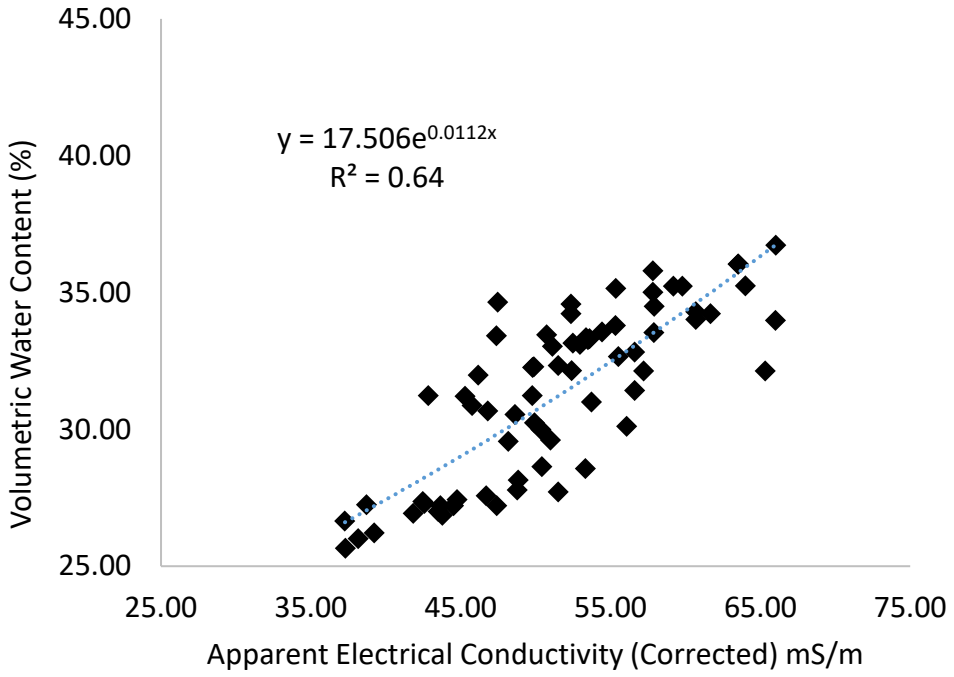

Figure A-3: Exponential model between corrected apparent electrical conductivity and Volumetric water content

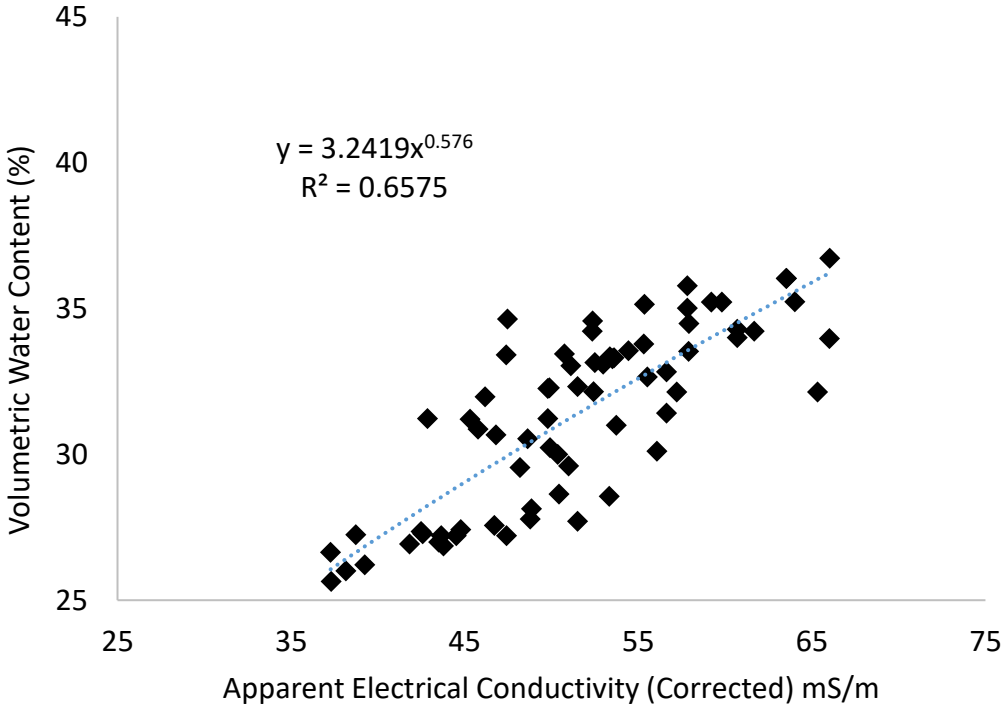

Figure A-4: Power model between corrected apparent electrical conductivity and Volumetric water content

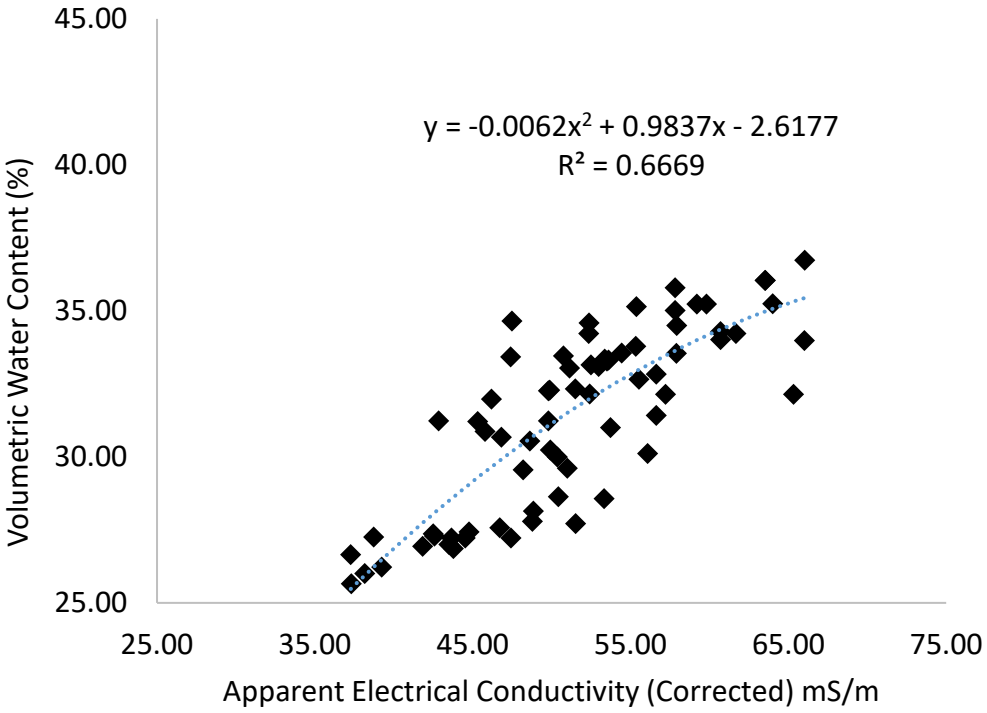

Figure A-5: Polynomial model between corrected apparent electrical conductivity and Volumetric water content

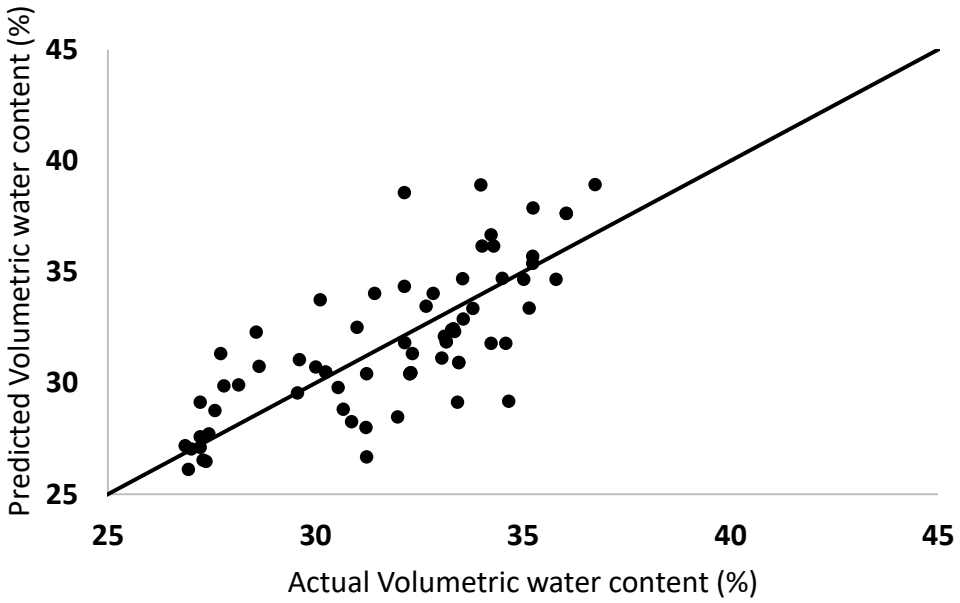

Figure A-6: Predicted Volumetric water content from Waxman and Smits model vs the actual volumetric water content

Appendix B - Fivefold analysis (Linear Models)

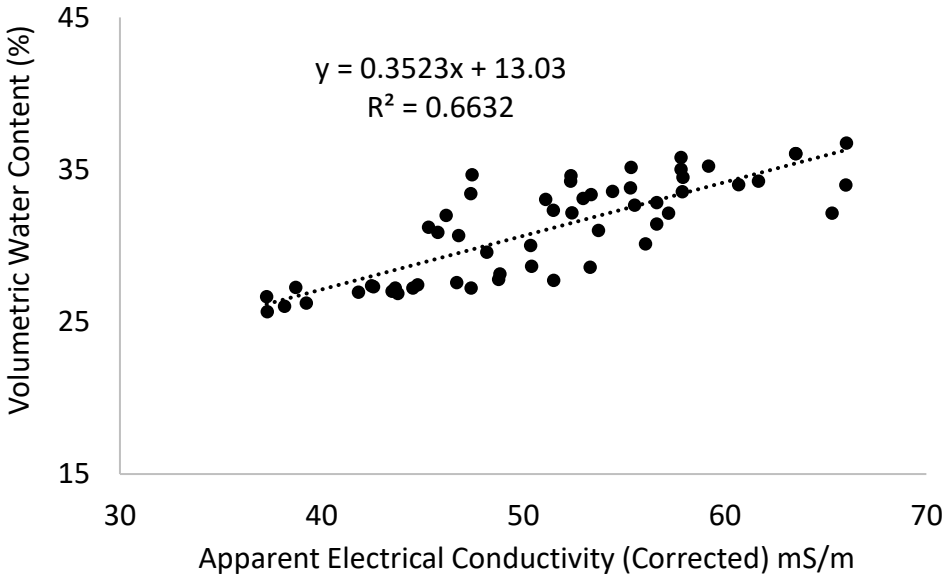

Figure B-1: The linear model for training data based on first random arrangement of data

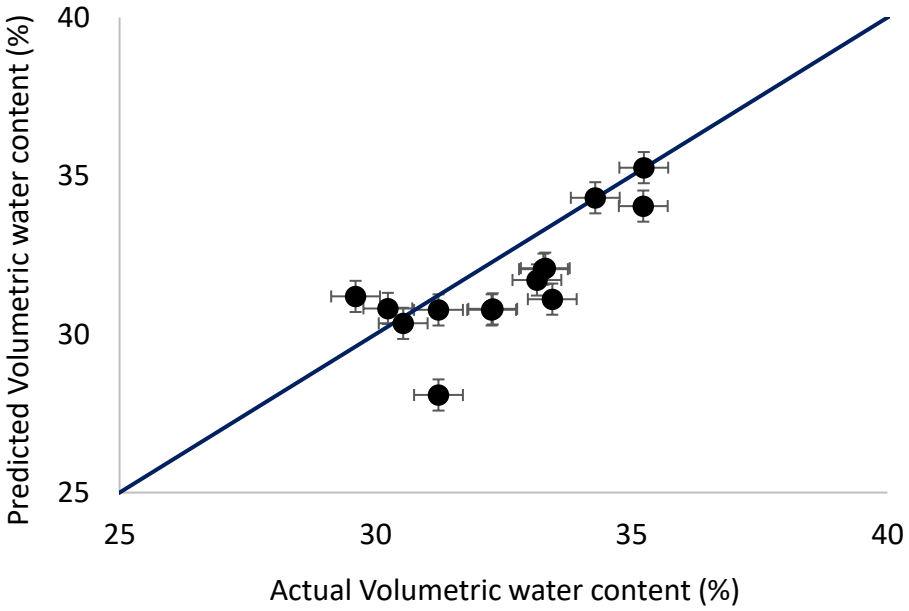

Figure B-2: Predicted value from the test dataset vs actual value of the test dataset for random 1 data

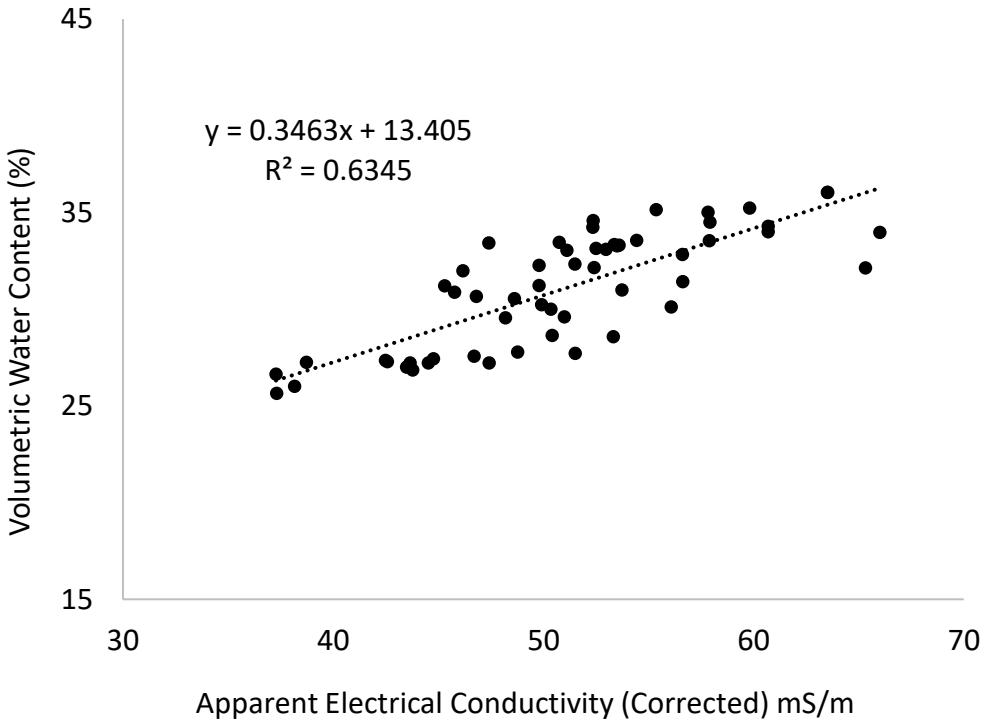

Figure B-3: The linear model for training data based on second random arrangement of data

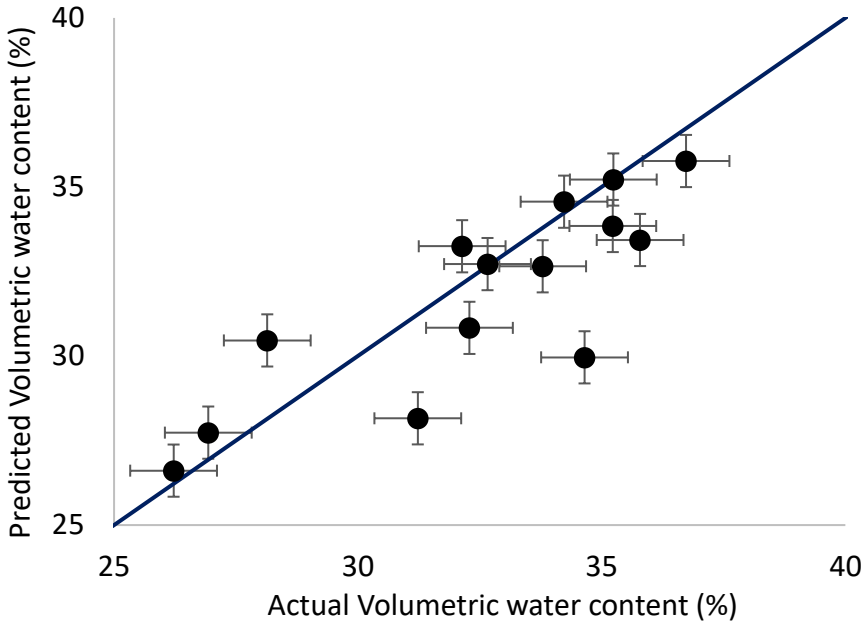

Figure B-4: Predicted value from the test dataset vs actual value of the test dataset for random 2 data

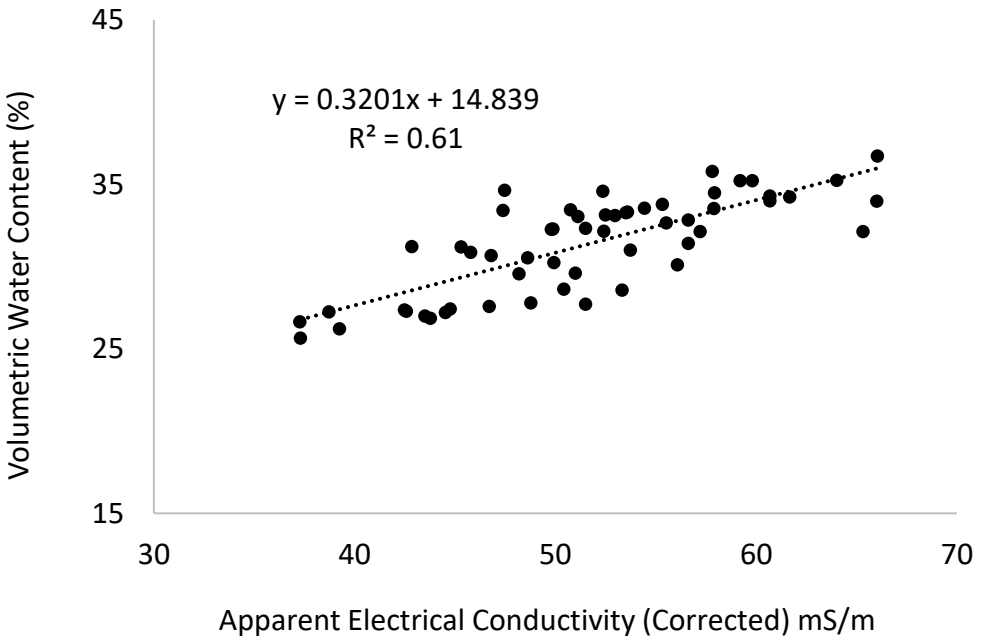

Figure B-5: The linear model for training data based on third random arrangement of data

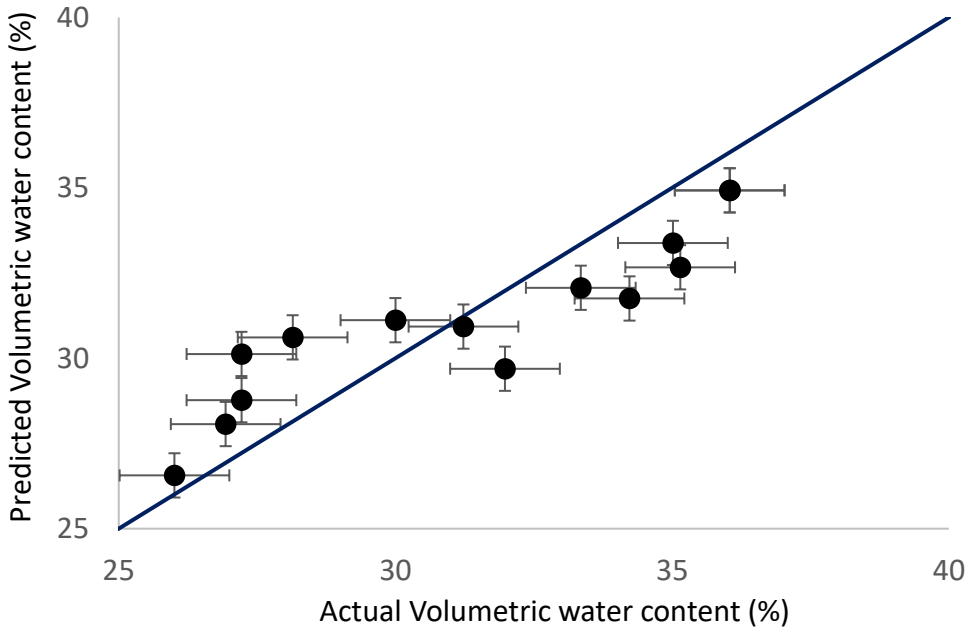

Figure B-6: Predicted value from the test dataset vs actual value of the test dataset for random 3 data

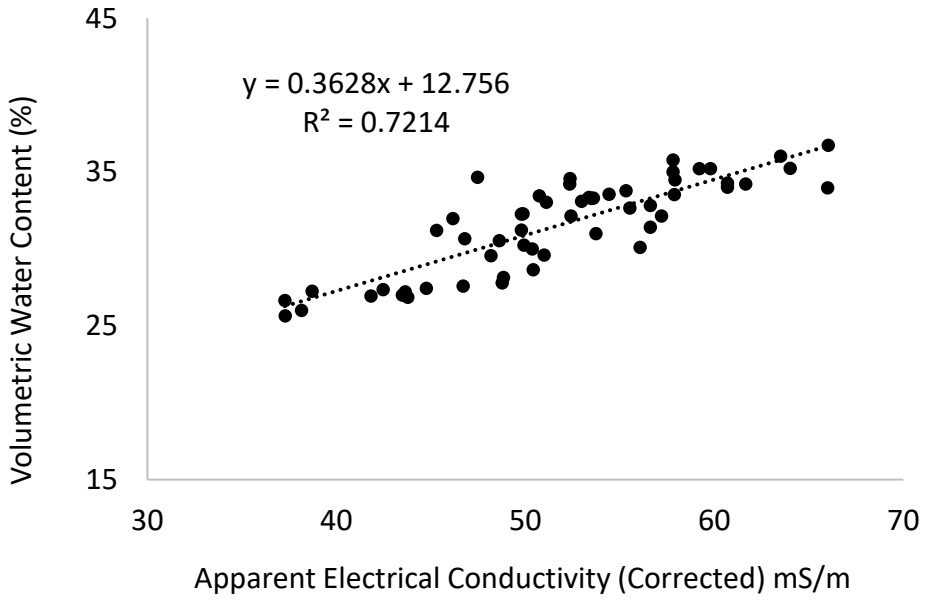

Figure B-7: The linear model for training data based on fourth random arrangement of data

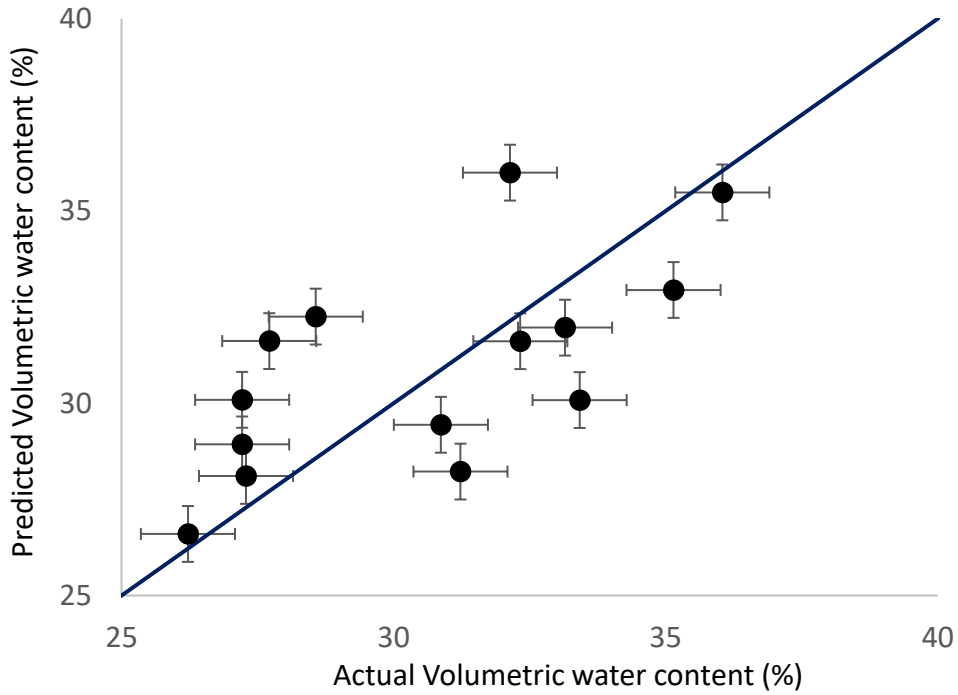

Figure B-8: Predicted value from the test dataset vs actual value of the test dataset for random 4 data

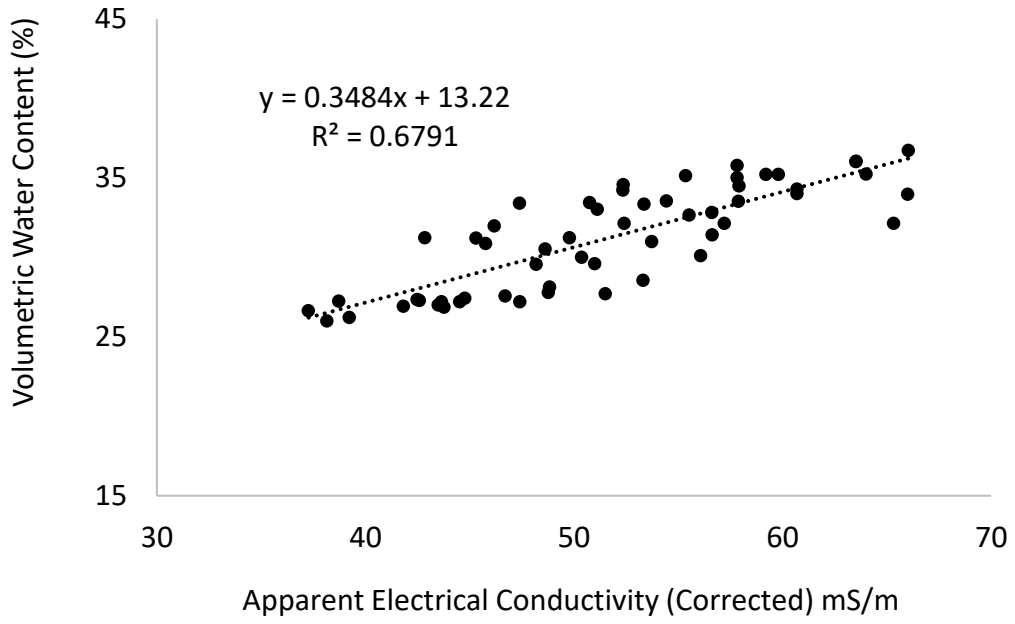

Figure B-9: The linear model for training data based on fifth random arrangement of data

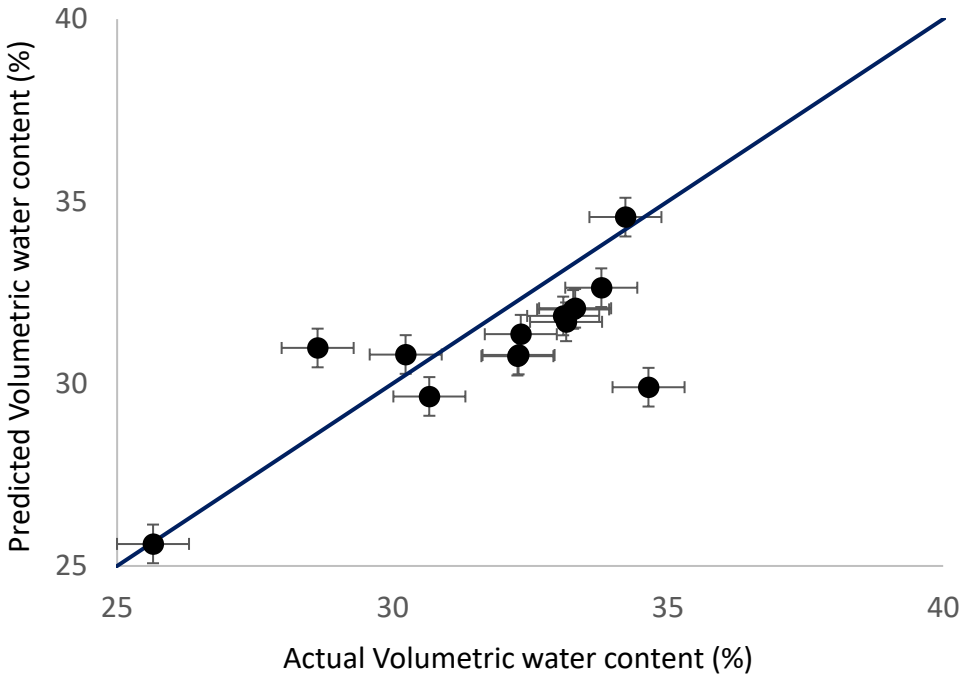

Figure B-10: Predicted value from the test dataset vs actual value of the test dataset for random 5 data

Appendix C - Fivefold analysis (Logarithmic Models)

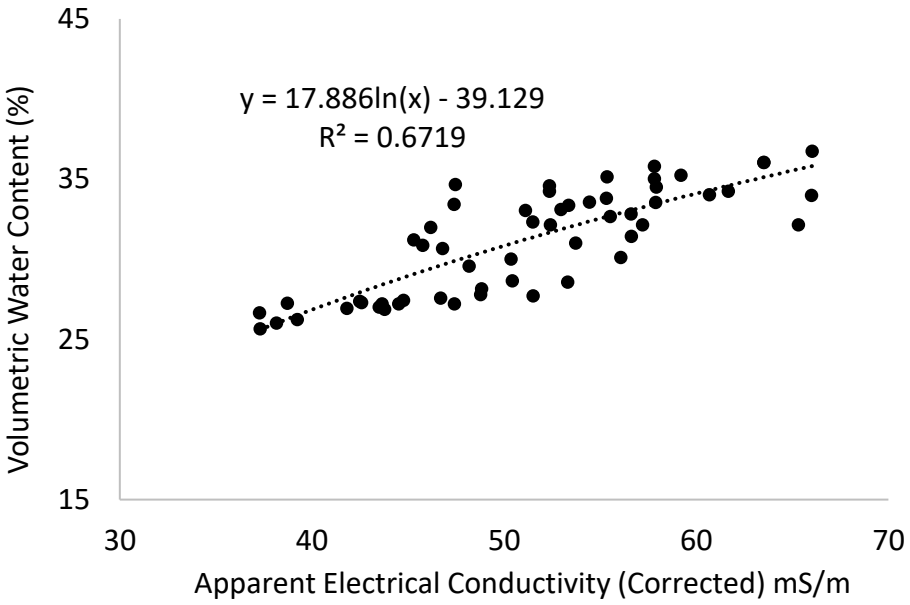

Figure C-1: The logarithmic model for training data based on first random arrangement of data

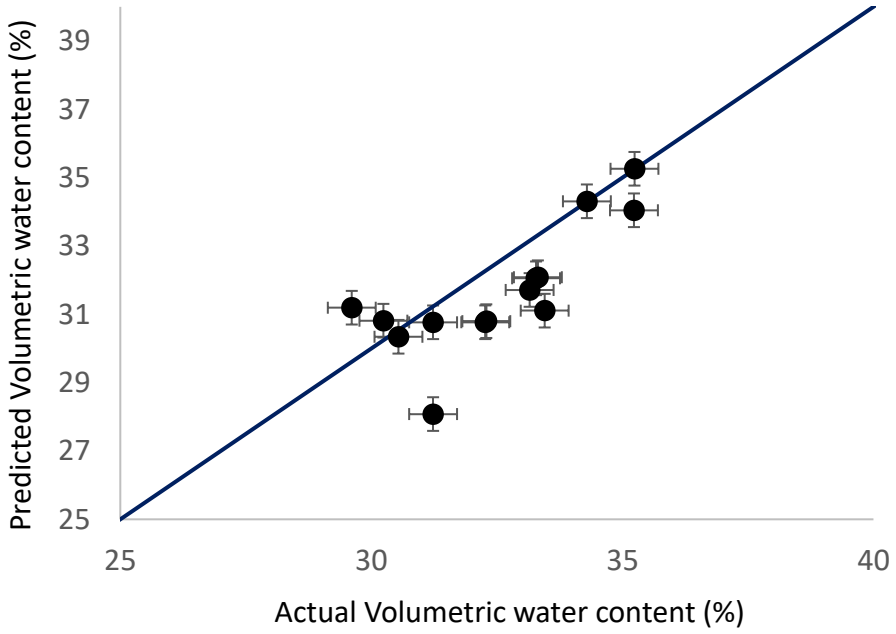

Figure C-2: Predicted value from the test dataset vs actual value of the test dataset for random 1 data

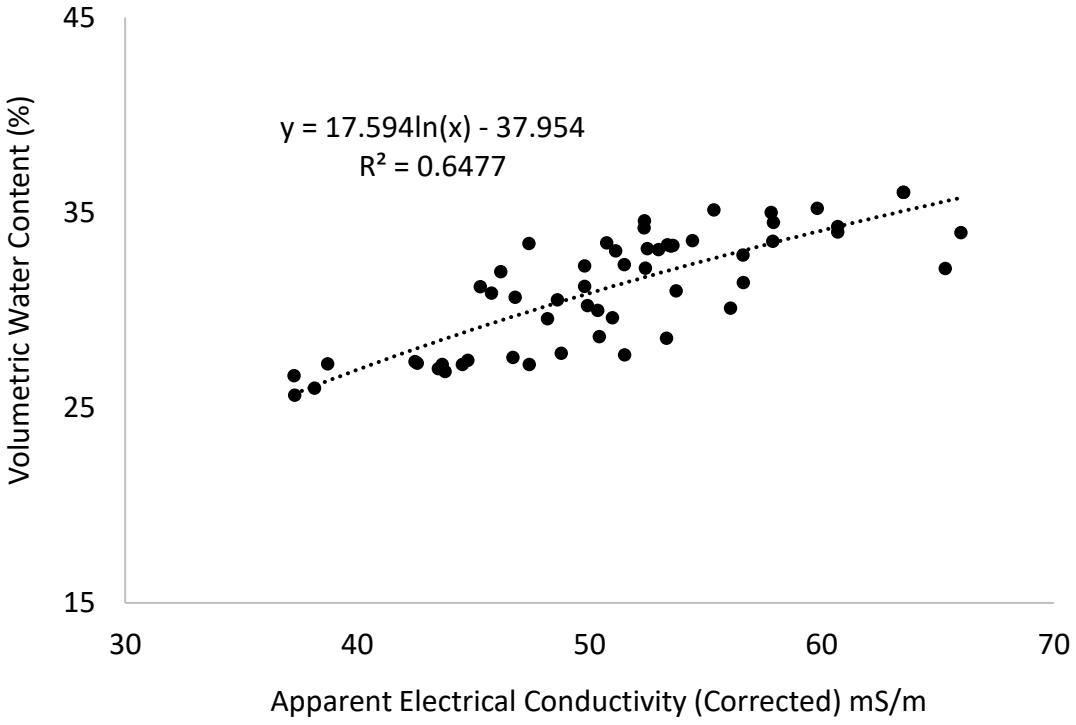

Figure C-3:The logarithmic model for training data based on second random arrangement of data

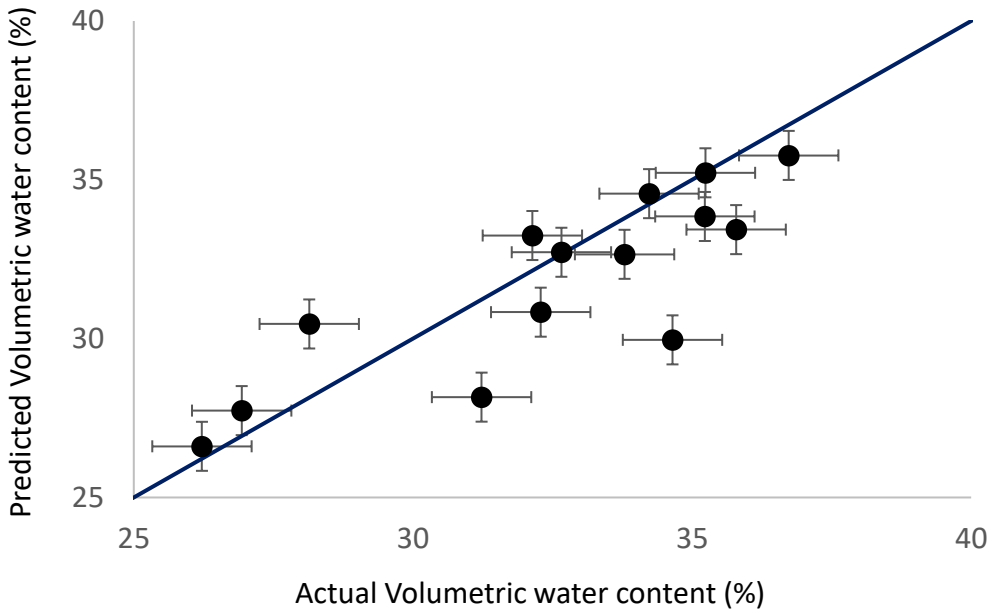

Figure C-4:Predicted value from the test dataset vs actual value of the test dataset for random 2 data

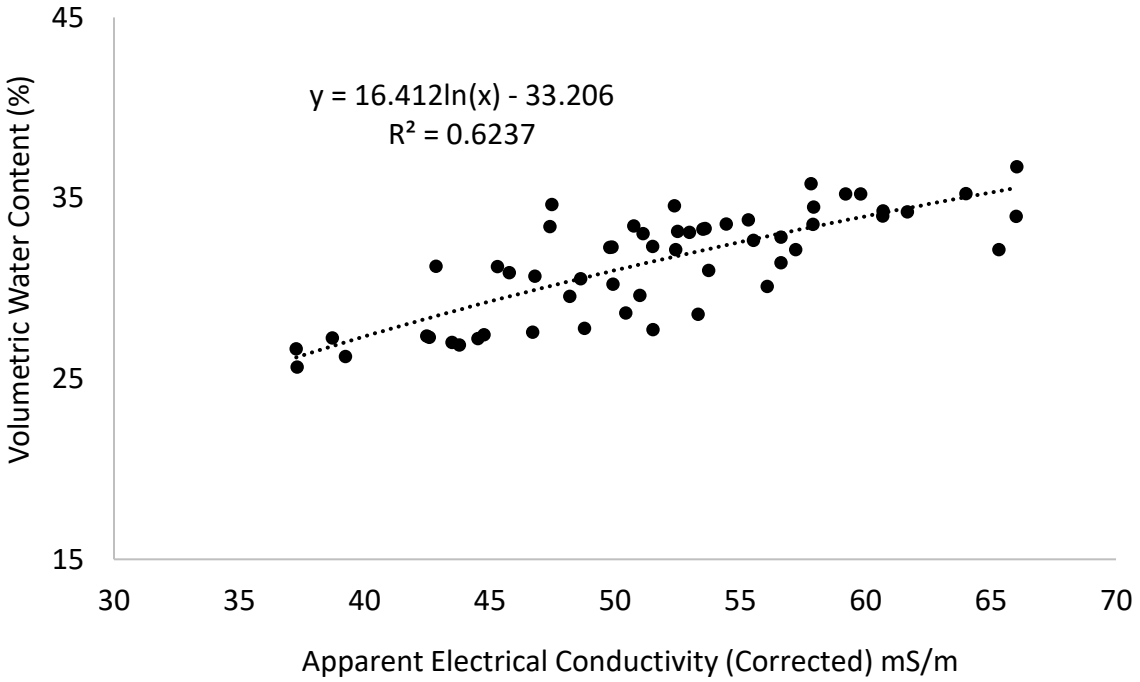

Figure C-5: The logarithmic model for training data based on third random arrangement of data

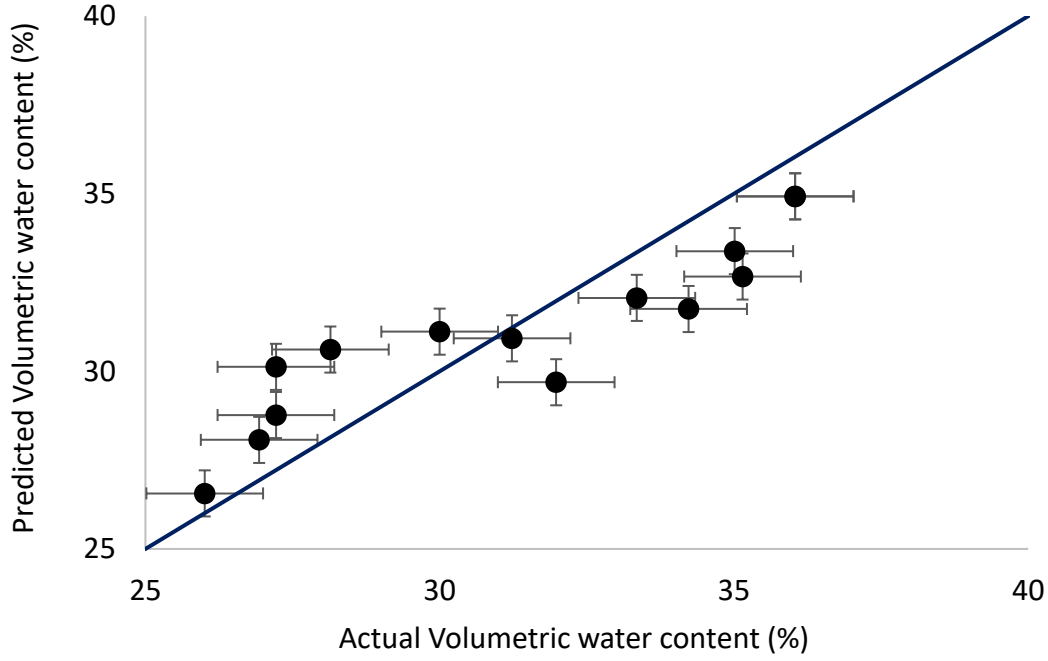

Figure C-6: Predicted value from the test dataset vs actual value of the test dataset for random 3 data

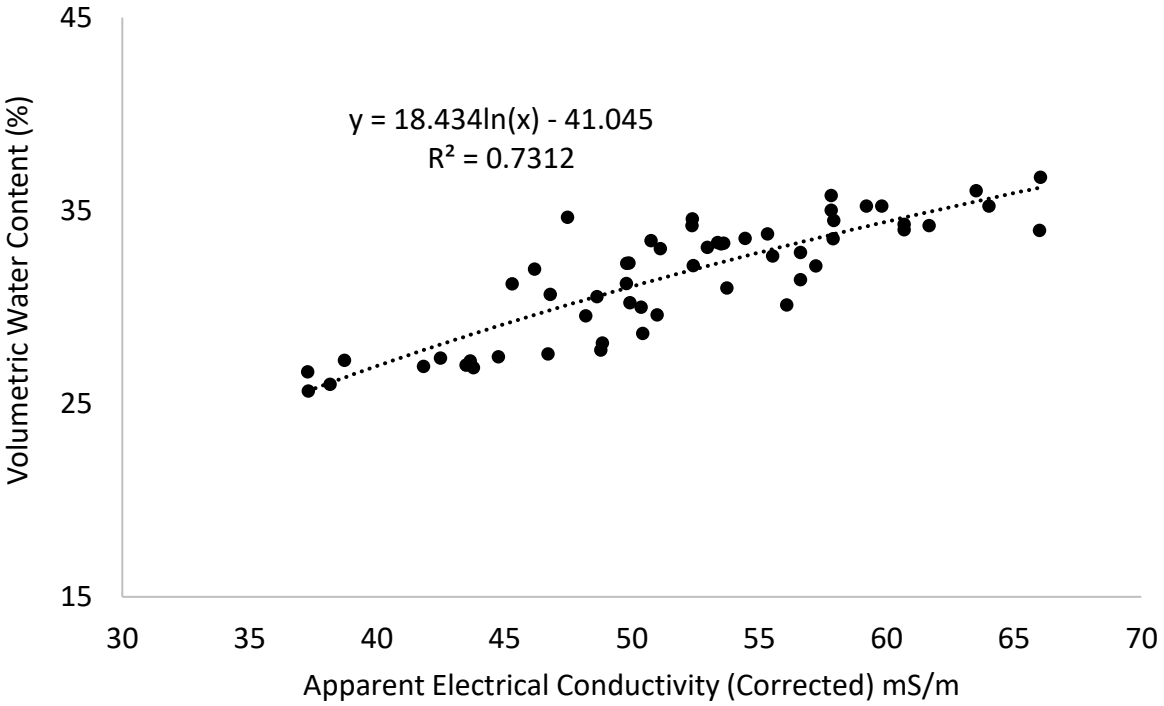

Figure C-7: The logarithmic model for training data based on fourth random arrangement of data

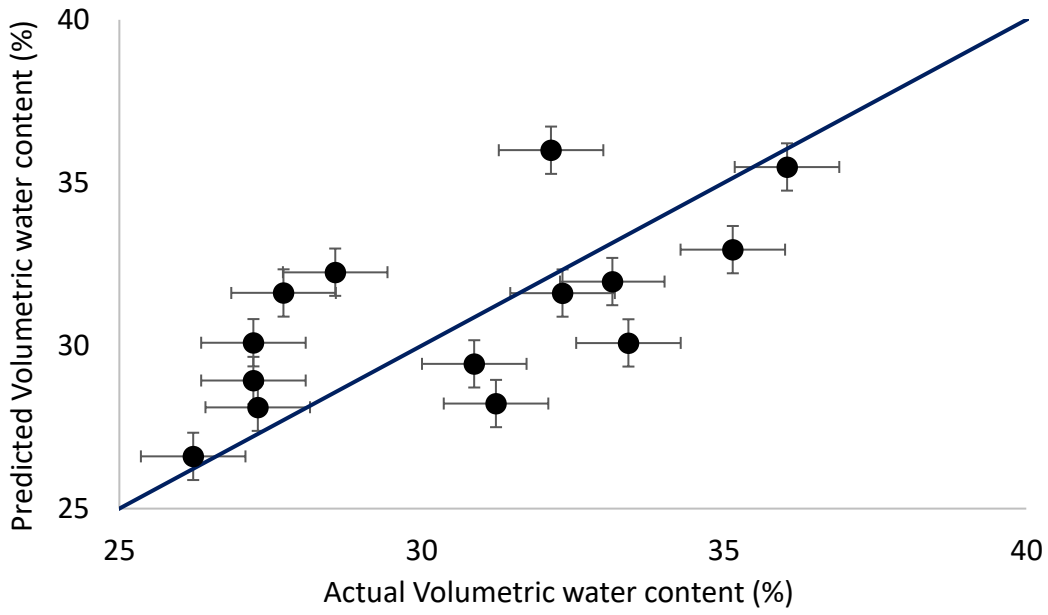

Figure C-8: Predicted value from the test dataset vs actual value of the test dataset for random 4 data

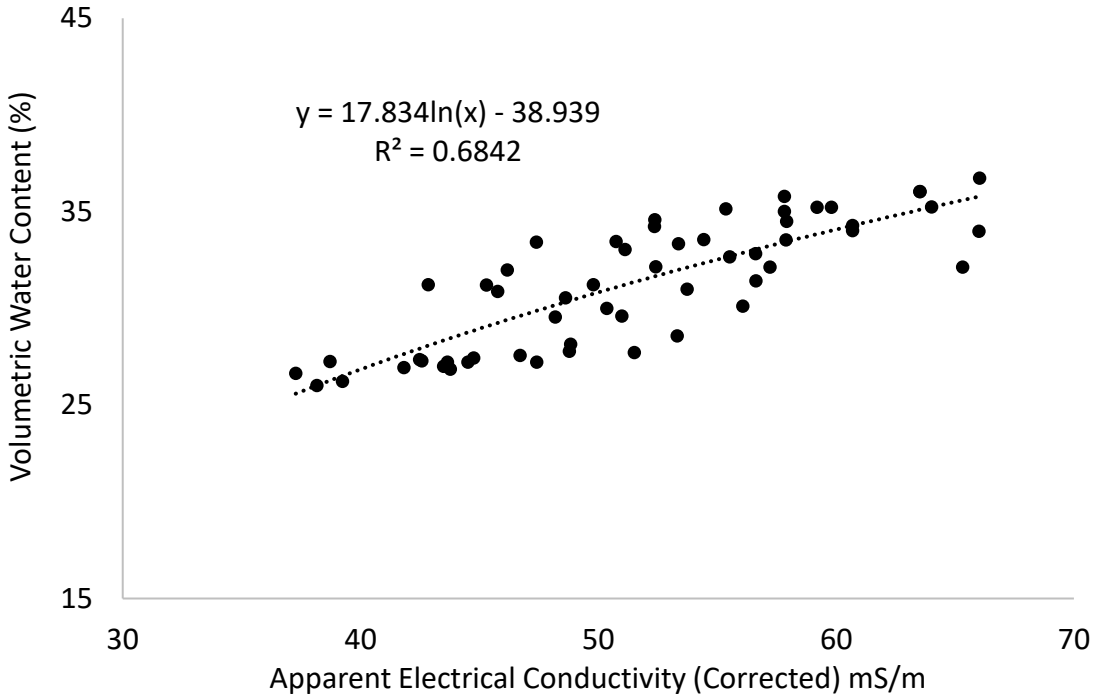

Figure C-9: The logarithmic model for training data based on fifth random arrangement of data

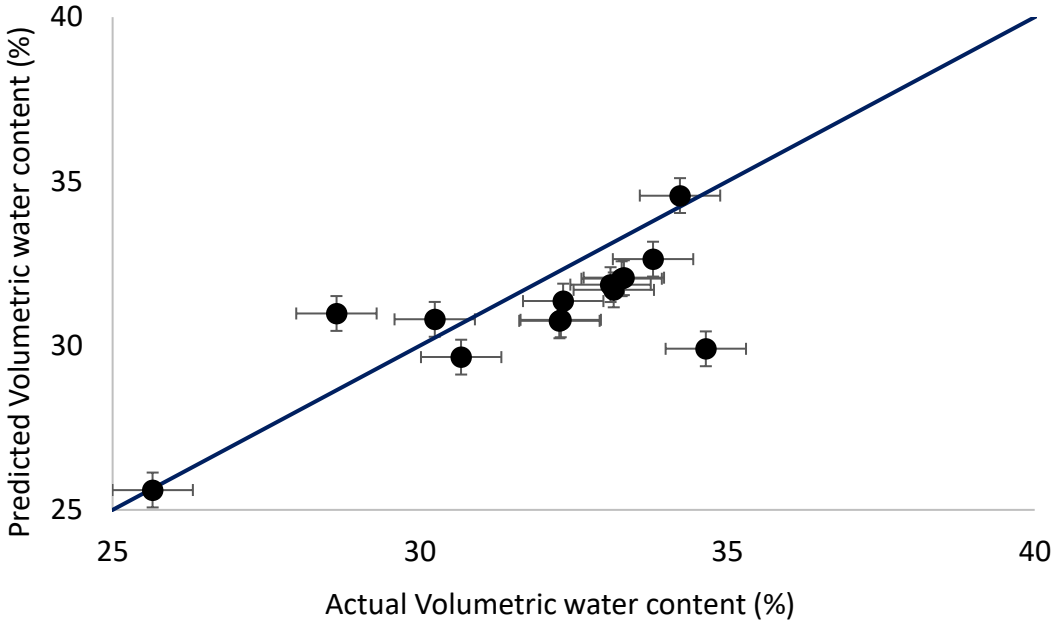

Figure C-10: Predicted value from the test dataset vs actual value of the test dataset for random 5 data

Appendix D - Precipitation, Evapotranspiration and temperature trends at Ashland Bottoms

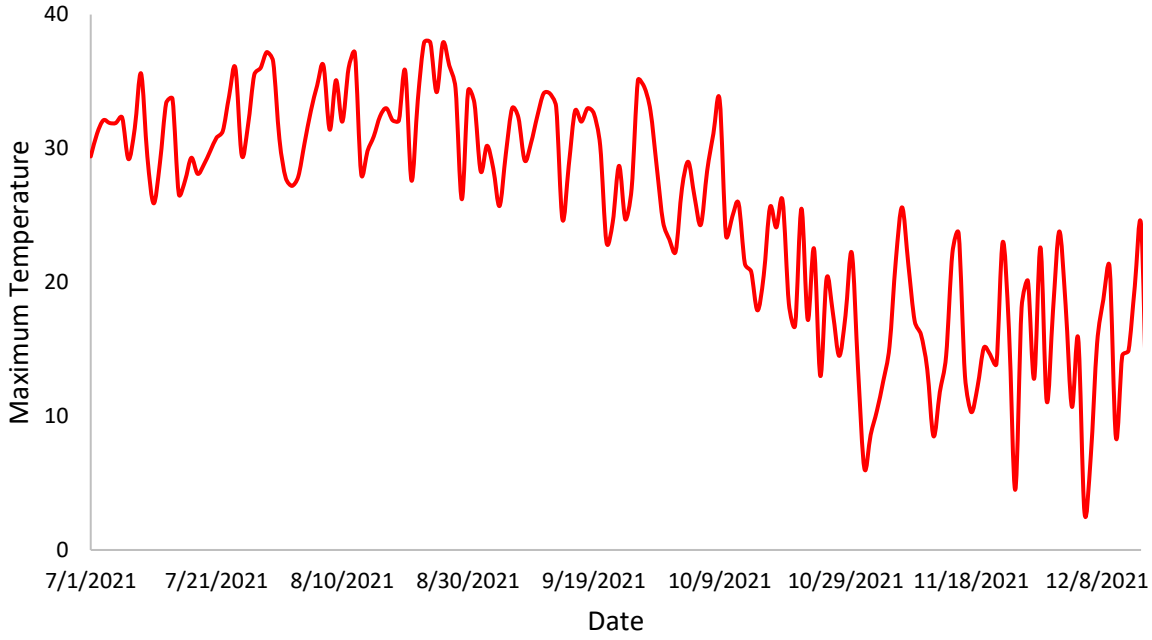

Figure D-1: Maximum Temperature in the study period (°C)

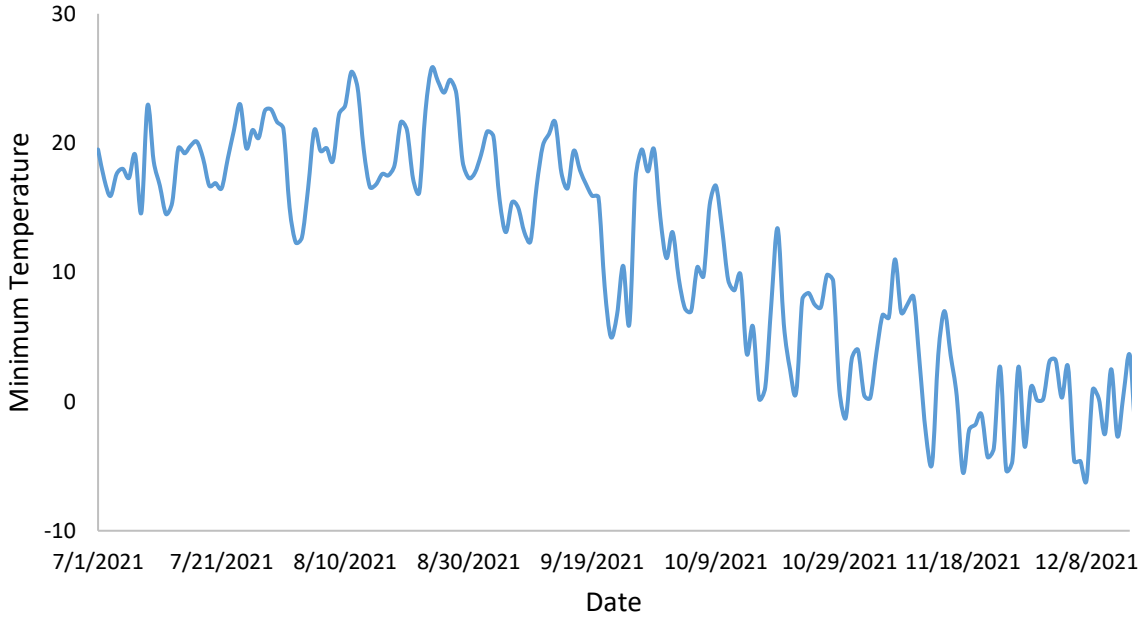

Figure D-2: Minimum Temperature in the study period (°C)

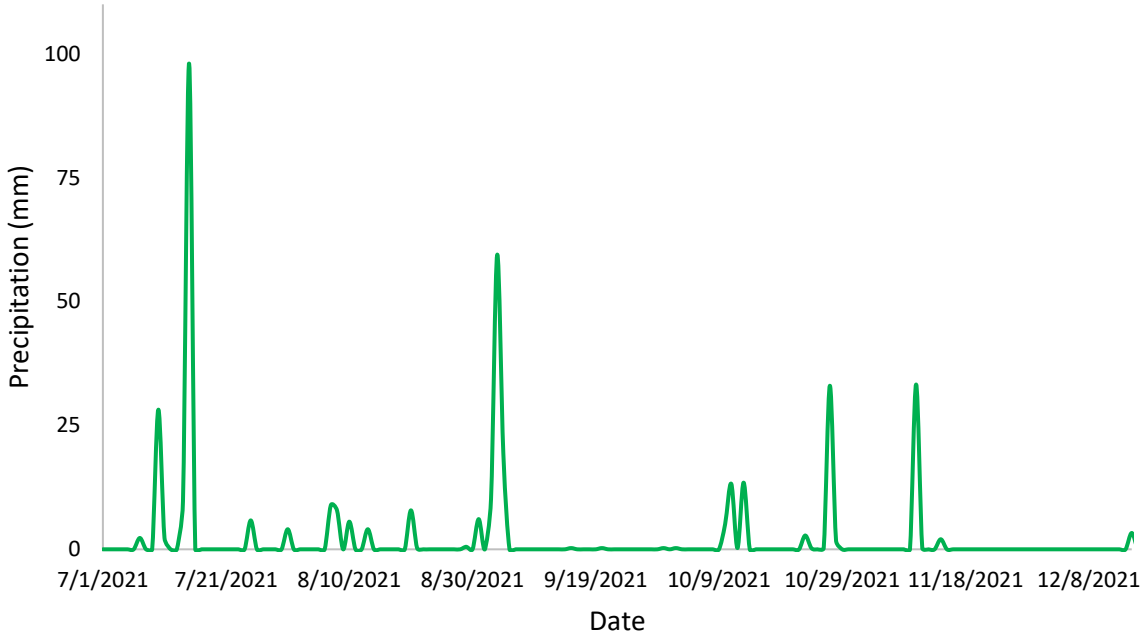

Figure D-3: Precipitation during the study period (mm)

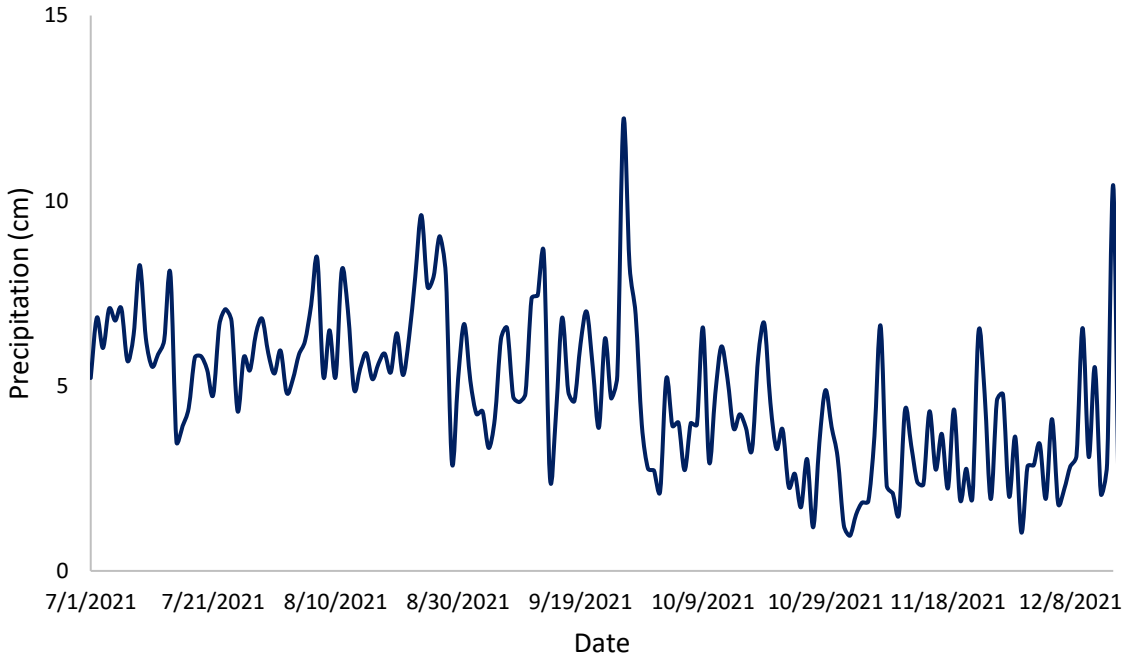

Figure D-4: ETo during the study period

Appendix E - Relative Models

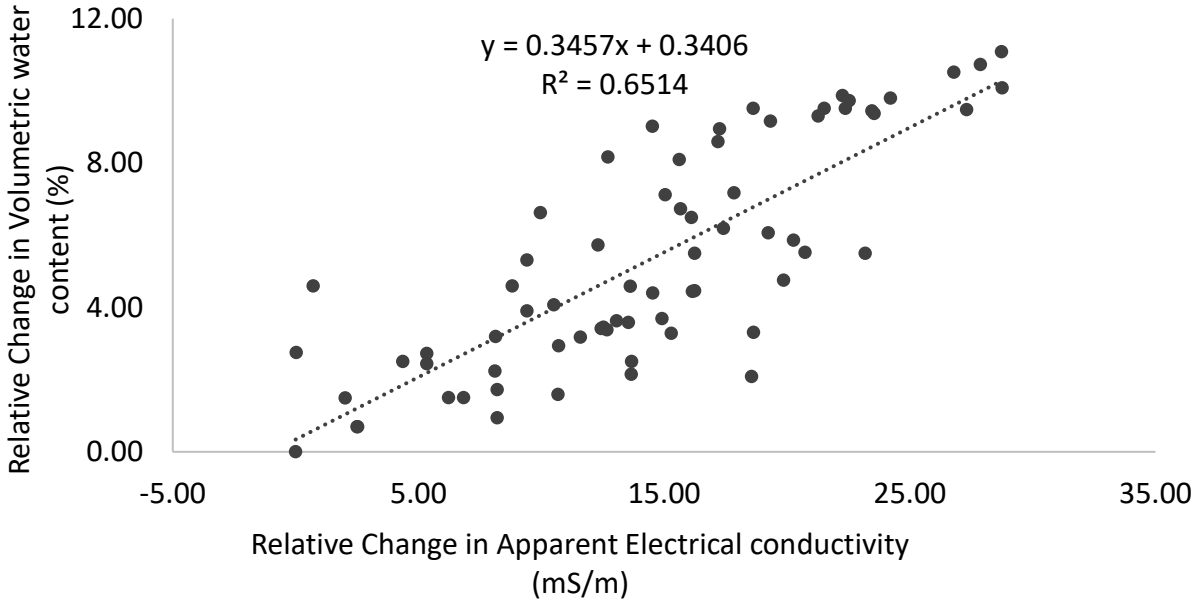

Figure E-1: Relative change in apparent electrical conductivity modelled against relative change in volumetric water content with maximum value as the reference value

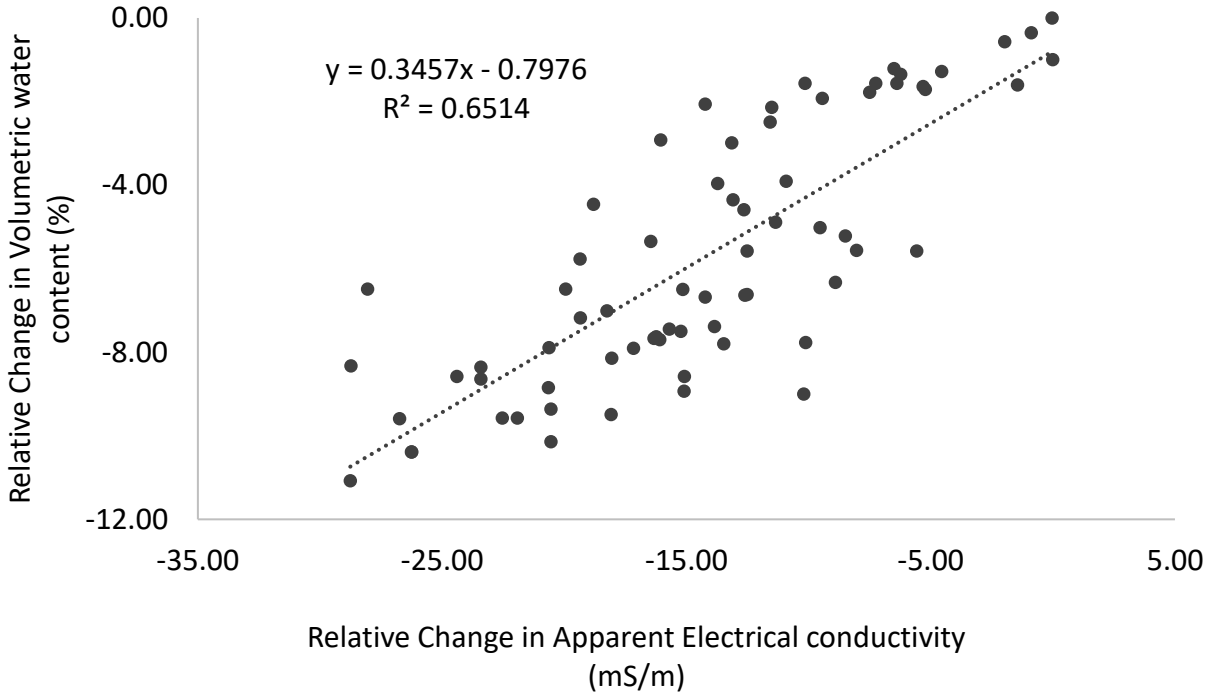

Figure E-2: Relative change in apparent electrical conductivity modelled against relative change in volumetric water content with minimum value as the reference value

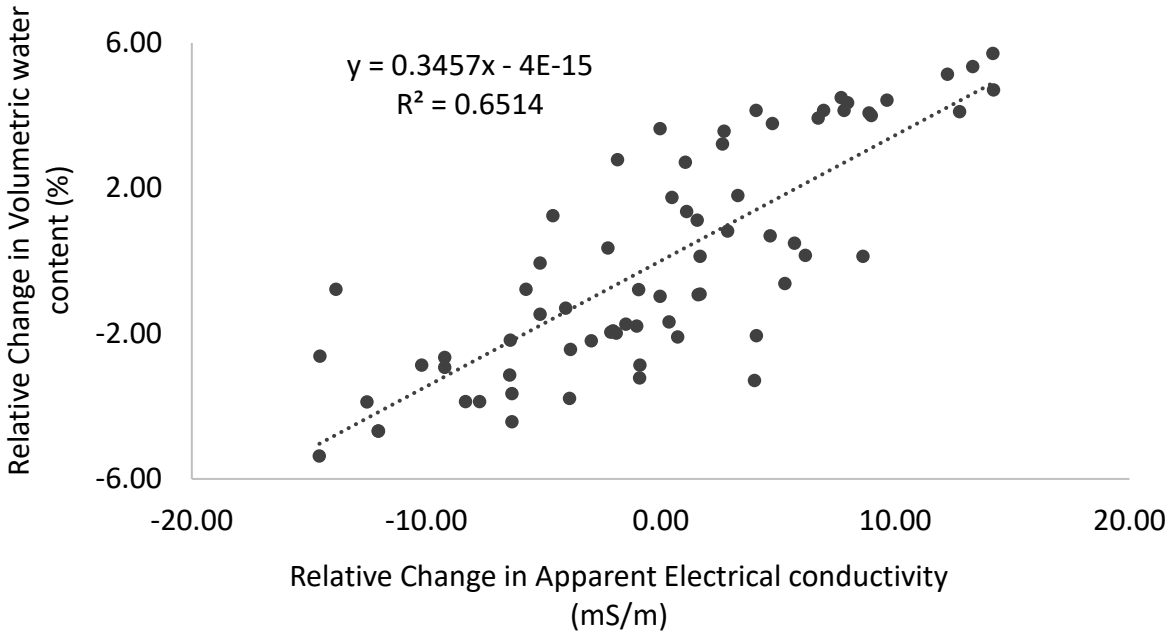

Figure E-3: Relative change in apparent electrical conductivity modelled against relative change in volumetric water content with average value as the reference value

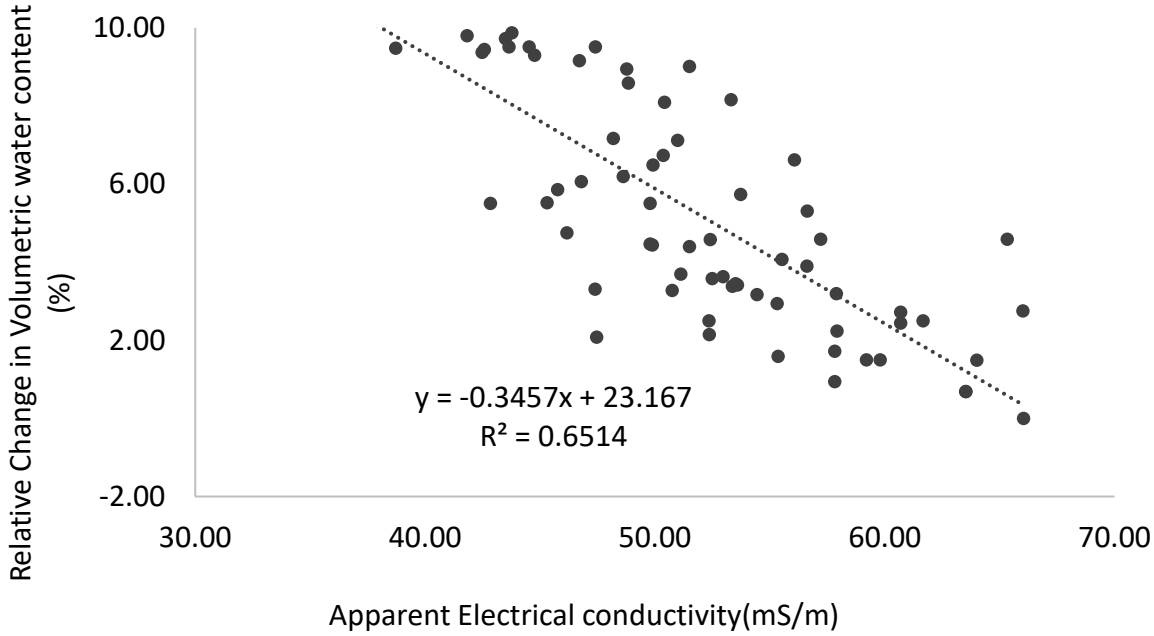

Figure E-4: Apparent electrical conductivity modelled against relative change in volumetric water content with maximum value as the reference value

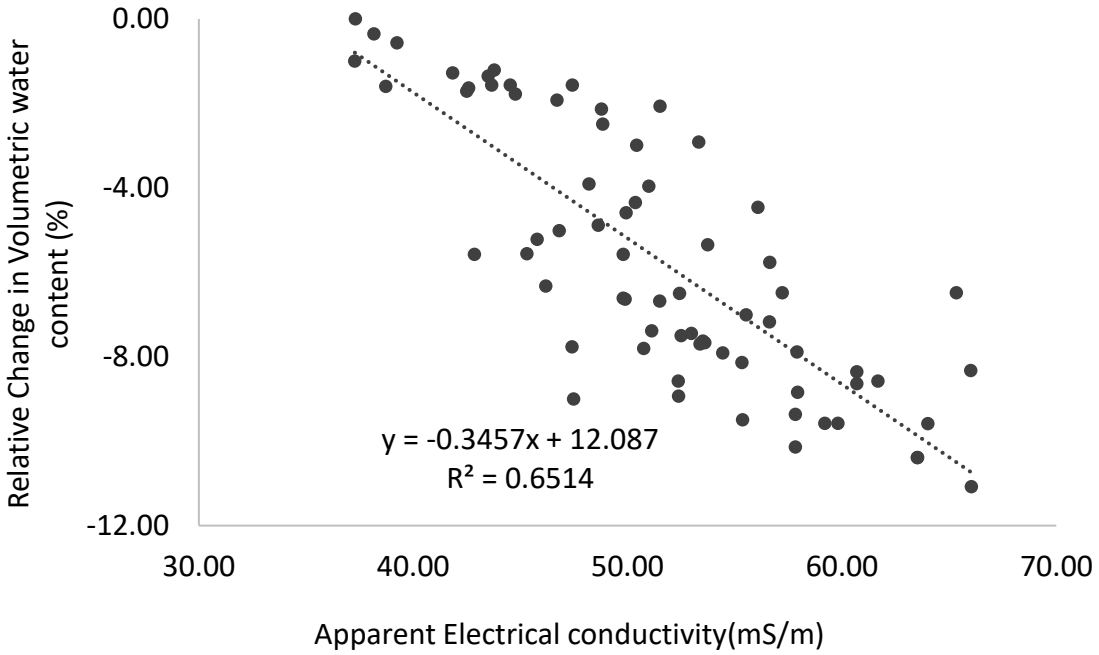

Figure E-5: Apparent electrical conductivity modelled against relative change in volumetric water content with minimum value as the reference value

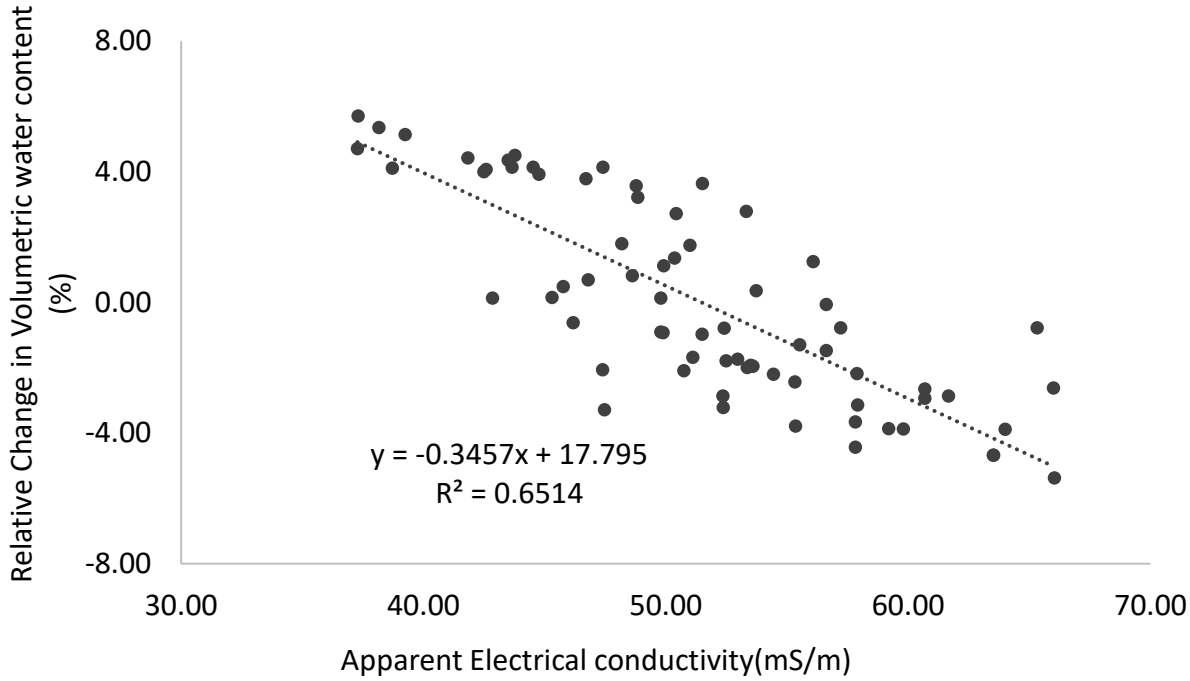

Figure E-6: Apparent electrical conductivity modelled against relative change in volumetric water content with average value as the reference value

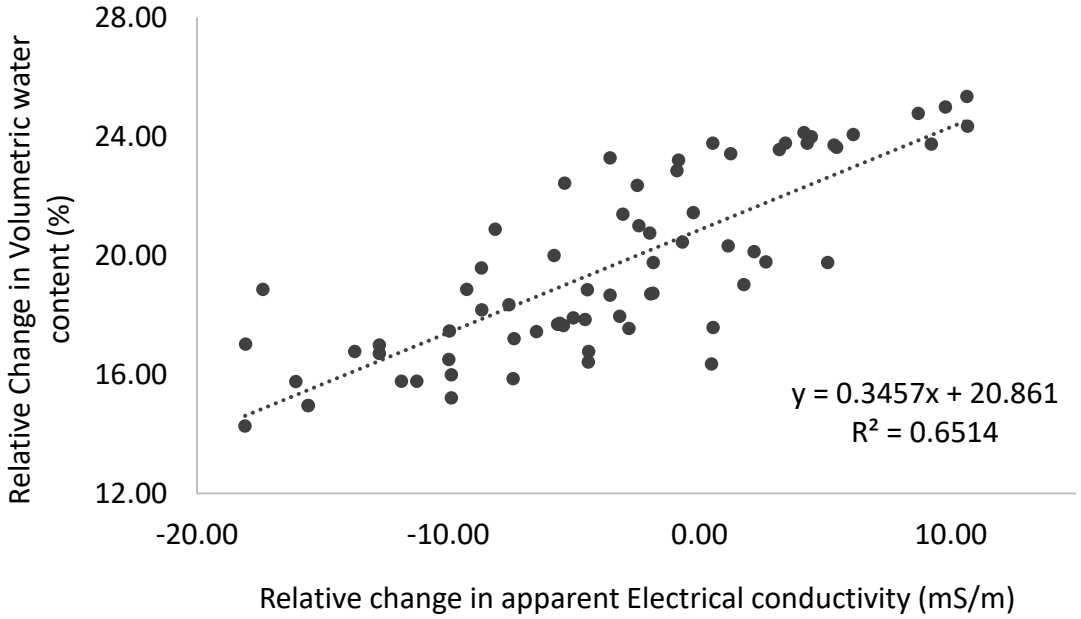

Figure E-7:Relative change in apparent electrical conductivity modelled against relative change in volumetric water content with known lab value as the reference value

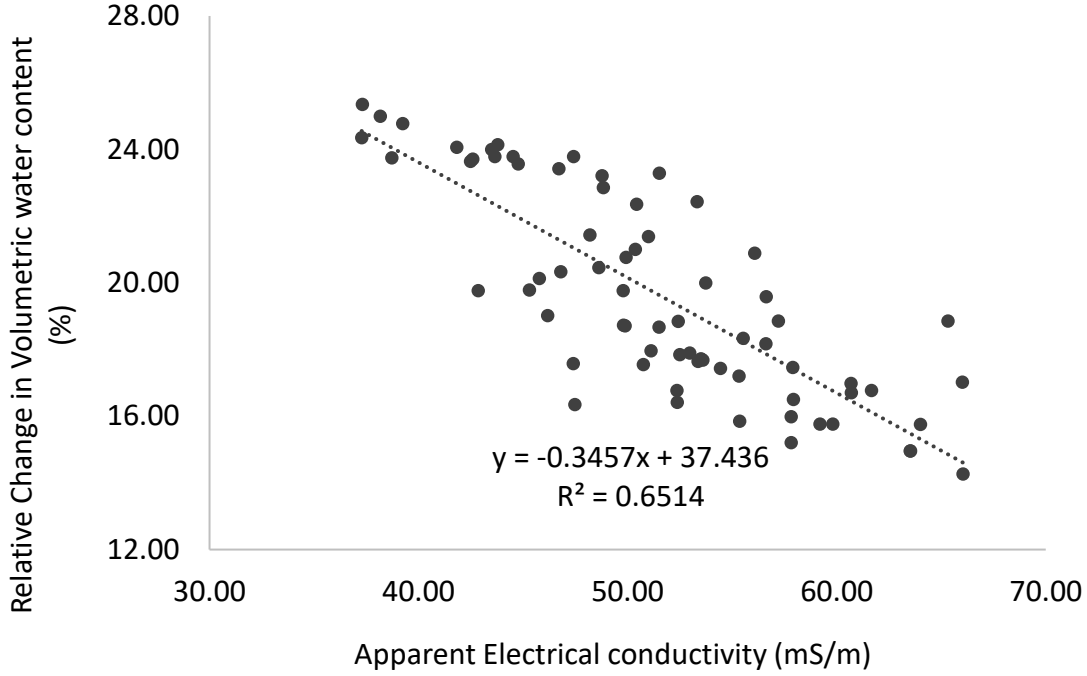

Figure E-8:Apparent electrical conductivity modelled against relative change in volumetric water content with known lab value as the reference value

Appendix F - Absolute models

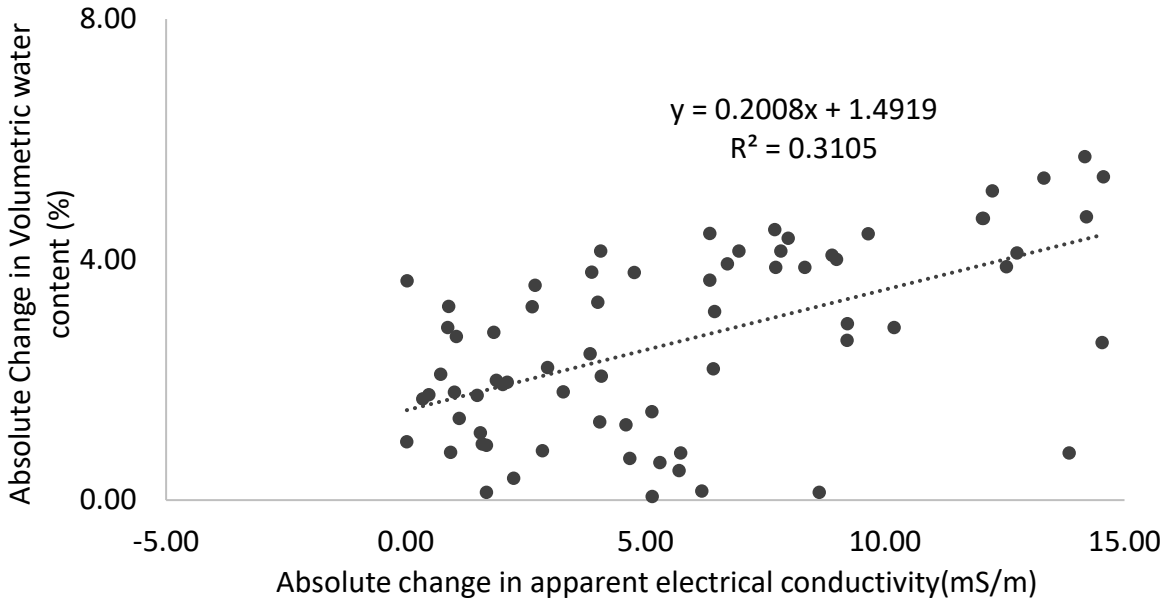

Figure F-1: Absolute change in apparent electrical conductivity modelled against absolute change in volumetric water content with average value as the reference value

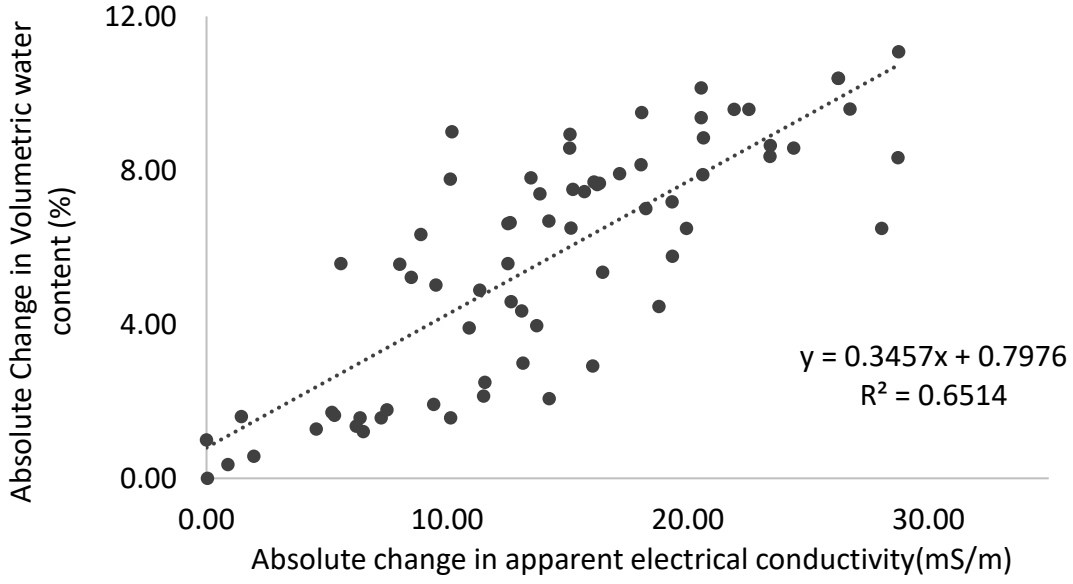

Figure F-2: Absolute change in apparent electrical conductivity modelled against absolute change in volumetric water content with minimum value as the reference value

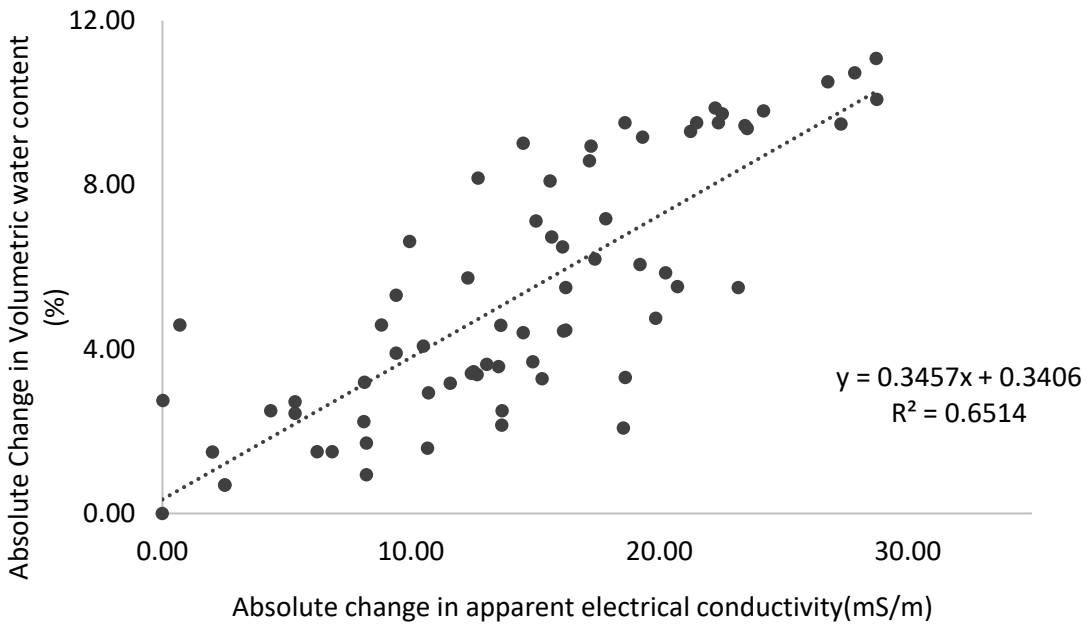

Figure F-3: Absolute change in apparent electrical conductivity modelled against absolute change in volumetric water content with maximum value as the reference value

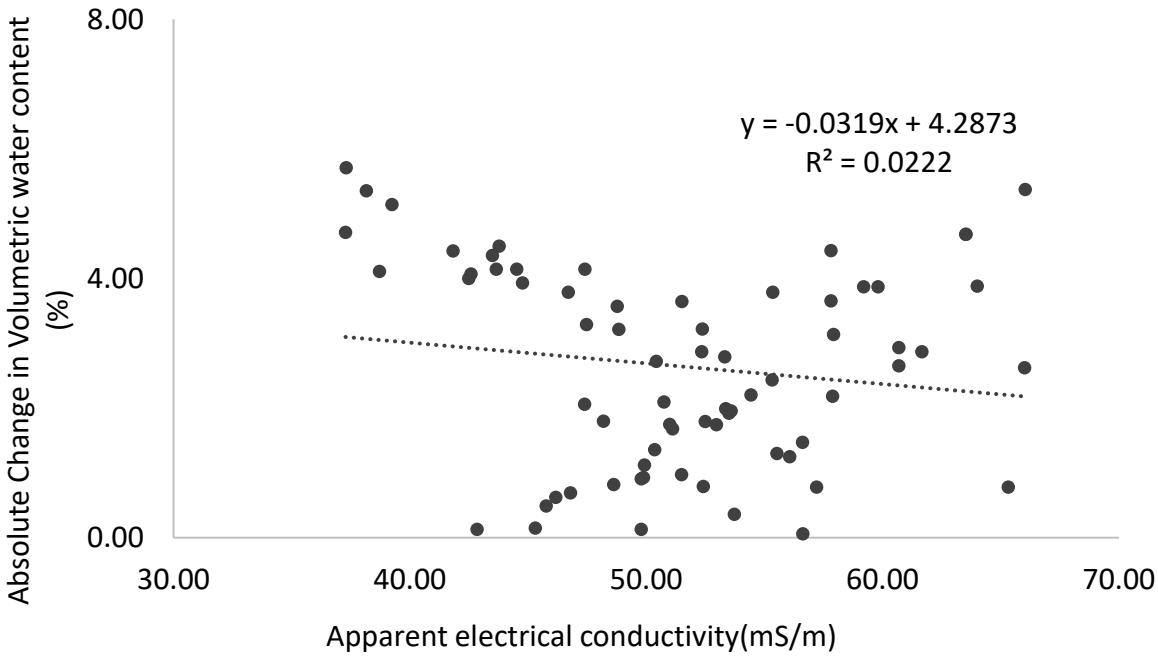

Figure F-4: Apparent electrical conductivity modelled against absolute change in volumetric water content with average value as the reference value

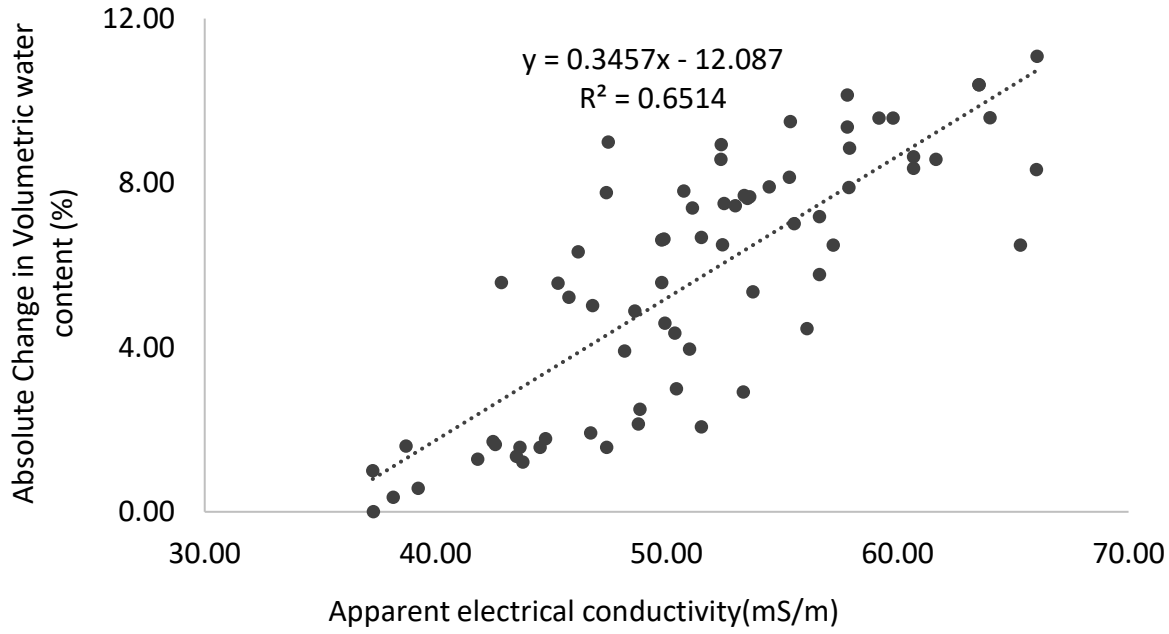

Figure F-5: Apparent electrical conductivity modelled against absolute change in volumetric water content with Minimum value as the reference value

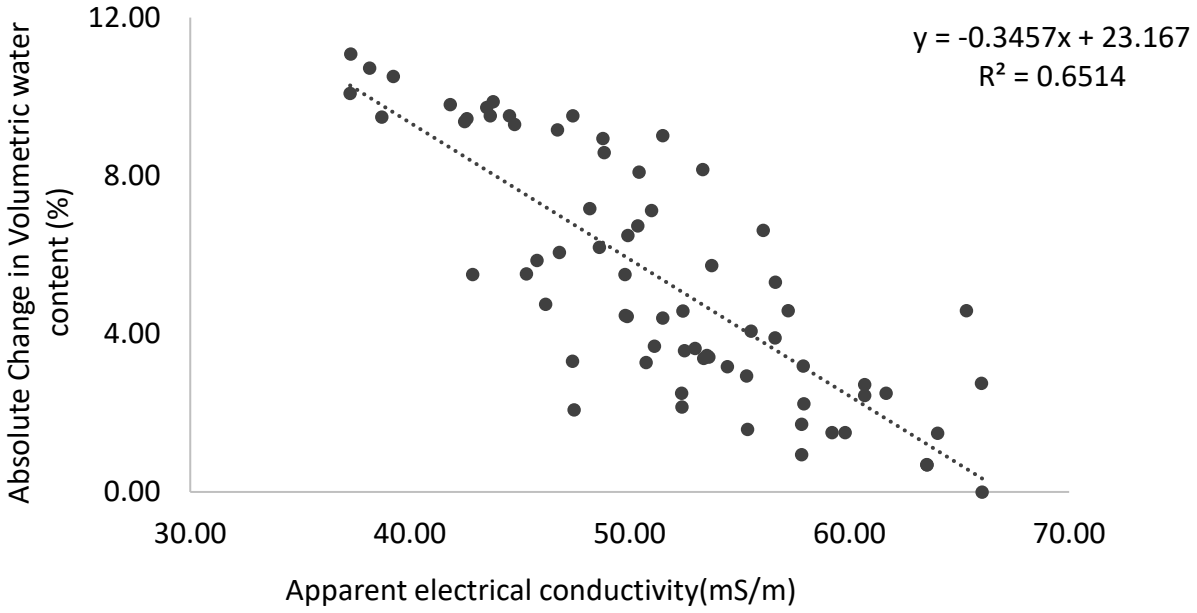

Figure F-6: Apparent electrical conductivity modelled against absolute change in volumetric water content with maximum value as the reference value

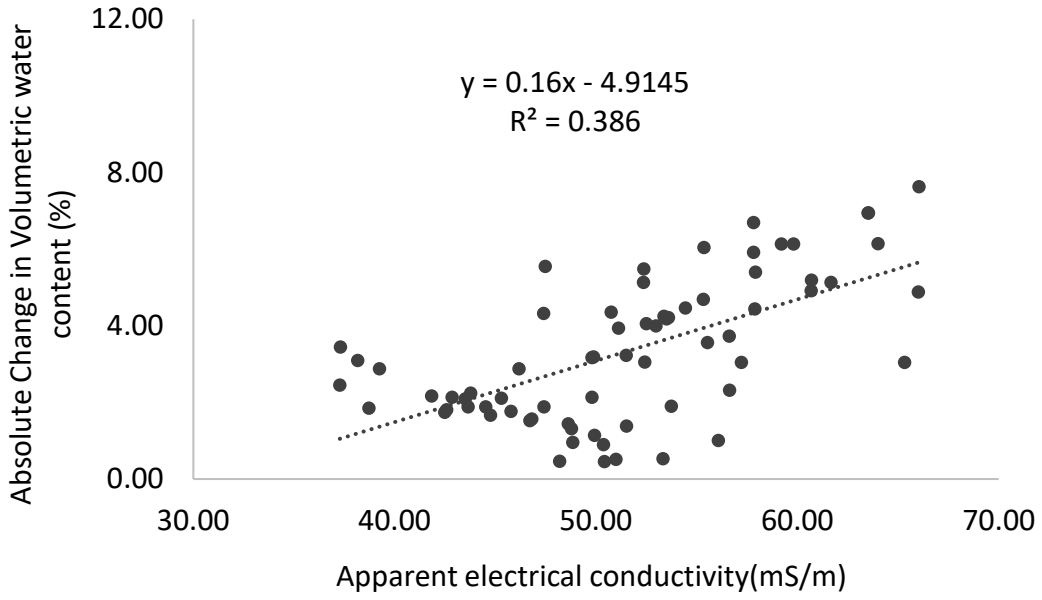

Figure F-7: Apparent electrical conductivity modelled against absolute change in volumetric water content with known lab value as the reference value

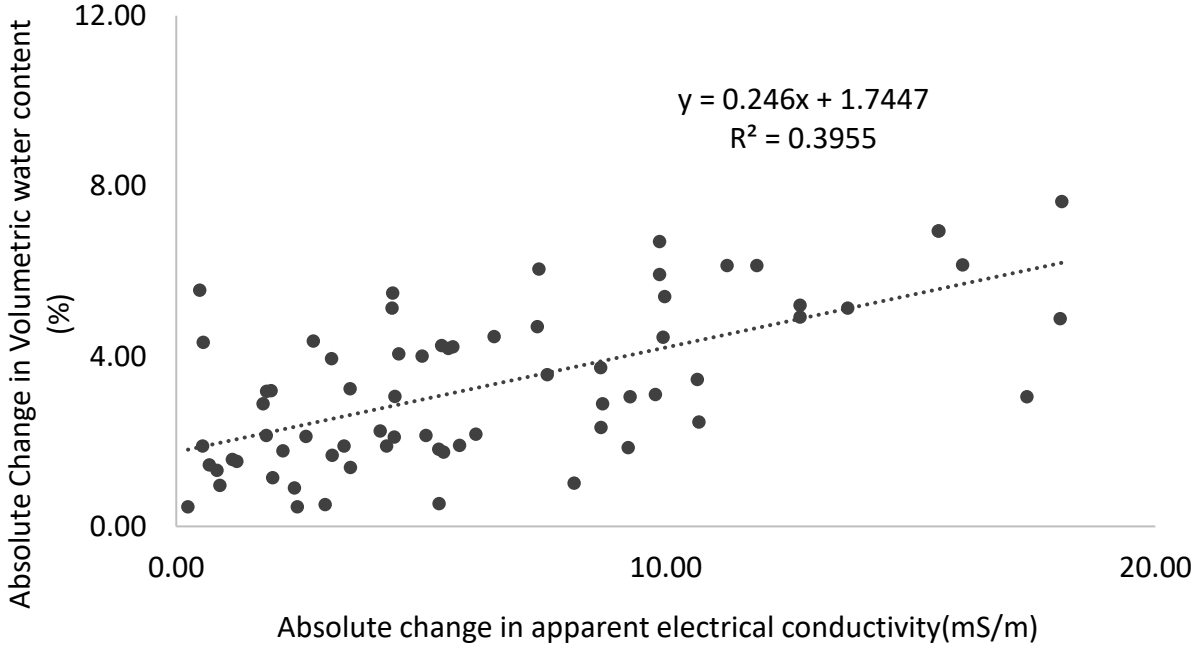

Figure F-8: Absolute change in apparent electrical conductivity modelled against absolute change in volumetric water content with known lab value as the reference value